IMPLEMENTING LOCKED NUCLEIC ACIDS AS A BIOINSPIRED COLLOIDAL ASSEMBLY AND DISASSEMBLY TOOL

A Dissertation
Presented to
The Academic Faculty

by

Ngozi Ada Eze

In Partial Fulfillment
of the Requirements for the Degree
Doctor of Philosophy in the
School of Materials Science and Engineering

Georgia Institute of Technology
May 2014

IMPLEMENTING LOCKED NUCLEIC ACIDS AS A BIOINSPIRED COLLOIDAL ASSEMBLY AND DISASSEMBLY TOOL

Approved by:

Dr. Valeria T. Milam, Advisor
School of Materials Science and Engineering
Georgia Institute of Technology

Dr. Vladimir V. Tsukruk
School of Materials Science and Engineering
Georgia Institute of Technology

Dr. Kenneth Gall
School of Materials Science and Engineering
Georgia Institute of Technology

Dr. Mark R. Prausnitz
School of Chemical & Biomolecular Engineering
Georgia Institute of Technology

Dr. Christopher J. Summers
School of Materials Science and Engineering
Georgia Institute of Technology

Date Approved: December 17, 2013

Ezi n’ụlọ m nye mụ ike ~ To my family, who gives me strength

ACKNOWLEDGEMENTS

I would like to thank everyone who has supported me over the course of my studies at Georgia Tech. First, to my advisor, Valeria Milam, I have appreciated your patience and helpful suggestions along the way as well as your dedication to making each member of your group a better scientist and engineer than at the start. I would also like to thank past and present members of the Milam group: James Hardin, Bryan Baker, Rick Sullivan, and Maeling Tapp, whose words of encouragement and commiseration have sustained me along the way. To Susan Bowman and Mechelle Kitchings, you both have given me lots of support, words of wisdom, encouragement, and consistently made my time at Tech cheerier. I owe a debt of gratitude to several people who brightened my time at Tech through laughter, conversation, commiseration, and food: thank you Kara, Sean, Ricky, Tamera, Lindsey, Selena, Chi, Deborah, and Mikel, along with several other people who have made me smile. I also would not have gotten through to the other end of the proverbial tunnel without the love and support from my surrogate family in Atlanta: Angie, Natashia, Jonas, Sean, and Annie. And to John, who has kept me motivated to finish, I look forward to the journey ahead. To my wonderful family, who has always believed in me and provided unwavering support, from wake-up calls, to care packages, to surprise trips to Atlanta. Thank you for learning early on not to ask the forbidden progress/graduation questions until it was time to buy the plane tickets, I love you.

TABLE OF CONTENTS

LIST OF TABLES

LIST OF FIGURES

LIST OF SYMBOLS

T_m	Melting Temperature
σ	Primary Duplex Density
k_1	Rate Constant for Primary Hybridization
k_d	Observed Displacement Rate Constant

LIST OF ABBREVIATIONS

DNA	Deoxyribonucleic Acid
LNA	Locked Nucleic Acid
RNA	Ribonucleic Acid
PNA	Peptide Nucleic Acid
ssDNA	Single-Stranded DNA
dsDNA	Double-Stranded DNA
dsLNA	Double-Stranded LNA
DNase I	Deoxyribonuclease I
RNase H	Ribonuclease H
mRNA	Messenger RNA
PCR	Polymerase Chain Reaction
MO	Modified Oligonucleotide
A	Adenine
T	Thymine
G	Guanine
C	Cytosine
EDAC	1-Ethyl-3-(3-dimethylaminopropyl) Carbodiimide
Oligo	Oligonucleotide

DLVO Theory	Derjaguin-Landau-Verwey-Overbeek Theory
MESF	Molecules of Equivalent Soluble Fluorochrome
PBS/T	Phosphate Buffered Saline with Tween-20 detergent
Au NP	Gold Nanoparticle
FAM	6-Carboxyfluorescein
Tris-EDTA	Tris(hydroxymethyl)aminomethane-Ethylenediaminetetraacetic Acid

SUMMARY

This dissertation extends prior work with DNA sequences to investigate incorporating locked nucleic acid (LNA), a synthetic oligonucleotide, in isothermal colloidal assembly and disassembly schemes as well as on hybridization kinetics between single-stranded and double-stranded probes immobilized on microspheres. Incorporation of LNA nucleotides into a DNA sequence is of particular interest as a means of enhancing the performance of DNA in a biomaterials context due to the increased resistance of LNA to nuclease degradation and its greater intrinsic affinity for oligonucleotide targets. The effects of LNA modification, target sequence length, sequence fidelity, and salt concentration are key variables explored. Chapter 1 provides an overview of DNA and its properties, synthetic oligonucleotides, colloidal particles, and previous applications of DNA and LNA in colloidal assembly schemes. Chapter 2 discusses first the selection and characteristics of appropriate pairs of hybridization partners for reversible colloidal assembly scenarios. Chapter 3 is a comparative investigation of the *in situ* primary hybridization kinetics between select LNA or DNA targets and single-stranded probes immobilized on colloidal surfaces. Chapter 4 discusses the *in situ* competitive displacement kinetics of hybridized LNA primary targets by either LNA or DNA secondary targets. For these *in situ* studies, flow cytometry was used to quantify the hybridization reactions as they occur on microsphere surfaces. While comparable rate constants were typically observed between target and single-stranded probes, LNA typically exhibited more extensive primary and secondary hybridization activity. Chapter 5 offers some concluding remarks and some research topics for future exploration in LNA-based materials systems.

CHAPTER 1

LITERATURE REVIEW: OLIGONUCLEOTIDES AS A BIOMATERIALS ASSEMBLY TOOL

Introduction

Oligonucleotides hold great promise as a recognition-based biomaterials assembly and disassembly tool. Chemically modified oligonucleotides such as locked nucleic acids (LNA) provide the added advantage of nuclease resistance. LNA is the most promising nucleic acid analogue due to its chemical similarity to RNA and DNA, reportedly low cytotoxicity effects, good *in vivo* stability, and ease of transfection into cells compared to other modified oligonucleotides.[1-4] LNA possesses a methylene linker between the 2′-oxygen and 4′-carbon of the ribose moiety that consequently locks the sugar into a C3′-*endo* conformation. This chemical modification confers nuclease resistance as well as higher affinity and greater specificity for oligonucleotide targets.[5-7]

1.1 Oligonucleotides as Biological Macromolecules

1.1.1 DNA and its Properties

DNA is a biological macromolecule that encodes the genetic information for living organisms. The structure of DNA is a double helix consisting of two long polymer strands of nucleotide units. Each nucleotide unit has one of four bases acting as a side group, as shown in Figure 1.1.1. The backbone of each nucleotide consists of an alternating five-carbon sugar group (2′-deoxyribose) and a negatively charged phosphate group. The coding information itself resides in the sequence of the bases—adenine (A), thymine (T), guanine (G), and cytosine (C). Hydrogen bonding between complementary bases stabilizes the helical structure, with each base binding to only one other to form base

pairs. The specific, complementary pairing that occurs between one purine base (C, T) and one pyrimidine base (G, A) to form A–T and C–G pairs is known as Watson-Crick base pairing and is depicted in Figure 1.1.1. The regular structure of the double helix and the data redundancy provided by the complementary strand make DNA optimal for the storage of genetic information; specific base pairing between DNA and other nucleotides provides the basis for both DNA replication and DNA transcription (to form RNA, and subsequently, proteins via RNA translation).

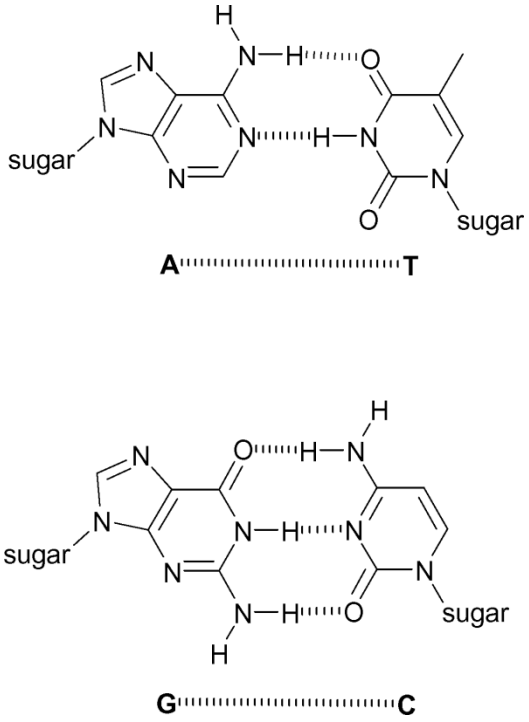

Figure 1.1.1. Hydrogen bonding and chemical structure of nucleotide bases in Watson-Crick base pairing. The guanine (G) – cytosine (C) pair involves three hydrogen bonds, resulting in greater thermal stability than the adenine (A) – thymine (T) pair involving only two hydrogen bonds. Reproduced from Gothelf and LaBean with permission of the Royal Society of Chemistry.[8]

1.1.2 Biological Function of DNA

The main function of DNA is the long-term storage of genetic information within cells. DNA directs the expression of this genetic information by controlling the synthesis of RNA and protein sequences through the processes of transcription and translation, respectively. The typical human (non-gamete) cell contains 46 chromosomes with a total length of approximately one meter. DNA is stored in the cell nucleus and is tightly wound around proteins called histones to form compact structures. Like DNA, histones can be chemically modified via methylation, acetylation, or phosphorylation to affect histone binding and to mediate access to and expression of specific genes.

Since DNA serves as the primary genetic information database, the mechanisms for copying this database (i.e., replication) and accessing it to respond to endogenous or exogenous stimuli are tightly regulated by very specific, recognition-based binding events between biomacromolecules. Due to this intrinsic selectivity for binding events, DNA offers a large degree of control in assembly-based schemes outside of the cell as described later in Section 1.3. Unlike other pairs of biological molecules that have fixed affinity values (e.g., biotin–avidin), DNA is becoming a particularly popular tool for materials assembly since the binding affinity of one strand for another can be tuned through choice in sequence length, number of base-pair mismatches, or salt concentration.[9] Ironically, however, there are some key obstacles that limit the utility of non-genomic DNA as an assembly tool for *in vivo* applications. Though stable inside the cell nucleus, DNA is susceptible to degradation by specific enzymes (deoxyribonucleases such as DNase I and DNase II) present in the cytoplasm as well as in physiological fluids (e.g., blood).[10] Deoxyribonucleases catalyze the hydrolytic cleavage of phosphodiester bonds in single- and double-stranded DNA. Nucleases are part of an organized multi-enzyme system that regulates gene expression as well as pathogenicity.[11] Within the past two decades, much research has been done to find acceptable nucleic acid analogues—

biocompatible molecules that retain the sequence-recognition capability of DNA and RNA, yet exhibit superior nuclease resistance.

1.1.3 General Chemical Properties of LNA and Other Synthetic Oligonucleotides

Modified oligonucleotides (MOs) such as peptide nucleic acid (PNA) and locked nucleic acid (LNA) have been explored for physiological applications due to their superior nuclease resistance over DNA as well as their typically stronger affinity for partner strands.[23,24] In phosphorothioate DNA,[24] for example, a non-bridging oxygen atom in the phosphodiester linkages of the backbone is replaced with a sulfur atom. Alternatively, the sugar moiety may be altered with atom substitutions such as fluorine (e.g., 2′-deoxy-2′-fluoro-β-D-arabino nucleic acid or FANA).[24] Both the backbone and the sugar are modified in PNA strands[24,25] which consist of a neutral pseudo-peptide backbone lacking a sugar moiety and which hybridize with high affinity to complementary RNA and DNA sequences.

These MOs are commonly used as antisense oligonucleotides for gene silencing by tightly binding an mRNA target either to block translation or to recruit RNase H.[26–29] RNase H is an RNA-specific nuclease that specifically degrades the RNA strand in RNA-DNA hybrid duplexes, thereby limiting subsequent transcription. The ability to recruit RNase H is important because MOs are usually designed to treat disorders and diseases caused by improper or undesired gene expression activity. Although these modified oligonucleotides, particularly PNA and phosphorothioate DNA, have been investigated,[30–33] several issues preclude their widespread use as an assembly tool under physiological conditions. Although the phosphorothioate linkages confer nuclease resistance to the modified DNA strands, base-pairing is less stable, and non-specific binding to proteins such as transcription factors is enhanced.[34] The use of PNA for cell cultures and *in vivo* applications is limited by cellular uptake issues stemming from its low solubility in water.[24] LNA is the most promising nucleic acid analog due to its

chemical similarity to RNA and DNA, reportedly low cytotoxicity effects, good *in vivo* stability, and ease of transfection into cells compared to other modified oligonucleotides.[24,35–37]

LNA is a hybrid mimic of DNA and RNA. It possesses the same bases as DNA. Similar to RNA, its ribose ring has a 2′-oxygen, whereas in DNA, the deoxyribose ring has a 2′-hydrogen atom bonded to the 2′-carbon. The distinctive feature of LNA oligonucleotides is a methylene linkage between the 2′-oxygen and the 4′-carbon in the ribose moiety that consequently locks the sugar in a C3′-*endo* conformation, as shown in Figure 1.1.3. The effect of each modification on either enthalpic or entropic factors, or both, is highly sequence- and context-specific.[12] Although the deoxyribose in DNA duplexes largely prefers the C2′-endo conformation, the sugar moiety can transition between two conformational states in single-stranded DNA (ssDNA).[13] Since the sugar moiety is already conformationally locked in LNA, the entropic penalty for LNA hybridization events is reduced.[4, 14-15] The increase in A-type helical structure reported for LNA-based duplexes is thought to promote stronger base-stacking interactions than found in the B-type helix for pure DNA-DNA duplexes.[15-16] Additionally, the chemical modification in LNA nucleotides confers resistance against nucleases.[17-19] LNA has, for example, been used in molecular beacons for real-time detection of oligonucleotide targets as illustrated in Figure 1.1.3.[20-22]

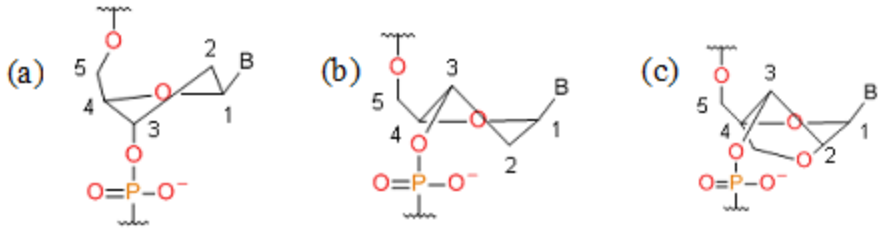

Figure 1.1.2. Schematic of DNA and LNA nucleotides. A single DNA nucleotide is shown with its (a) C2′-*endo* and (b) C3′-*endo* sugar puckers. While single-stranded DNA readily transitions between these two sugar conformations, the deoxyribose groups in natural double-stranded DNA are primarily C2′-*endo*. The (c) LNA ribose is locked into a C3′-*endo* sugar pucker due to the 2′O-4′C methylene bridge.

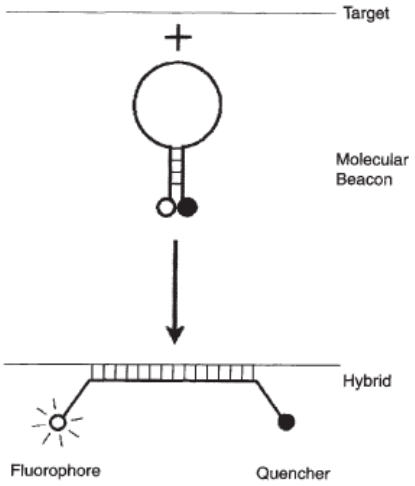

Figure 1.1.3. Schematic representation of a molecular beacon. *Top*: Single-stranded oligonucleotide target in the presence of a folded molecular beacon. The stem-loop structure of the single-stranded molecular beacon maintains the fluorophore and quenching moiety in close proximity, thus causing energy absorbed by the fluorophore to be transferred to the quencher via fluorescence-resonance energy transfer (FRET) and then dissipated as heat. *Bottom*: Hybridization of loop sequence with target induces a conformational change that allows the previously quenched fluorophore reporter to now emit a fluorescent signal. Reprinted from Tyagi and Kramer by permission from MacMillan Publishers Ltd: Nature Biotechnology, copyright 1996.[23]

1.2 Colloidal Particles, Interactions and Aggregation

Colloidal particles have extensive use in materials applications, such as paints,[24] food,[25] pharmaceuticals,[26] and optoelectronics.[27] Colloids serve as useful materials building blocks because they can be synthesized with a great degree of control over their size and chemical composition. One significant feature of colloidal particles is their high surface area to volume ratio. Thus, surface chemistry (e.g., the presence of charged functional groups, adsorbed macromolecules, etc.) plays an important role in colloidal interactions and resulting suspension structure. Suspensions can range in phase behavior from fluids (comprised of a dilute suspension of repulsive particles) to colloidal crystals (comprised of a concentrated suspension of either repulsive particles or very weakly attractive particles) to gels (comprised of a modest to high concentration of attractive particles).[28] These suspensions can be characterized with a variety of tools such as flow cytometry, microscopy, and rheology. Traditional approaches[28] to controlling colloidal interactions that govern phase behavior have focused on nonspecific interactions such as (1) attractive van der Waals interactions arising from induced dipole-dipole interactions, (2) repulsive electrostatic interactions between like-charged colloidal particles, and (3) repulsive steric interactions between polymer strands on opposing particle surfaces. Electrostatic and van der Waals interactions are accounted for in Derjaguin, Landau, Verwey and Overbeek (DLVO) theory and used to predict colloidal stability in polar environments for homogeneous spherical particles. Much of the early work used DLVO theory to model colloidal particles as hard-sphere suspensions in which the interaction is infinitely repulsive when the particles are in contact, and zero otherwise.[29] In addition to the experimental difficulties involved in achieving truly hard-sphere suspensions (e.g., index-matching the solvent to particles), this repulsion-based approach restricts the arrangement of neighboring particles.

A greater degree of control over the phase behavior of colloidal particles can be induced by functionalizing the particle surfaces with particular macromolecules that

interact in a specific manner. Depending on the chemical nature of the macromolecule (e.g., charged vs. neutral, natural vs. synthetic polymers), surface-bound macromolecules can further stabilize a suspension by introducing entropic contributions to steric repulsion effects. This steric repulsion, in turn, hinders aggregation by overcoming attractive van der Waals attractive wells at small separation distances. On the other hand, biological macromolecules such as proteins and oligonucleotides can serve as a source of "directed" attractive interaction to mediate colloidal aggregation or assembly. Colloidal aggregation involves disordered clusters or fractal clusters of varying size, as shown in Figure 1.2.1(a). Colloidal assembly implies some degree of order in the form of colloidal crystals or well-defined colloidal structures such as colloidal satellites, as shown in Figure 1.2.1(b). In this dissertation, compact colloidal assemblies called colloidal satellites or colloidal micelles (as shown in Figure 1.2.1(b)), will be explored as a central colloidal structure. In order for both the assembly and disassembly of these colloidal particles to be programmable, the effect of nonspecific interactions (e.g., van der Waals, electrostatic) must be minimized such that specific interactions (e.g., oligonucleotide duplex formation between particle surfaces) dominate suspension behavior.

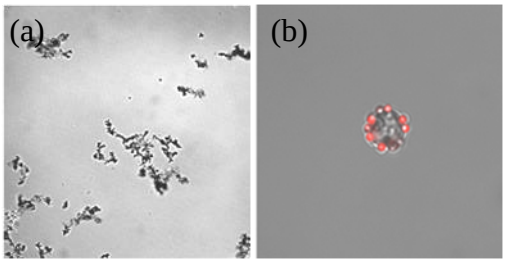

Figure 1.2.1. Confocal micrographs of DNA-linked colloidal structures: (a) colloidal aggregates comprised of 1 μm particles and (b) a colloidal satellite or micelle assembly comprised of a 5 μm particle surrounded by a layer of fluorescent 1 μm particles. All particles in this study were polystyrene microspheres. Reprinted with permission from Tison and Milam.[30] Copyright 2007 American Chemical Society.

1.3 Oligonucleotides as a Colloidal Assembly Tool

1.3.1 DNA-Mediated Colloidal Assembly

In 1996, Mirkin *et al*. and Alivisatos *et al*. published the first reports of DNA-based nanoparticle assembly.[31-32] Both research groups used gold nanoparticles (Au NPs) functionalized with surface-bound, thiolated DNA strands that bridged surfaces together through hybridization events. Alivisatos used soluble 'linker' DNA strands as an assembly tool, but for different colloidal structures. Rather than promote the formation of duplex-bridged nanoparticle aggregates, Alivisatos designed long segments of single-stranded DNA (ssDNA) templates that could hybridize with short single-stranded segments (oligomers) immobilized on Au NPs to produce either parallel (head-to-head) or antiparallel (head-to-tail) duplexes as shown in Figure 1.3.1. By adding complementary soluble strands, Alivisatos assembled Au nanoparticles into linear chains on the long DNA template strand. The stoichiometry of gold to double-stranded DNA (dsDNA) was confirmed by comparing the relative maximum absorbances of the suspensions at 420 nm (Au). Since ssDNA and dsDNA exhibit maximum absorbances at different wavelengths of UV light (260 nm and 280 nm, respectively), the extent of duplex-driven nanoparticle assembly on long DNA strands was measured using the change in the 280/260 absorbance ratio of a colloidal suspension over time. Alivisatos also demonstrated that the aggregation was reversible by raising the temperature above the melting temperature, T_m, for the linker–oligomer duplexes.

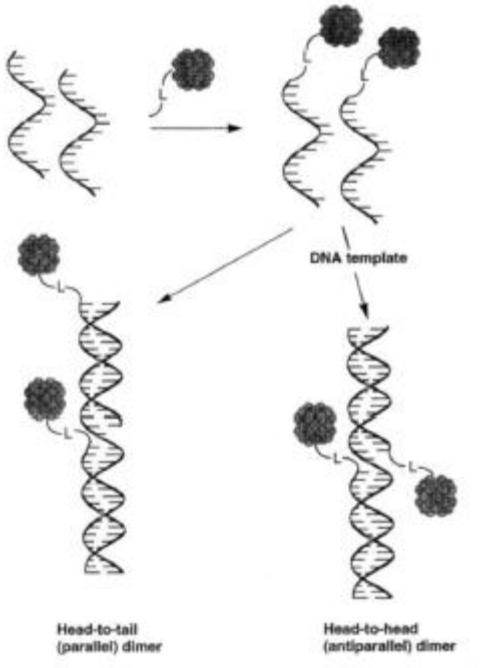

Figure 1.3.1. Schematic of nanoparticle assembly structures. Assembly of Au NPs is mediated by hybridization of DNA strands attached to the particle surface. The head-to-tail and head-to-head particle orientations are controlled by attachment of the Au NPs to the 5′ or 3′ end of the DNA strands. Reprinted from Alivisatos *et al.*[32] by permission from Macmillan Publishers Ltd: Nature, copyright 1996.

Mirkin used a similar chemical technique to prepare DNA-functionalized Au NPs. However, Mirkin designed a short "linker" possessing 5′ overhangs to drive hybridization events between two populations of Au nanoparticles functionalized with short oligonucleotide sequences as shown in Figure 1.3.2. Colloidal aggregation of the Au nanoparticles was observed upon addition of the linker. A control experiment using a linker with noncomplementary bases on the "sticky ends" confirmed that only hybridization induced colloidal aggregation. Mirkin demonstrated that the process was reversible via thermal denaturation by monitoring the change in absorbance at 260 nm (DNA hybridization) and 700 nm (degree of nanoparticle aggregation) while cycling the temperature between 0° and 80 °C. The seminal experiments reported by Alivisatos and Mirkin on reversible DNA-mediated colloidal assembly inspired a new avenue of re-

search in colloidal assembly that took advantage of the recognition capabilities of DNA as a materials assembly tool. Though redispersion was induced in Mirkin's system by heating the suspensions well past the duplex melting point, the conditions for programming the time or extent of redispersion of the aggregated nanoparticles were not specifically addressed in either study.

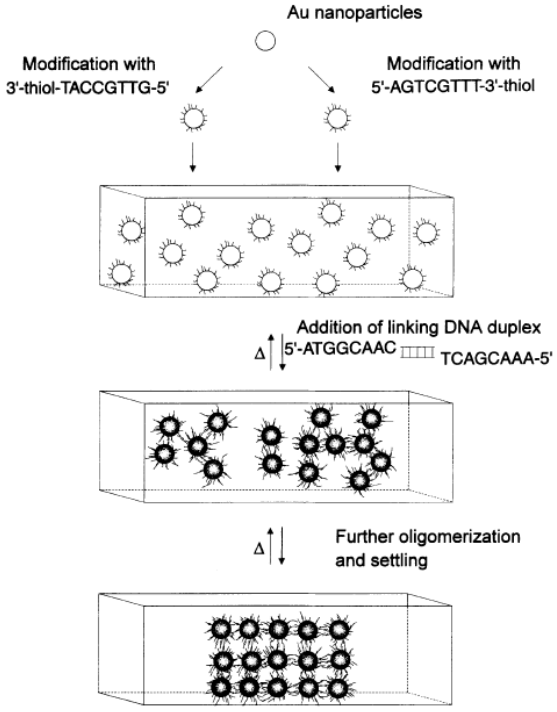

Figure 1.3.2. Schematic of a DNA-mediated gold nanoparticle aggregation strategy, which demonstrates the thermally reversible nature of the aggregation. Reprinted from Mirkin *et al*.[31] by permission from Macmillan Publishers Ltd: Nature, copyright 1996.

Much of the subsequent research in DNA-mediated meso- and nano-scale assembly has focused on characterizing and tuning the assembly/disassembly process. DNA hybridization has been used to assemble a variety of materials, including polystyrene microspheres,[33-35] quantum dots,[36] organic molecules for FRET analysis,[37] and nanowires.[38] In 2003, Milam *et al*. first investigated the DNA-driven assembly of

polystyrene microspheres.[33] Milam used a biotin–avidin linkage to immobilize complementary DNA strands on two populations of microspheres (e.g., one green fluorescent population and a second population of larger, nonfluorescent microspheres). With bidisperse colloids, DNA-directed aggregation (resulting in heterogeneous clusters) could be distinguished from nonspecific aggregation (resulting in both homogeneous and heterogeneous clusters). Her work demonstrated that interactions between complementary surface-bound DNA strands can induce aggregation. Milam also characterized the effect of ionic strength and sequence length on the extent of DNA-mediated colloidal aggregation, in order to show the possibility of tuning the degree of attraction between particles by controlling the affinity between pairs of complementary DNA strands.[33, 35] More recent work has incorporated an efficient method for immobilizing DNA on polystyrene microspheres by adapting a carbodiimide coupling process initially used to couple hydrogels in aqueous media.[39] Since this coupling process for covalently linking aminated DNA to carboxylated polystyrene microspheres via 1-ethyl-3-(3-dimethylaminopropyl) carbodiimide (EDAC) chemistry results in a stronger and smaller linkage than the biotin–avidin linkage used in Milam's 2003 experiments, the functionalized microspheres contain a stronger tether to DNA and better possibilities for increasing the surface DNA density.[40]

In 2005, Valignat *et al*. first described a process for reversible DNA-mediated aggregation using micron-sized colloids, instead of nanoparticles.[41] Valignat studied DNA-mediated polystyrene colloidal aggregation using two types of 61 base-long oligonucleotides: G-type and R-type. The eleven bases at the free end of G-type strands are complementary to the eleven bases at the free end of R-type strands, and act as sticky ends. The remaining fifty bases are the same in both types of sequences. Prior to combining the two bead populations, each functionalized with multiple copies of one strand type, the homologous 50-base sequences are hybridized with their soluble complements to effectively create a 111 base-pair spacer between particles. Valignat used laser tweezers

to spatially direct assembly of the colloidal particles into rigid rectangular shapes. Though not a high throughput approach, this experiment showed that it is possible to produce ordered, reversible DNA-hybridized colloidal structures.

Several groups have been interested in using DNA to mediate three-dimensional colloidal crystallization for applications such as photonics, electronics, and acoustics. The Crocker group was the first to report well-ordered crystals resulting from DNA-mediated assembly.[42] Close-packed crystal structures were observed for colloidal suspensions with DNA immobilized to microspheres via poly(ethylene glycol) (PEG) linkages. No crystallization was observed for suspensions with DNA anchored to microspheres via either carbodiimide chemistry or avidin–biotin coupling. Crocker discovered that the difference in phase behavior arose from differences in surface chemistry or nanostructure that induced transient, nonspecific interactions that interfered with the particle-on-particle rolling necessary for crystallization. Kinetic studies also indicated that the rate of crystallization increased with the density of surface-bound DNA. Crocker's key findings were as follows. First, crystallization could only occur by overcoming the nonspecific binding interactions that facilitate aggregation. Second, the concentration of surface-bound DNA affects crystallization kinetics. The Gang and Mirkin groups have since also demonstrated DNA-mediated assembly of colloidal crystals comprised of nanoparticles instead of microspheres.[43-44] The central issue in directing crystallization is maximizing the entropic degrees of freedom available to the colloids and hybridizing DNA strands. Both Gang and Mirkin observed a transition from aggregates to ordered packing as the length of hybridizing strands increased. In addition, decreasing the number of available interparticle linkages decreased the association rates and slowed particle motion to avoid kinetically trapped cluster formation and allow crystallization to occur.

1.3.2 Synthetic Oligonucleotide-Mediated Colloidal Assembly

There has been much interest in developing nucleic acid analogues for biotechnology applications, given their superior binding properties and stability compared to DNA.[21-22, 45-47] In the past decade, several analogues have been synthesized, each with their advantages and disadvantages. These include peptide nucleic acid (PNA) and LNA. The structure of PNA is a synthetic protein-derived backbone which is achiral and uncharged. As an electrically neutral macromolecule, PNA exhibits poor water solubility—a major obstacle for physiological applications. The unique hybridization characteristics of PNA to DNA have been studied, and studies reveal that PNA recognizes homopurine sequences (i.e., AAAA or GGGG) in double-stranded DNA, and subsequently forms stable PNA:DNA:PNA triplexes.[48] In addition to poor water solubility, the uncharged backbone in PNA is the cause of observed cytotoxicity, thus compromising the use of PNA as a potential biomaterials assembly tool. The hybridization characteristics of LNA are less understood than that of PNA, but LNA is a much more promising candidate, due to its charged backbone, water solubility, and lack of cytotoxicity. In 2007, the Mirkin group functionalized gold nanoparticles with LNA and used these conjugates in an antisense capacity to down-regulate gene expression in cells.[49] There has been little investigation, however, into the use of nucleic acid analogues to mediate colloidal assembly. In 2005, Ng investigated the hybridization of LNA to PNA, motivated by its potential use as an alternative to DNA in mediating programmable assembly of nanoparticles.[50] However, the results reported by Ng involved primarily proof-of-concept experiments to characterize the hybridization parameters of soluble LNA and PNA oligomers rather than materials assembly experiments involving LNA or PNA strands immobilized on nonnucleotide components. LNA has potential as an assembly tool, but fundamental research on its hybridization activity as a surface-immobilized macromolecule is lacking in the literature.

1.4 Redispersing Oligonucleotide-Linked Assemblies

Disassembly of oligonucleotide-linked objects has been performed using selective enzymatic digests or more commonly, elevated temperature conditions to melt partner strands. Enzymatic digests provide an isothermal method of disassembly; however, subsequent assembly formation (for reversible cycles) is precluded by the fragmentation of DNA strands. Melting immobilized partner strands is a convenient way to induce disassembly, and multiple assembly-disassembly cycles are in fact possible via thermal cycling. Such thermal cycling, however, precludes assembly and disassembly under physiologically relevant conditions (i.e., maintaining temperatures at or near 37 °C). Although several groups have explored schemes involving thermally reversible DNA-linked particles,[40-42, 51-52] only a few groups have investigated the use of competitive displacement of DNA to program colloidal disassembly.[30, 53-54] Moreover, to our knowledge, there have been no studies extending these competitive displacement strategies to LNA:LNA duplexes either in solution (i.e., not immobilized) or immobilized to a substrate. In addition to reversible assembly schemes, hybridization studies—particularly kinetics studies—could reveal valuable information to help optimize real-time, LNA-based monitoring of *in situ* or intracellular targets. To clarify, competitive hybridization in general involves the replacement of one strand of a duplex by another strand, and two scenarios are commonly studied for this phenomenon. The first involves the simultaneous addition of two or more distinct oligonucleotide targets to probe strands (two- or multi-component hybridization). This scenario would be applicable to microarrays in which there are several potential targets.[55-56] The second scenario involves an initial incubation step to promote primary hybridization between single-stranded probes and single-stranded targets with subsequent removal of any unhybridized target through wash steps. Secondary or competitive targets are then introduced to drive subsequent displacement of the original hybridization partner or primary target from the probe strand. This scenario,

known as competitive displacement, has been explored in oligonucleotide solutions[57-61] and particle studies.[62-64]

A kinetics model for competitive displacement has been developed by Reynaldo *et al.*[65] for DNA solutions involving primary and competitive targets of the same length. In this model, an unlabeled competitive DNA target, T_2, replaces an identical, labeled DNA target that is originally hybridized to an unlabeled DNA probe strand in the primary duplex PT_1^*, to form an unlabeled duplex, PT_2. According to Reynaldo, replacement of T_1^* in the original hybridization duplex by T_2 to form the new PT_2 duplex can proceed either via dissociation or via sequential displacement. In the dissociative pathway, the PT_1^* duplex completely dissociates, which then allows for rapid hybridization of P and T_2. In the sequential displacement pathway, however, PT_1^* becomes partly denatured (likely due to random base pair fluctuations) and forms an intermediate complex, $PT_1^*T_2$, with T_2, followed by rapid branch migration to displace T_1^*. The dissociative pathway dominates near the T_m of the primary duplex, whereas the sequential displacement pathway dominates near room temperature and when the competitive target is used in excess, which are the conditions relevant for this dissertation.

To better favor displacement of the primary target, a longer, and thereby stronger, secondary target can be employed to drive toehold-mediated competitive displacement activity. As illustrated in Figure 1.4.1, the initial hybridization of the competitive target occurs with bases outside the original duplex segment to help "anchor" or nucleate a secondary duplex. Afterwards, rapid branch migration ensues until the primary target is completely displaced and released to the surrounding solution.[59-61, 66-67] Competitive displacement involving immobilized sequences has been used to investigate a diverse array of research topics, including DNA-based machines,[67-69] genotyping,[70-72] biosensing,[73-74] and finally DNA-mediated colloidal assembly and disassembly under isothermal conditions[30, 54, 63, 75] as discussed further below.

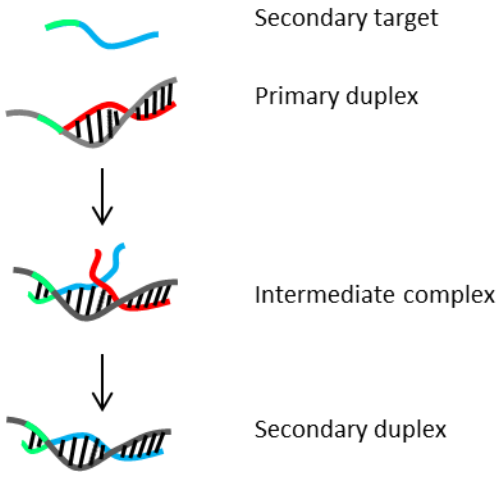

Figure 1.4.1. Schematic of toehold-mediated competitive displacement. Following the addition of a secondary target to a primary duplex consisting of a probe (gray) hybridized to a shorter primary target (red), the green segment of the secondary target hybridizes to the complementary green toehold region of the probe, thereby nucleating a secondary duplex and forming an intermediate complex between the probe and both primary and secondary targets. Following the formation of this complex, each base of the primary target is sequentially replaced by a base of the secondary target until the primary target is completely displaced, leaving a fully hybridized secondary duplex.

In 2007, Tison and Milam reported an isothermal process to reverse DNA-mediated colloidal assembly.[30] Competitive hybridization events between DNA-linked microspheres and soluble oligonucleotides directed the redispersion of colloidal satellite assemblies as shown in Figure 1.4.2. Tison demonstrated control over the relative affinities of the original (causing aggregation) and replacement (reversing aggregation) target strands for the DNA probe strands by changing the sequence characteristics such as length and base-pair mismatches.[75] Tison was able to control the extent of assembly and disassembly by titrating the surface density of conjugated probe strands with nonsense oligonucleotides (diluent strands). The research done by Tison and Milam in developing a successful isothermal disassembly method is an essential step in using a colloidal assembly system under physiological conditions. However, the clinical potential of this reversible, isothermal system is hindered by the use of DNA which is susceptible to

enzymatic degradation. The incorporation of nucleic acid analogues, such as LNA, into the sequence design should confer the additional stability against nucleases needed for successful clinical applications.

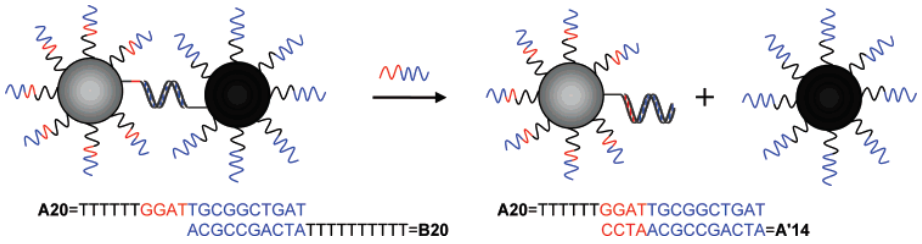

Figure 1.4.2. Schematic of toehold-mediated disassembly of DNA-linked particles via competitive displacement events resulting in particle redispersion. For simplicity, only one linkage is shown, though several duplexes are estimated to occur between pairs of particles. Reprinted with permission from Tison and Milam.[30] Copyright 2007 American Chemical Society.

LNA has been used to investigate physiologically relevant applications due to its reportedly low cytotoxic effects, good *in vivo* stability, and ease of transfection into cells.[1, 76-77] Prior work has demonstrated the potential for *in situ* displacement of double-stranded LNA (dsLNA) mixmers (sequences containing a mix of LNA and DNA bases) by cellular mRNA targets by quantifying the transfection efficiency and inducible gene expression of dsLNA probes; however, there is no displacement rate analysis, as the prior kinetics studies examined the fluorescence lifetimes of prehybridized probe:quencher and probe:target pairs.[78] Another study uses LNA mixmers in displacement-based strategies to improve the efficiency of real-time PCR. Though useful information about the higher melting temperature values and greater specificity of the LNA duplexes over DNA is reported, there is no detailed information about the kinetics of the LNA-based displace-

ment behavior.[79] While displacement kinetics studies are lacking, similar primary hybridization rate constants have been reported for LNA and DNA sequences in solution.[80-81] *In situ* hybridization experiments for immobilized sequences carry particular challenges such as potential nonspecific binding of primary and secondary targets to the material surface. To minimize nonspecific binding, wash studies are often employed; however, these wash steps can induce dissociation of target into the target-poor solution surrounding oligonucleotide-functionalized surfaces, even for the most robust hybridization partners.[62, 64, 82] In addition, the inclusion of any wash steps typically eliminates the ability to monitor *in situ* hybridization for colloidal particles. This dissertation complements prior work by the Milam group to assess *in situ* primary hybridization and competitive displacement kinetics of immobilized DNA probe sequences[64] as well as DNA-mediated colloidal assembly and disassembly studies[63, 75] and extends these studies to LNA sequences. The results presented in this dissertation help further the understanding of LNA hybridization activity and its potential as a programmable, reversible colloidal assembly tool.

1.5 Thermodynamics of LNA Hybridization

While the hybridization activity of natural oligonucleotides has been studied for decades, less is known about the hybridization activity of synthetic oligonucleotides, which are relatively newer. Existing reports on LNA hybridization have focused on thermodynamic studies of oligonucleotide solutions in which no strands are conjugated to a material surface[12, 14-16, 83-86] and on biotechnological applications of LNA hybridization, such as microarrays and gene therapy, in which strands may or may not be immobilized to a surface. [2, 68, 83-90]

Much of the solution-based thermodynamic studies of LNA have extracted sequence-dependent thermodynamic parameters from experimentally determined melting temperature values and heat capacity data. While a robust nearest neighbor model was developed for DNA-DNA hybridization that encompassed internal and end mismatches,[87-88] this model could not be directly extended to LNA hybridization since any effects of including LNA nucleotides on duplex stability and base pairing specificity are strongly dependent on the sequence itself (e.g., order of bases, inclusion of LNA vs. DNA nucleotide). Nearest-neighbor models based on experimental hybridization of several sets of LNA-DNA duplexes[75, 78, 82] include an expanded set of sequence parameters that allow for control over the number, composition, and order of both bases and sugar groups (i.e., deoxyribose vs. ribose for LNA) in a given sequence and its partner strand. Current models, for example, can account for both internal mismatches and consecutive LNA nucleotides in a sequence; however, they are only applicable to the hybridization of a pure LNA sequence or an LNA-DNA chimera sequence to a pure DNA sequence, and not to the pairs of LNA-DNA mixmers studied in this dissertation. A similar model is lacking for LNA:LNA hybridization, and would be useful for the sequences studied here and in previous work, since these sequences are designed to have either DNA:DNA or LNA:DNA interactions at each base pair.[89] Importantly, it has been demonstrated that incorporation of LNA nucleotides in a DNA sequence has additive effects on the melting temperature up to 50%.[15-16, 90] This finding is important for LNA-based applications because of the substantially greater cost of LNA nucleotides. For example, the unlabeled version of the 9 base-long DNA sequence used here costs approximately $140, whereas the corresponding LNA-DNA mixmer sequence, in which only one-third of the bases are LNA costs approximately $300, for a 1 μmole synthesis scale and HPLC purification.[91]

While less explored than DNA solutions, particle-based DNA hybridization activity appears to be more sensitive to experimental conditions[92] such as probe density, sequence

length, and salt concentration, with conflicting reports of enhanced[92-93] or suppressed[94-95] duplex stability compared to oligonucleotide solutions. The thermodynamics of LNA hybridization on particles has been studied to a lesser extent, but one study reports a degree of enhancement in the melting temperature values of immobilized LNA duplexes over analogous DNA duplexes in solution.[49] Direct comparison of the same LNA sequences in another study indicates that the duplex melting temperature is increased by immobilizing LNA duplexes.[96]

To provide a quantitative comparison of the effect of LNA substitution on duplex stability at the base pair level, thermodynamic parameters for solution-based duplex formation for DNA:DNA and LNA:DNA interactions are available from the literature. Appendix A lists the relevant ΔG°_{37} values of hybridization for doublets (e.g., AC/TG) relevant to the sequences used in this dissertation. Notably, ΔG°_{37} values are reported at 37 °C based on reported values and not at room temperature because at least one study has shown that differences in enthalpy, or ΔH, cannot be assumed to be independent of temperature (i.e., the change in heat capacity, $\Delta C_p \neq 0$), especially for LNA sequences. One of two online LNA calculators available does, however, assume a constant ΔH to report free energies,[97] and the other only reports melting temperatures.[91]

1.6 Kinetics of LNA Hybridization

Similar to the limited number of studies that have demonstrated the enhanced stability of LNA-based duplexes via thermal melting experiments to extract thermodynamic parameters,[12, 14, 83, 85-86, 98-99] there are relatively few kinetics studies for either solution-based or surface-based LNA systems.[80-81, 84, 100-103] There are reportedly no significant differences in the kinetics of duplex formation in solution for various combinations of DNA-DNA, LNA-DNA, and LNA-LNA duplexes in solution.[80-81] It was found, however, that the enhanced thermal stability of LNA-based duplexes may be due to a slower

spontaneous target dissociation rate constant. If both target and substrate contain substantial secondary structures within a single strand (e.g., stem-loop or hairpin structure), however, there is an apparent sequence context-specific dependence of the kinetic profile, though there is no agreement among these particular studies regarding the ultimate effect of LNA modification on the dissociation rate constants. [102-104] In contrast, the kinetics of duplex formation between single-stranded DNA sequences in solution has been well studied, even providing functional kinetic models.[105-106] Reported solution-based association rate constants for DNA hybridization are ~10^5–10^{-6} $M^{-1}s^{-1}$.[107-110] By comparison, reported solution-based association rate constants for duplex formation between LNA and either DNA or LNA are ~10^6–10^7 $M^{-1}s^{-1}$,[80-81] but in each case, the association rate constants for equivalent DNA sequences are the same order of magnitude as their LNA counterparts.

It has been shown, however, similar to the thermodynamics studies, that the solution-based parameters (e.g., salt concentration) for DNA do not necessarily allow for accurate prediction of surface-based hybridization activity.[110] For example, analysis of hybridization kinetics on planar substrates requires the use of flow conditions to avoid depletion of the initial target concentration at the diffusion boundary layer.[111] Analysis of hybridization kinetics on particle-based substrates, however, can be performed under static solution conditions because diffusion barriers to the surface decrease with decreasing particle radius, thus making the depletion effect on hybridization kinetics at the diffusion boundary layer minimal.[111] In both cases, for planar substrates or colloidal particles, the presence of a solid-phase support leads to slower kinetics compared to oligonucleotide solutions. A decrease in the association rate constant was observed from ~10^4–10^5 $M^{-1}s^{-1}$ in solution to 10^4 $M^{-1}s^{-1}$ when immobilized to microspheres,[111] and an even greater decrease of up to three orders of magnitude, from ~10^3–10^5 $M^{-1}s^{-1}$ in solution to ~10^2 $M^{-1}s^{-1}$ after immobilization occurs with increasing secondary structure of the probe sequence.[110] One study by the Milam group reported a similar association rate

constant of ~10^4 $M^{-1}s^{-1}$ between DNA-functionalized microspheres and DNA targets despite varying base-length and sequence fidelity.[64] These prior studies on DNA hybridization serve as useful comparative systems for LNA, which are discussed next.

Expanding these kinetics studies for immobilized strands to include LNA nucleotides indicates a similar dependence on several parameters including the temperature, sequence context of LNA substitutions and mismatches, total sequence length, and type of assay used.[101, 112-113] Hybridization kinetics studies[100-101] on planar substrates indicate a nearly ten-fold reduction in the target dissociation rate constant for LNA-based strands over DNA, somewhat smaller than reported in solution-based LNA kinetics studies.[81] To our knowledge, however, these kinetics studies on planar substrates have not been extended to monitor the in situ hybridization activity of LNA on colloidal particles. Here, this dissertation expands on previous work[64] on DNA-based colloidal systems to monitor early LNA hybridization events using flow cytometry as a high throughput analytical tool.

1.7 References

1. Kaur, H.; Babu, B. R.; Maiti, S. Perspectives on chemistry and therapeutic applications of locked nucleic acid (LNA). *Chem. Rev.* **2007,** *107* (11), 4672-4697.

2. Jepsen, J. S.; Pfundheller, H. M.; Lykkesfeldt, A. E. Downregulation of p21((WAF1/CIP1)) and estrogen receptor alpha in MCF-7 cells by antisense oligonucleotides containing locked nucleic acid (LNA). *Oligonucleotides* **2004,** *14* (2), 147-156.

3. Grunweller, A.; Wyszko, E.; Bieber, B.; Jahnel, R.; Erdmann, V. A.; Kurreck, J. Comparison of different antisense strategies in mammalian cells using locked nucleic acids, 2 '-o-methyl RNA, phosphorothioates and small interfering RNA. *Nucleic Acids Res.* **2003,** *31* (12), 3185-3193.

4. Koshkin, A. A.; Nielsen, P.; Meldgaard, M.; Rajwanshi, V. K.; Singh, S. K.; Wengel, J. LNA (locked nucleic acid): An RNA mimic forming exceedingly stable LNA:LNA duplexes. *J. Am. Chem. Soc.* **1998,** *120* (50), 13252-13253.

5. Singh, S. K.; Wengel, J. Universality of LNA-mediated high-affinity nucleic acid recognition. *Chem. Commun.* **1998,** (12), 1247-1248.

6. Wengel, J.; Petersen, M.; Nielsen, K. E.; Jensen, G. A.; Hakansson, A. E.; Kumar, R.; Sorensen, M. D.; Rajwanshi, V. K.; Bryld, T.; Jacobsen, J. P. LNA (locked nucleic acid) and the diastereoisomeric alpha-l-LNA: Conformational tuning and high-affinity recognition of DNA/RNA targets. *Nucleos. Nucleot. Nucl.* **2001,** *20* (4-7), 389-396.

7. Singh, S. K.; Nielsen, P.; Koshkin, A. A.; Wengel, J. LNA (locked nucleic acids): Synthesis and high-affinity nucleic acid recognition. *Chemical Communications* **1998,** (4), 455-456.

8. Gothelf, K. V.; LaBean, T. H. DNA-programmed assembly of nanostructures. *Org. Biomol. Chem.* **2005,** *3*, 4023-4037.

9. Kwon, Y. W.; Lee, C. H.; Choi, D. H.; Jin, J. I. Materials science of DNA. *J. Mater. Chem.* **2009,** *19* (10), 1353-1380.

10. Cherepanova, A.; Tamkovich, S.; Pyshnyi, D.; Kharkova, M.; Vlassov, V.; Laktionov, P. Immunochemical assay for deoxyribonuclease activity in body fluids. *J. Immunol. Methods* **2007,** *325* (1-2), 96-103.

11. Wilson, S. H.; Strauss, P. R., *The eukaryotic nucleus: Molecular biochemistry and macromolecular assemblies*. Telford Press: Caldwell, NJ, 1990; Vol. 2, p 881.

12. McTigue, P. M.; Peterson, R. J.; Kahn, J. D. Sequence-dependent thermodynamic parameters for locked nucleic acid (LNA)−DNA duplex formation. *Biochemistry* **2004,** *43* (18), 5388-5405.

13. Saenger, W.; Hunter, W. N.; Kennard, O. DNA conformation is determined by economics in the hydration of phosphate groups. *Nature* **1986,** *324* (6095), 385-388.

14. Kaur, H.; Arora, A.; Wengel, J.; Maiti, S. Thermodynamic, counterion, and hydration effects for the incorporation of locked nucleic acid nucleotides into DNA duplexes. *Biochemistry* **2006,** *45* (23), 7347-7355.

15. Petersen, M.; Nielsen, C. B.; Nielsen, K. E.; Jensen, G. A.; Bondensgaard, K.; Singh, S. K.; Rajwanshi, V. K.; Koshkin, A. A.; Dahl, B. M.; Wengel, J.; Jacobsen, J. P. The conformations of locked nucleic acids (LNA). *J. Mol. Recognit.* **2000,** *13* (1), 44-53.

16. Nielsen, K. E.; Singh, S. K.; Wengel, J.; Jacobsen, J. P. Solution structure of an LNA hybridized to DNA: NMR study of the d(CT(L)GCT(L)T(L)CT(L)GC):d(GCAGAAGCAG) duplex containing four locked nucleotides. *Bioconjugate Chem.* **2000,** *11* (2), 228-238.

17. Kurreck, J.; Wyszko, E.; Gillen, C.; Erdmann, V. A. Design of antisense oligonucleotides stabilized by locked nucleic acids. *Nucleic Acids Res.* **2002,** *30* (9), 1911-1918.

18. Crinelli, R.; Bianchi, M.; Gentilini, L.; Magnani, M. Design and characterization of decoy oligonucleotides containing locked nucleic acids. *Nucleic Acids Res.* **2002,** *30* (11), 2435-2443.

19. Frieden, M.; Hansen, H. F.; Koch, T. Nuclease stability of LNA oligonucleotides and LNA-DNA chimeras. *Nucleosides, Nucleotides and Nucleic Acids* **2003,** *22* (5-8), 1041-1043.

20. Dong, H.; Ding, L.; Yan, F.; Ji, H.; Ju, H. The use of polyethylenimine-grafted graphene nanoribbon for cellular delivery of locked nucleic acid modified molecular beacon for recognition of microRNA. *Biomaterials* **2011,** *32*, 3875-3882.

21. Yang, C. J.; Wang, L.; Wu, Y.; Kim, Y.; Medley, C. D.; Lin, H.; Tan, W. Synthesis and investigation of deoxyribonucleic acid/locked nucleic acid chimeric molecular beacons. *Nucleic Acids Res.* **2007,** *35* (12), 4030-4041.

22. Martinez, K.; Estevez, M. C.; Wu, Y.; Phillips, J. A.; Medley, C. D.; Tan, W. Locked nucleic acid based beacons for surface interaction studies and biosensor development. *Anal. Chem.* **2009,** *81* (9), 3448-3454.

23. Tyagi, S.; Kramer, F. R. Molecular beacons: Probes that fluoresce upon hybridization. *Nat. Biotechnol.* **1996,** *14* (3), 303-308.

24. Croll, S. DLVO theory applied to TiO2 pigments and other materials in latex paints. *Prog. Org. Coat.* **2002,** *44* (2), 131-146.

25. Le Reverend, B. J. D.; Norton, I. T.; Cox, P. W.; Spyropoulos, F. Colloidal aspects of eating. *Curr. Opin. Colloid Interface Sci.* **2010,** *15* (1-2), 84-89.

26. Mishra, B.; Patel, B. B.; Tiwari, S. Colloidal nanocarriers: A review on formulation technology, types and applications toward targeted drug delivery. *Nanomedicine: NBM* **2010,** *6* (1), 9-24.

27. Talapin, D. V.; Lee, J. S.; Kovalenko, M. V.; Shevchenko, E. V. Prospects of colloidal nanocrystals for electronic and optoelectronic applications. *Chem. Rev.* **2010,** *110* (1), 389-458.

28. Pusey, P. N.; van Megen, W. Phase behaviour of concentrated suspensions of nearly hard colloidal spheres. *Nature* **1986,** *320* (6060), 340-342.

29. Underwood, S. M.; Taylor, J. R.; Vanmegen, W. Sterically stabilized colloidal particles as model hard-spheres. *Langmuir* **1994,** *10* (10), 3550-3554.

30. Tison, C. K.; Milam, V. T. Reversing DNA-mediated adhesion at a fixed temperature. *Langmuir* **2007,** *23* (19), 9728-9736.

31. Mirkin, C. A.; Letsinger, R. L.; Mucic, R. C.; Storhoff, J. J. A DNA-based method for rationally assembling nanoparticles into macroscopic materials. *Nature* **1996,** *382* (6592), 607-609.

32. Alivisatos, A. P.; Johnsson, K. P.; Peng, X. G.; Wilson, T. E.; Loweth, C. J.; Bruchez, M. P.; Schultz, P. G. Organization of 'nanocrystal molecules' using DNA. *Nature* **1996,** *382* (6592), 609-611.

33. Milam, V. T.; Hiddessen, A. L.; Crocker, J. C.; Graves, D. J.; Hammer, D. A. DNA-driven assembly of bidisperse, micron-sized colloids. *Langmuir* **2003,** *19* (24), 10317-10323.

34. Biancaniello, P. L.; Kim, A. J.; Crocker, J. C. Colloidal interactions and self-assembly using DNA hybridization. *Phys. Rev. Lett.* **2005,** *94* (5), 4.

35. Biancaniello, P. L.; Crocker, J. C.; Hammer, D. A.; Milam, V. T. DNA-mediated phase behavior of microsphere suspensions. *Langmuir* **2007,** *23* (5), 2688-2693.

36. Mitchell, G. P.; Mirkin, C. A.; Letsinger, R. L. Programmed assembly of DNA functionalized quantum dots. *J. Am. Chem. Soc.* **1999,** *121* (35), 8122-8123.

37. Shi, J. F.; Bergstrom, D. E. Assembly of novel DNA cycles with rigid tetrahedral linkers. *Angew. Chem., Int. Ed. Engl.* **1997,** *36* (1-2), 111-113.

38. Braun, E.; Eichen, Y.; Sivan, U.; Ben-Yoseph, G. DNA-templated assembly and electrode attachment of a conducting silver wire. *Nature* **1998,** *391* (6669), 775-778.

39. Nakajima, N.; Ikada, Y. Mechanism of amide formation by carbodiimide for bioconjugation in aqueous media. *Bioconjugate Chem.* **1995,** *6* (1), 123-130.

40. Rogers, P. H.; Michel, E.; Bauer, C. A.; Vanderet, S.; Hansen, D.; Roberts, B. K.; Calvez, A.; Crews, J. B.; Lau, K. O.; Wood, A.; Pine, D. J.; Schwartz, P. V. Selective, controllable, and reversible aggregation of polystyrene latex microspheres via DNA hybridization. *Langmuir* **2005,** *21* (12), 5562-5569.

41. Valignat, M. P.; Theodoly, O.; Crocker, J. C.; Russel, W. B.; Chaikin, P. M. Reversible self-assembly and directed assembly of DNA-linked micrometer-sized colloids. *Proc. Natl. Acad. Sci. U. S. A.* **2005,** *102* (12), 4225-4229.

42. Kim, A. J.; Biancaniello, P. L.; Crocker, J. C. Engineering DNA-mediated colloidal crystallization. *Langmuir* **2006,** *22* (5), 1991-2001.

43. Nykypanchuk, D.; Maye, M. M.; van der Lelie, D.; Gang, O. DNA-guided crystallization of colloidal nanoparticles. *Nature* **2008,** *451* (7178), 549-552.

44. Park, S. Y.; Lytton-Jean, A. K. R.; Lee, B.; Weigand, S.; Schatz, G. C.; Mirkin, C. A. DNA-programmable nanoparticle crystallization. *Nature* **2008,** *451* (7178), 553-556.

45. Wahlestedt, C.; Salmi, P.; Good, L.; Kela, J.; Johnsson, T.; Hokfelt, T.; Broberger, C.; Porreca, F.; Lai, J.; Ren, K. K.; Ossipov, M.; Koshkin, A.; Jakobsen, N.; Skouv, J.; Oerum, H.; Jacobsen, M. H.; Wengel, J. Potent and nontoxic antisense oligonucleotides containing locked nucleic acids. *Proceedings of the National Academy of Sciences of the United States of America* **2000,** *97* (10), 5633-5638.

46. Jacobsen, N.; Bentzen, J.; Meldgaard, M.; Jakobsen, M. H.; Fenger, M.; Kauppinen, S.; Skouv, J. LNA-enhanced detection of single nucleotide polymorphisms in the apolipoprotein E. *Nucl. Acids Res.* **2002,** *30* (19), e100-.

47. Kubota, K.; Ohashi, A.; Imachi, H.; Harada, H. Improved in situ hybridization efficiency with locked-nucleic-acid-incorporated DNA probes. *Appl. Environ. Microbiol.* **2006,** *72* (8), 5311-5317.

48. Larsen, H. J.; Bentin, T.; Nielsen, P. E. Antisense properties of peptide nucleic acid. *Biochim. Biophys. Acta, Gene Struct. Expression* **1999,** *1489* (1), 159-166.

49. Seferos, D. S.; Giljohann, D. A.; Rosi, N. L.; Mirkin, C. A. Locked nucleic acid-nanoparticle conjugates. *ChemBioChem* **2007,** *8* (11), 1230-1232.

50. Ng, P. S.; Bergstrom, D. E. Alternative nucleic acid analogues for programmable assembly: Hybridization of LNA to PNA. *Nano Lett.* **2005,** *5* (1), 107-111.

51. Park, S. Y.; Stroud, D. Theory of melting and the optical properties of gold/DNA nanocomposites. *Phys. Rev. B* **2003,** *67*, 212202.

52. Maye, M. M.; Nykypanchuk, D.; van der Lelie, D.; Gang, O. DNA-regulated micro- and nanoparticle assembly. *Small* **2007,** *3* (10), 1678-1682.

53. Chi, C.; Maye, M. M.; Stadler, A. L.; van der Lelie, D.; Gang, O. Sensing nucleic acids with dimer nanoclusters. *Adv. Funct. Mater.* **2011,** *21*, 1051-1057.

54. Hazarika, P.; Ceyhan, B.; Niemeyer, C. M. Reversible switching of DNA-gold nanoparticle aggregation. *Angew. Chem. Int. Edit.* **2004,** *43* (47), 6469-6471.

55. Bishop, J.; Wilson, C.; Chagovetz, A. M.; Blair, S. Competitive displacement of DNA during surface hybridization. *Biophys. J.* **2007,** *92* (1), L10-L12.

56. Tawa, K.; Yao, D.; Knoll, W. Matching base-pair number dependence of the kinetics of DNA–DNA hybridization studied by surface plasmon fluorescence spectroscopy. *Biosens. Bioelectron.* **2005,** *21* (2), 322-329.

57. Green, C.; Tibbetts, C. Reassociation rate limited displacement of DNA strands by branch migration. *Nucleic Acids Res.* **1981,** *9* (8), 1905-1918.

58. Vary, C. P. H. A homogeneous nucleic-acid hybridization assay based on strand displacement. *Nucleic Acids Res.* **1987,** *15* (17), 6883-6897.

59. Ellwood, M. S.; Collins, M.; Fritsch, E. F.; Williams, J. I.; Diamond, S. E.; Brewen, J. G. Strand displacement applied to assays with nucleic acid probes. *Clin. Chem.* **1986,** *32* (9), 1631-1636.

60. Li, Q.; Luan, G.; Guo, Q.; Liang, J. A new class of homogeneous nucleic acid probes based on specific displacement hybridization. *Nucleic Acids Res.* **2002,** *30* (2), e5.

61. Zhang, D. Y.; Winfree, E. Control of DNA strand displacement kinetics using toehold exchange. *J. Am. Chem. Soc.* **2009,** *131* (47), 17303-17314.

62. Baker, B. A.; Milam, V. T. Hybridization kinetics between immobilized double-stranded DNA probes and targets containing embedded recognition segments. *Nucleic Acids Res.* **2011,** *39* (15).

63. Tison, C. K.; Milam, V. T. Programming the kinetics and extent of colloidal disassembly using a DNA trigger. *Soft Matter* **2010,** *6* (18), 4446-4453.

64. Hardin, J. O.; Milam, V. T. Measuring in situ primary and competitive DNA hybridization activity on microspheres. *Biomacromolecules* **2013,** *14* (4), 986-992.

65. Reynaldo, L. P.; Vologodskii, A. V.; Neri, B. P.; Lyamichev, V. I. The kinetics of oligonucleotide replacements. *J. Mol. Biol.* **2000,** *297* (2), 511-520.

66. Genot, A. J.; Zhang, D. Y.; Bath, J.; Turberfield, A. J. Remote toehold: A mechanism for flexible control of DNA hybridization kinetics. *J. Am. Chem. Soc.* **2011,** *133* (7), 2177-2182.

67. Yurke, B.; Turberfield, A. J.; Mills, A. P.; Simmel, F. C.; Neumann, J. L. A DNA-fuelled molecular machine made of DNA. *Nature* **2000,** *406* (6796), 605-608.

68. Yan, H.; Zhang, X. P.; Shen, Z. Y.; Seeman, N. C. A robust DNA mechanical device controlled by hybridization topology. *Nature* **2002,** *415* (6867), 62-65.

69. Frezza, B. M.; Cockroft, S. L.; Ghadiri, M. R. Modular multi-level circuits from immobilized DNA-based logic gates. *J. Am. Chem. Soc.* **2007,** *129* (48), 14875-14879.

70. Khodakov, D. A.; Khodakova, A. S.; Linacre, A.; Ellis, A. V. Toehold-mediated nonenzymatic DNA strand displacement as a platform for DNA genotyping. *J. Am. Chem. Soc.* **2013,** *135* (15), 5612-5619.

71. Golubev, D. B.; Zolotarev, F. N. The method of competitive dot hybridization for genotyping of influenza-a viruses. *Vopr. Virusol.* **1993,** *38* (5), 198-201.

72. Kaller, M.; Hultin, E.; Zheng, B. Y.; Gharizadeh, B.; Wallin, K. L.; Lundeberg, J.; Ahmadian, A. Tag-array based HPV genotyping by competitive hybridization and extension. *J. Virol. Methods* **2005,** *129* (2), 102-112.

73. Wang, D.; Tang, W.; Wu, X.; Wang, X.; Chen, G.; Chen, Q.; Li, N.; Liu, F. Highly selective detection of single-nucleotide polymorphisms using a quartz crystal microbalance biosensor based on the toehold-mediated strand displacement reaction. *Anal. Chem.* **2012,** *84* (16), 7008-7014.

74. Briones, C.; Moreno, M. Applications of peptide nucleic acids (PNAs) and locked nucleic acids (LNAs) in biosensor development. *Anal. Bioanal. Chem.* **2012,** *402* (10), 3071-3089.

75. Parpart, S. T.; Tison, C. K.; Milam, V. T. Effects of mismatches on DNA as an isothermal assembly and disassembly tool. *Soft Matter* **2010,** *6* (16), 3832-3840.

76. Veedu, R. N.; Wengel, J. Locked nucleic acids: Promising nucleic acid analogs for therapeutic applications. *Chem. Biodiversity* **2010,** *7* (3), 536-542.

77. Lundin, K. E.; Højland, T.; Hansen, B. R.; Persson, R.; Bramsen, J. B.; Kjems, J.; Koch, T.; Wengel, J.; Smith, C. I. E. Biological activity and biotechnological aspects of locked nucleic acids. In *Advances in genetics*, Theodore Friedmann, J. C. D.; Stephen, F. G., Eds. Academic Press: 2013; Vol. Volume 82, pp 47-107.

78. Riahi, R.; Dean, Z.; Wu, T.-H.; Teitell, M. A.; Chiou, P.-Y.; Zhang, D. D.; Wong, P. K. Detection of mRNA in living cells by double-stranded locked nucleic acid probes. *Analyst* **2013,** *138* (17), 4777-4785.

79. Kennedy, B.; Arar, K.; Reja, V.; Henry, R. J. Locked nucleic acids for optimizing displacement probes for quantitative real-time pcr. *Anal. Biochem.* **2006,** *348* (2), 294-299.

80. Christensen, U.; Jacobsen, N.; Rajwanshi, V. K.; Wengel, J.; Koch, T. Stopped-flow kinetics of locked nucleic acid (LNA)-oligonucleotide duplex formation: Studies of LNA-DNA and DNA-DNA interactions. *Biochem. J.* **2001,** *354* (3), 481-484.

81. Christensen, U. Thermodynamic and kinetic characterization of duplex formation between 2′-o, 4′-c-methylene-modified oligoribonucleotides, DNA and RNA. *Biosci. Rep.* **2007,** *27* (6), 327-333.

82. Zhang, Y.; Hammer, D. A.; Graves, D. J. Competitive hybridization kinetics reveals unexpected behavior patterns. *Biophys. J.* **2005,** *89* (5), 2950-2959.

83. Hughesman, C. B.; Turner, R. F. B.; Haynes, C. A. Role of the heat capacity change in understanding and modeling melting thermodynamics of complementary duplexes containing standard and nucleobase-modified LNA. *Biochemistry* **2011,** *50* (23), 5354-5368.

84. Bruylants, G.; Boccongelli, M.; Snoussi, K.; Bartik, K. Comparison of the thermodynamics and base-pair dynamics of a full LNA:DNA duplex and of the isosequential DNA:DNA duplex. *Biochemistry* **2009,** *48* (35), 8473-8482.

85. Owczarzy, R.; You, Y.; Groth, C. L.; Tataurov, A. V. Stability and mismatch discrimination of locked nucleic acid-DNA duplexes. *Biochemistry* **2011,** *50* (43), 9352-9367.

86. You, Y.; Moreira, B. G.; Behlke, M. A.; Owczarzy, R. Design of LNA probes that improve mismatch discrimination. *Nucleic Acids Res.* **2006,** *34* (8), 11.

87. SantaLucia, J.; Allawi, H. T.; Seneviratne, A. Improved nearest-neighbor parameters for predicting DNA duplex stability. *Biochemistry* **1996,** *35* (11), 3555-3562.

88. SantaLucia, J.; Hicks, D. The thermodynamics of DNA structural motifs. *Annu. Rev. Biophys. Biomol. Struct.* **2004,** *33*, 415-440.

89. Eze, N. A.; Milam, V. T. Exploring locked nucleic acids as a bio-inspired materials assembly and disassembly tool. *Soft Matter* **2013,** *9* (8), 2403-2411.

90. Singh, S. K.; Wengel, J. Universality of LNA-mediated high-affinity nucleic acid recognition. *Chem. Commun.* **1998,** (12), 1247-1248.

91. Exiqon. http://www.exiqon.com (accessed 10/4/2013).

92. Akamatsu, K.; Kimura, M.; Shibata, Y.; Nakano, S.; Miyoshi, D.; Nawafune, H.; Sugimoto, N. A DNA duplex with extremely enhanced thermal stability based on controlled immobilization on gold nanoparticles. *Nano Lett.* **2006,** *6* (3), 491-495.

93. Lytton-Jean, A. K. R.; Mirkin, C. A. A thermodynamic investigation into the binding properties of DNA functionalized gold nanoparticle probes and molecular fluorophore probes. *J. Am. Chem. Soc.* **2005,** *127* (37), 12754-12755.

94. Xu, J.; Craig, S. L. Thermodynamics of DNA hybridization on gold nanoparticles. *J. Am. Chem. Soc.* **2005,** *127* (38), 13227-13231.

95. Chen, C. L.; Wang, W. J.; Ge, J.; Zhao, X. S. Kinetics and thermodynamics of DNA hybridization on gold nanoparticles. *Nucleic Acids Res.* **2009,** *37* (11), 3756-3765.

96. McKenzie, F.; Faulds, K.; Graham, D. Sequence-specific DNA detection using high-affinity LNA-functionalized gold nanoparticles. *Small* **2007,** *3* (11), 1866-1868.

97. IDT biophysics. http://biophysics.idtdna.com (accessed 10/6/2013).

98. Obika, S.; Nanbu, D.; Hari, Y.; Andoh, J.; Morio, K.; Doi, T.; Imanishi, T. Stability and structural features of the duplexes containing nucleoside analogues with a fixed n-type conformation, 2 '-o,4 '-c-methyleneribonucleosides. *Tetrahedron Lett* **1998,** *39* (30), 5401-5404.

99. Wengel, J.; Petersen, M.; Frieden, M.; Koch, T. Chemistry of locked nucleic acids (LNA): Design, synthesis, and bio-physical properties. *Lett. Pept. Sci.* **2004,** *10* (3-4), 237-253.

100. Arora, A.; Kaur, H.; Wengel, J.; Maiti, S. Effect of locked nucleic acid (LNA) modification on hybridization kinetics of DNA duplex. *Nucleic Acids Symposium Series* **2008,** *52* (1), 417-418.

101. Mohrle, B. P.; Kumpf, M.; Gauglitz, G. Determination of affinity constants of locked nucleic acid (LNA) and DNA duplex formation using label free sensor technology. *Analyst* **2005,** *130* (12), 1634-1638.

102. Donini, S.; Clerici, M.; Wengel, J.; Vester, B.; Peracchi, A. The advantages of being locked: Assessing the cleavage of short and long RNAs by locked nucleic acid-containing 8-17 deoxyribozymes. *J. Biol. Chem.* **2007**.

103. Ormond, T. K.; Spear, D.; Stoll, J.; Mackey, M. A.; St. John, P. M. Increase in hybridization rates with oligodeoxyribonucleotides containing locked nucleic acids. *J. Biomol. Struct. Dyn.* **2006,** *24* (2), 171-182.

104. Hull, C.; Szewcyk, C.; St John, P. M. Effects of locked nucleic acid substitutions on the stability of oligonucleotide hairpins. *Nucleosides, Nucleotides and Nucleic Acids* **2012,** *31* (1), 28-41.

105. Wetmur, J. G. Hybridization and renaturation kinetics of nucleic acids. *Annu. Rev. Biophys. Bioeng.* **1976,** *5* (1), 337-361.

106. Livshits, M. A.; Mirzabekov, A. D. Theoretical analysis of the kinetics of DNA hybridization with gel-immobilized oligonucleotides. *Biophys. J.* **1996,** *71* (5), 2795-2801.

107. Porschke, D.; Uhlenbec.Oc; Martin, F. H. Thermodynamics and kinetics of helix-coil transition of oligomers containing gc base pairs. *Biopolymers* **1973,** *12* (6), 1313-1335.

108. Parkhurst, K. M.; Parkhurst, L. J. Kinetic studies by fluorescence resonance energy transfer employing a double-labeled oligonucleotide: Hybridization to the oligonucleotide complement and to single-stranded DNA. *Biochemistry* **1995,** *34* (1), 285-292.

109. Gao, Y.; Wolf, L. K.; Georgiadis, R. M. Secondary structure effects on DNA hybridization kinetics: A solution versus surface comparison. *Nucleic Acids Res.* **2006,** *34* (11), 3370-3377.

110. Sekar, M. M. A.; Bloch, W.; St John, P. M. Comparative study of sequence-dependent hybridization kinetics in solution and on microspheres. *Nucleic Acids Res.* **2005,** *33* (1), 366-375.

111. Henry, M. R.; Wilkins Stevens, P.; Sun, J.; Kelso, D. M. Real-time measurements of DNA hybridization on microparticles with fluorescence resonance energy transfer. *Anal. Biochem.* **1999,** *276* (2), 204-214.

112. Diaz, M. R.; Jacobson, J. W.; Goodwin, K. D.; Dunbar, S. A.; Fell, J. W. Molecular detection of harmful algal blooms (HABs) using locked nucleic acids and bead array technology. *Limnol. Oceanogr. Meth.* **2010,** *8*, 269-284.

113. Diercks, S.; Gescher, C.; Metfies, K.; Medlin, L. Evaluation of locked nucleic acids for signal enhancement of oligonucleotide probes for microalgae immobilised on solid surfaces. *J. Appl. Phycol.* **2009,** *21* (6), 657-668.

CHAPTER 2

ASSESSING THE EXTENT OF PRIMARY HYBRIDIZATION AND COMPETITIVE DISPLACEMENT FOR REVERSIBLE COLLOIDAL ASSEMBLY[1]

Introduction

Oligonucleotides are popular recognition-based biomaterials assembly and disassembly tools due to their specificity and ease of control. Their susceptibility to degradation by nucleases and false positive signals under certain conditions, however, has led to great interest in chemically modified oligonucleotides such as locked nucleic acids (LNA) that enhance both nuclease resistance and target specificity. LNA is commonly used due to its chemical similarity to DNA and RNA, and several positive effects have been reported, such as low cytotoxicity effects, good *in vivo* stability, and ease of transfection into cells compared to other modified oligonucleotides.[1-4] These properties stem from the LNA structure, which possesses a methylene linker between the 2′-oxygen and 4′-carbon of the ribose moiety that consequently locks the sugar into a C3′-*endo* conformation. This chemical modification confers nuclease resistance as well as higher affinity and greater specificity for oligonucleotide targets.[5-7]

Thermodynamic analysis of LNA hybridization, however, is empirical and focuses on soluble oligonucleotides such as pure LNA duplexes, pure LNA strands hybridized to perfectly matched DNA or RNA strands, or mixmers (DNA sequences that possess LNA residues) hybridized to perfectly matched DNA targets.[8-12] When mismatches are introduced in these studies, the hybridization partners for mismatch-containing strands are typically pure DNA targets, but not mixmers or pure LNA targets.[9, 13-17] Prior work[13, 18]

[1] Much of the experimental work presented in this chapter is taken from the following publication: [Eze, N. A. and V. T. Milam. Exploring Locked Nucleic Acids as a Bio-inspired Materials Assembly and Disassembly Tool. *Soft Matter* **2013**, *9*, 2403-2411] – Reproduced by permission of The Royal Society of Chemistry.

illustrates the interdependent, complex roles that both mismatch location and base composition play on the resulting hybridization activity in not only pure DNA oligonucleotide solutions but also LNA-based solutions; center mismatches are more destabiliz-destabilizing than by off-center mismatches. The experimental work in this chapter employs short duplexes that are either 1) perfectly matched or 2) possess a single, center mismatch. First, soluble target studies of both primary hybridization activity and competitive displacement activity involving two perfectly matched or mismatched LNA-LNA, LNA-DNA, or DNA-DNA strands are quantified as a function of sequence length and complementarity. Unlike subsequent chapters, wash steps are employed prior to duplex analysis via flow cytometry. Select pairs of promising mixmers (referred to as LNA for simplicity) with modest primary hybridization activity are then explored in colloidal satellite assembly studies with longer, perfectly matched targets then added to drive disassembly events via competitive displacement.

2.1 Materials and Methods

2.1.1 Oligonucleotide Selection and Coupling to Colloidal Particles

Table 2.1.1 lists all DNA sequences (Integrated DNA Technologies; Coralville, IA) and LNA sequences (Exiqon; Woburn, MA). All oligonucleotides were purified by the manufacturer using HPLC. Upon arrival, the sequences were aliquoted in Tris–EDTA (TE) buffer at a 100 μM concentration and stored at -20 °C until used. Oligonucleotides labeled with 6-carboxyfluorescein (FAM) were stored in TE pH 8.0; aminated and unlabeled oligonucleotides were stored in TE pH 7.4. FAM is a single-isomer derivative and spectral mimic of fluorescein that is less susceptible to hydrolysis. FAM-labeled oligonucleotides are received from the manufacturer with a FAM fluorophore covalently attached to the 5′ end of the oligonucleotide sequence via a six-carbon linker with a 3′ phosphate group. Aminated oligonucleotides are received from the manufacturer with a terminal -NH_2 group attached to the 5′ end of the sequence via a six-carbon linker with a

3′ phosphate group. Sequence selection was based on prior work on pure DNA sequences.[19] The nomenclature of the sequences is as follows: complementary strands used as primary hybridization partners are labeled as **A** or **B**, according to their function, followed by either the total number of bases (for probes) or the total number of bases intended for duplex formation (for soluble as well as immobilized targets). The presence of LNA at every third residue is indicated by the lettering $\mathbf{L^3}$ which precedes the **A**/**B** label. For example, the 20 base-long DNA probe is labeled **A20**, whereas a 20 base-long, immobilized LNA target with 9 complementary bases is labeled $\mathbf{L^3B9}$. Mismatched targets include the letter **M** in their nomenclature. For soluble target studies, the soluble primary targets are fluorescently tagged with 6-FAM whereas the soluble secondary targets are unlabeled. Multiple copies of the probe sequence (**A20** or $\mathbf{L^3A20}$) were immobilized on nonfluorescent 1.1 μm diameter microspheres (Bangs Laboratories, Fishers, IN) for soluble target hybridization, assembly, and disassembly experiments. Multiple copies of a 20 base-long derivative of the unlabeled primary target sequence ($\mathbf{L^3B9}$ or $\mathbf{L^3M9}$) were immobilized on red fluorescent 200 nm diameter nanoparticles (Molecular Probes, Eugene, OR) for assembly and disassembly experiments.

Table 2.1.1. List of oligonucleotide sequence function and nomenclature. Values of the difference in Gibbs Free Energy of Hybridization, ΔG_{hyb}, are provided for select DNA probe-target duplexes. Superscript "3" in sequence nomenclature indicates an LNA base at every third residue. Superscript "L" after base indicates LNA modification. Underlined base in target sequences indicates a mismatch. ΔG_{hyb} values for the **A20** probe and DNA targets were calculated from the Zuker Mfold Web Server using a two-state melting function (http://mfold.rna.albany.edu/?q=DINAMelt/Two-state-melting; accessed 10/8/2013).[20] Notably, analogous analytic tools for determining ΔG_{hyb} values for strands possessing LNA residues were unavailable.

Function	**Nomenclature**	**ΔG_{hyb} (kcal/mol)**
immobilized DNA probe	**A20** = 3′-TAGTCGGCGTTAGGTTTTTT-5′	---
immobilized LNA probe	**L^{3}A20** = 3′-TA^{L}GTC^{L}GGC^{L}GTT^{L}AGG^{L}TTTTTT-5′	---
soluble DNA 1° target	**B9F** = 5′-ATCAGCCGC-3′	-12.6
soluble LNA 1° target	**L^{3}B9F =** 5′-AT^{L}CAG^{L}CCG^{L}C-3′	---
soluble mis-matched DNA 1° target	**M9F** = 5′-ATCA<u>C</u>CCGC-3′	-6.3
soluble mis-matched LNA 1° targets	**L^{3}M9F** = 5′-AT^{L}CA<u>C</u>^{L}CCG^{L}C-3′	---
	L^{3}M11F = 5′-AT^{L}CAG^L<u>G</u>CG^{L}CAA^L-3′	---
	L^{3}M13F = 5′-AT^{L}CAG^{L}C<u>G</u>G^{L}CAA^{L}TC-3′	---
	L^{3}M15F = 5′-AT^{L}CAG^{L}CC<u>C</u>^{L}CAA^{L}TCC^{L}A-3′	---
immobilized LNA 1° targets	**L^{3}B9 =** 5′-TTTTTTTTTTTAT^{L}CAG^{L}CCG^{L}C-3′	---
	L^{3}M9 = 5′-TTTTTTTTTTTAT^{L}CA<u>C</u>^{L}CCG^{L}C-3′	---
soluble DNA 2° target	**B15U** = 5′-ATCAGCCGCAATCCA-3′	-20.2
soluble LNA 2° target	**L^{3}B15U** = 5′-AT^{L}CAG^{L}CCG^{L}CAA^{L}TCC^{L}A-3′	---
soluble non-complementary 1° target	**NC14F** = 5′-TAGTCGGCGTTAGG-3′	-4.2
soluble non-complementary 2° target	**NC12U** = 5′-TAGTCGGCGTTA-3′	-4.2

The polystyrene particles used in this study possess carboxyl groups on their surfaces to allow for coupling with aminated oligonucleotide sequences using 1-ethyl-3-[3-dimethylaminopropyl]-carbodiimide hydrochloride (EDAC) at a final concentration of either 71 mM (for flow cytometry experiments) or 7.1 mM (for assembly and disassembly experiments). Coupling of probe and target sequences to polystyrene particles was carried out similarly as described before for microspheres,[19] with 10 µL of microspheres (at 10% w/v loading) added to 90 µL coupling buffer (CB) and centrifuged at 9900×*g* for 3.5 min (after vortexing and sonication) with the supernatant removed from the pelleted beads. The pellet was then resuspended in 100 µL CB and centrifuged at 9900×*g* for 3.5 min. After an additional wash step, the particles were resuspended in 150 µL CB after which 25 µL 1.1 M EDAC (110 mM EDAC for assembly and disassembly studies) is added. After 200 µL of 10 µM aminated probe strands is mixed into the suspension with vortexing, the particles are incubated for 2 h at room temperature, followed by 3 washes in 100 µL of phosphate buffered saline containing 0.2% v/v Tween-20 (PBS/Tween), and a final resuspension to 100 µL in PBS/Tween buffer. To couple aminated target strands to the fluorescent nanoparticles, 50 µL of the particles was added to 50 µL CB and centrifuged at 15,000×*g* for 7 min (after vortexing and sonication) and then resuspended in 100 µL CB. The nanoparticles underwent the same wash steps once, with resuspension in 150 µL CB. Then, 50 µL of 110 mM EDAC in CB is added to the particles followed by 200 µL of 10 µM amine-terminated oligonucleotides with vortexing. After a 2 h incubation with end-over-end mixing, the particles were washed 3× in 100 µL of PBS/Tween buffer and then resuspended in 100 µL of PBS/Tween (for a final 1% w/v suspension).[19]

2.1.2 Flow Cytometry

The primary hybridization activity of immobilized **A20** and **L^{3}A20** probe strands to FAM-labeled primary targets was quantified using flow cytometry. Samples were prepared by incubating FAM-labeled target sequences (100 µL of 5 µM solution) with probe-functionalized, nonfluorescent microspheres (2 µL of 1% w/v suspension) for 24 h

at room temperature in 100 μL PBS/Tween. Samples were then washed by centrifuging (9900×*g* for 3.5 min) and resuspending the pellet three times in 100 μL PBS/Tween. Flow cytometry samples were prepared by diluting 100 μL of the 0.02% w/v suspension in 900 μL of PBS/Tween buffer. These 1 mL suspensions were then run on a Becton Dickinson LSR II flow cytometer (Becton Dickinson, San Jose, CA) in which FACSDiva software (Becton Dickinson) was used for all data acquisition. A calibration curve was obtained prior to each experiment using Quantum FITC-5 MESF standards (Bangs Laboratories), which were diluted in the same buffer as the samples. The standards allow for quantitation of the fluorescence intensity in terms of molecules of equivalent soluble fluorochrome (MESF) and data comparison over time. QuickCal template software (Bangs Laboratories) was used to analyze the calibration curve, determine the instrument fluorescence detection threshold, and the instrument linearity (expressed as the regression coefficient), perform data analysis, and to compare data sets over time and between multiple instruments. In all experiments the regression coefficient was at least 0.995. The molecules of equivalent soluble fluorochrome (MESF) units from standards are used to convert the mean fluorescence value measured for each sample into the average number of fluorescently tagged targets associated with each particle. Each sample series included probe-functionalized microspheres (a) alone (to determine autofluorescence baseline); (b) incubated with noncomplementary targets (to assess nonspecific binding of targets to either the polystyrene particle surface or to immobilized probe strands); or (c) incubated with complementary or nearly complementary targets (to measure average duplex densities).

Competitive hybridization activity of secondary targets was also quantified via flow cytometry. Samples were prepared by first incubating **L^{3}A20**-functionalized microspheres with various FAM-labeled primary targets for 24 h, washing three times, and finally resuspending in 400 μL PBS/Tween. An 80 μL volume of microspheres (0.015% w/v) was then incubated in the absence (only buffer added) or presence of (a) noncomplementary **NC12** targets (1 μM) to assess spontaneous primary target dissociation from probes or (b) complementary unlabeled **B15** DNA or **L^{3}B15** LNA secondary target strands (1 μM) to assess displacement of primary targets. After a 24 h incubation at either

room temperature or 37 °C and subsequent wash steps, the samples were run on the flow cytometer.

2.1.3 Colloidal Assembly, Disassembly and Image Analysis

Aminated, 20 base-long versions of select mixmers identified in the soluble target studies described above are then immobilized onto fluorescent nanoparticles for assembly and disassembly studies. Each satellite assembly is comprised of an individual 1.1 μm diameter microsphere surrounded by a layer of 200 nm diameter red fluorescent nanoparticles. To then drive disassembly, longer, perfectly matched LNA or DNA target strands are added to the suspension to competitively displace the weaker original partner strands (that are bridging particles together) to release the fluorescent nanoparticles from the template microspheres, as illustrated in Figure 2.1.1. During the coupling reaction to immobilize probe and target to their respective particle surfaces, a tenfold dilution of EDAC was used for the assembly and disassembly experiments to minimize nonspecific particle aggregation. For the assembly experiments, separate suspensions of LNA-functionalized nonfluorescent microspheres and fluorescent nanoparticles were resuspended in PBS/Tween at 0.5% w/v particle loading. In a 0.5 mL Eppendorf tube, 5 μL of microspheres and 22.3 μL of nanoparticles were added to 48 μL PBS/Tween, and briefly vortexed and sonicated. The samples were incubated at room temperature for 48 h. The samples were washed in 100 μL PBS/Tween three times with centrifugation at 2000×*g* for 2 min, then three times with centrifugation at 1300×*g* for 2 min, and once with centrifugation at 2000×*g* for 2 min before the pellet was finally resuspended in 100 μL PBS/Tween. Samples were briefly sonicated between each wash step.

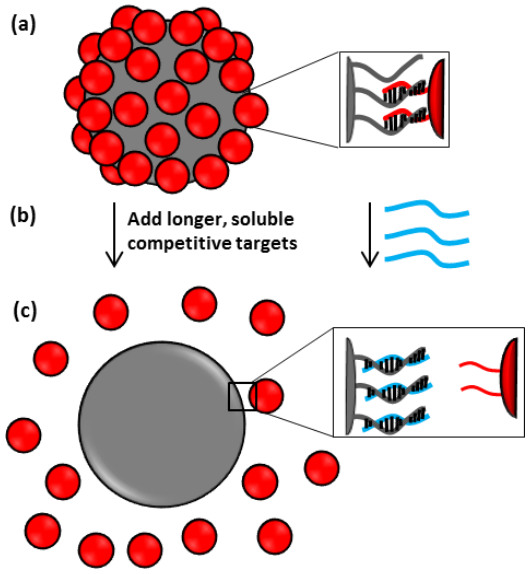

Figure 2.1.1. Schematic illustration of disassembly via competitive hybridization. (a) An LNA-linked colloidal satellite is incubated with (b) secondary target strands that displace the primary hybridization partners and (c) induce the redispersion of particles, leaving a bare non-fluorescent particle. Only a few duplexes are shown for simplicity. Reproduced from Eze and Milam.[21]

For imaging, 10 µL of the suspension was added to 15 µL PBS/Tween then vortexed and briefly sonicated to mix. The 25 µL volume was added to an adhesive glass slide well, sealed with a poly-l-lysine-coated glass cover slip and imaged with a Zeiss LSM 510 confocal microscope (Carl Zeiss AG, Oberkochen, Germany) using a 63× oil objective in DIC and fluorescence modes. Glass cover slips were incubated for 15-20 min in a 10-fold dilution of 0.1% w/v poly-l-lysine solution, rinsed with 70% ethanol, and air dried. For disassembly experiments, 10 µL of the "assembly" suspension and 20 µL of 10 µM unlabeled secondary target DNA were carefully added to 10 µL PBS/Tween with gentle vortexing to mix. The samples were incubated at 37 °C for 24 h. To prepare samples for microscopy, 25 µL of the disassembly suspension was added to a slide well and imaged using confocal microscopy (Zeiss LSM 510 confocal microscope, Carl Zeiss AG) using both fluorescence and DIC modes.

2.2 Results and Discussion

2.2.1 Analysis of Primary Hybridization Activity of Soluble Targets

Figure 2.2.1 is a quantitative comparison of the hybridization activity between immobilized probes and soluble primary targets listed in Table 2.1.1. In order to evaluate the effects of LNA on primary hybridization activity, the same DNA target (**B9**) was incubated with either a DNA (**A20**) or LNA (**L^{3}A20**) microsphere probe system. Negative controls with **NC14** (not shown) confirmed negligible nonspecific interactions. The resulting duplex densities were consistently higher for LNA probes (e.g., 18,600 oligos/μm^2 for **L^{3}A20**:**B9**) than for DNA probes (e.g., 9200 oligos/μm^2 for **A20**:**B9**). This trend is substantiated for primary targets possessing LNA residues in which, for example, the resulting duplex densities increased to 29,760 oligos/μm^2 for **L^{3}A20**:**L^{3}B9**. For both LNA and DNA probes, however, the introduction of a central mismatch in the **M9** and **L^{3}M9** primary targets results in a drastic reduction in duplex densities (16 oligos/μm^2 and 630 oligos/μm^2, respectively with the **L^{3}A20** probe) compared with their perfectly-matched analogs, **B9** and **L^{3}B9**. Three of the mismatched LNA targets (**L^{3}M11**, **L^{3}M13**, and **L^{3}M15**) have very similar duplex densities despite differences in sequence length perhaps due to probe saturation. In contrast, earlier work on DNA analogs of these mismatched targets indicated that analogous differences in sequence length typically correspond to differences in duplex densities.[22]

The overall increase in duplex density upon the introduction of LNA residues in either the probe or the primary target sequence is an indicator of an increase in affinity between primary hybridization partners. Compared to the longer, mismatched targets, the low duplex density observed for the mismatched nine base-long primary targets may signify a sequence-length dependent threshold for mismatch destabilization. Although it has been shown that LNA mismatches are more destabilizing than equivalent DNA mismatches in a DNA:DNA duplex,[13] these destabilizing effects are less clear for du-

plexes in which both partner strands possess LNA and DNA nucleotides. Moreover, the central mismatch is a DNA nucleotide in **L^{3}M11** and **L^{3}M13** and an LNA nucleotide in **L^{3}M9** and **L^{3}M15**. Thermodynamic models can account for numerous combinations of sequence and solution characteristics for soluble DNA strands. Current models for LNA and mixmers, on the other hand, are empirical and typically involve modifying a DNA-based model for a small group of experimentally-tested sequences.[14, 23-24] In the absence of predictive models to assess LNA hybridization (either intrastrand or interstrand) relative affinity differences between the mismatched LNA targets were further assessed using competitive displacement studies.

.

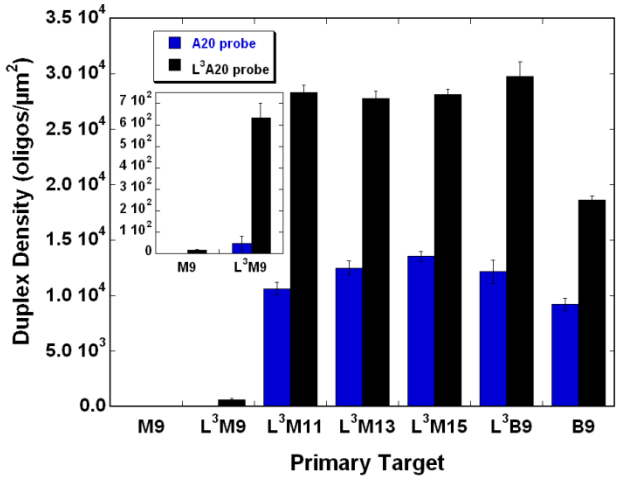

Figure 2.2.1. Surface density of primary duplexes formed between various soluble DNA (**M9** or **B9**) and LNA (**L^{3}M9**, **L^{3}M11**, **L^{3}M13**, **L^{3}M15** or **L^{3}B9**) targets and either **A20** DNA probes or **L^{3}A20** LNA probes immobilized on nonfluorescent microspheres. Inset shows the surface density of primary duplexes formed between the **M9** or **L^{3}M9** targets and **A20** or **L^{3}A20** probes. Reprinted from Eze and Milam.[21]

2.2.2 Analysis of Competitive Displacement Activity at Room Temperature

Figure 2.2.2 shows a quantitative comparison of primary mismatched duplexes remaining hybridized following incubation with various secondary targets for 24 h at room

temperature. With the addition of TE buffer only, LNA–LNA duplexes retain nearly the same duplex densities as shown in Figure 2.2.1.

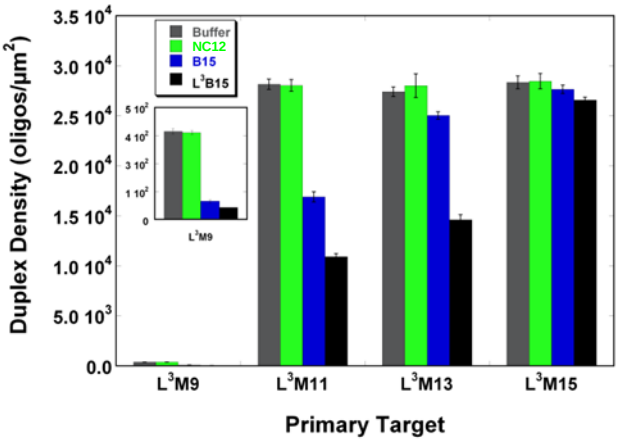

Figure 2.2.2. Surface density of primary LNA–LNA duplexes remaining following 24 h incubation with various secondary DNA (**NC12** or **B15**) or LNA (**L^{3}B15**) target strands at room temperature. Reprinted from Eze and Milam.[21]

Similar densities also occur for **L^{3}M11**-, **L^{3}M13**- and **L^{3}M15**-based duplexes in the presence of the noncomplementary **NC12** secondary target. These control experiments indicate that dissociation of the primary target from the probe is not appreciably induced by addition of either TE buffer or noncomplementary DNA. Following incubation with complementary secondary **B15** or **L^{3}B15** targets, however, the duplex densities drop for all cases involving shorter, mismatched primary duplexes. Since duplex dissociation at room temperature appears negligible, this decrease in the primary duplex density is attributed to competitive displacement of the original hybridization partner by the complementary secondary target. Moreover, as the length of the primary target increases, more primary duplexes remained hybridized in the presence of either **B15** or **L^{3}B15** secondary target. Thus, despite the similar initial primary duplex densities shown in Figure 2.2.1 for **L^{3}M11**, **L^{3}M13**, and **L^{3}M15**, all the mismatched LNA targets in Figure 2.2.2 exhibit a sequence length dependence with respect to their displacement activity by

both **B15** and **L^{3}B15**. One can infer from these trends in displacement activity that increasing the total number of base-pair matches results in stronger primary duplexes that are less likely to allow for partner exchange. Thus, while quantifying primary hybridization activity is one indicator of relative affinity between oligonucleotide partner strands, measurable differences in competitive displacement activity may be a better indicator of relative affinity. While significant displacement activity by **L^{3}B15** is evident for both **L^{3}M11** (reduced from 28,150 to 10,920 oligos/μm^2) and **L^{3}M13** (reduced from 27,400 to 14,610 oligos/μm^2) primary targets, the weaker **L^{3}M9** (reduced from 390 to 50 oligos/μm^2) holds better promise for promoting assembly as well as disassembly of colloidal satellites. To validate this sequence choice, competitive displacement experiments for select, closely related primary targets (**L^{3}M9** and **L^{3}B9**) were carried out next under conditions mimicking disassembly experiments (i.e., 37 °C conditions; diluted probe coupling step).

2.2.3 Analysis of Competitive Displacement Activity at 37 °C

Figure 2.2.3 shows the duplex densities of fluorescently labeled, perfectly matched (**L^{3}B9**) and mismatched (**L^{3}M9**) LNA primary targets remaining hybridized to **L^{3}A20** LNA probes after incubation with various secondary targets at 37 °C. The case involving the addition of buffer only provides the baseline for the primary duplex density at 37 °C and provides a reference for any possible TE buffer-induced dissociation. Separate experiments at room temperature (not shown) indicated that thermal dissociation accounts for a less than 2% reduction in duplex densities for most primary target studies. Both the **L^{3}B9** and **L^{3}M9** targets were exceptions to this trend and exhibited a 22% and 35% reduction in duplex density, respectively. The noncomplementary **NC12** case also provides a baseline for dissociation. The resulting duplex densities for **L^{3}A20**:**L^{3}B9** as well as for **L^{3}A20**:**L^{3}M9** were not appreciably different for these two incubation condi-

tions. In contrast, there is a significant drop in primary duplex density values for both **L^{3}A20**:**L^{3}B9** and **L^{3}A20**:**L^{3}M9** following incubation with either a DNA or LNA complementary secondary target. In the presence of **L^{3}B15**, there is a 94.6% and 96.7% drop in primary duplex density for **L^{3}B9** and **L^{3}M9**, respectively. Since dissociation of the primary target in the presence of **NC12** was shown to be negligible relative to the buffer only control, the drop in duplex density must stem from displacement activity by the secondary target. In comparing duplex densities, **L^{3}B15** displaces the mismatched **L^{3}M9** primary target more extensively than the perfectly-matched **L^{3}B9** target. This result indicates that LNA secondary targets are likely to promote extensive disassembly of colloids bridged together with 9-base-long duplexes, especially mismatched ones. In addition to relative affinity issues considered so far, the ultimate selection of appropriate sequences for subsequent assembly and disassembly of colloidal particles for physiological applications also depends on the nuclease resistance of duplexes which is explored in the next section.

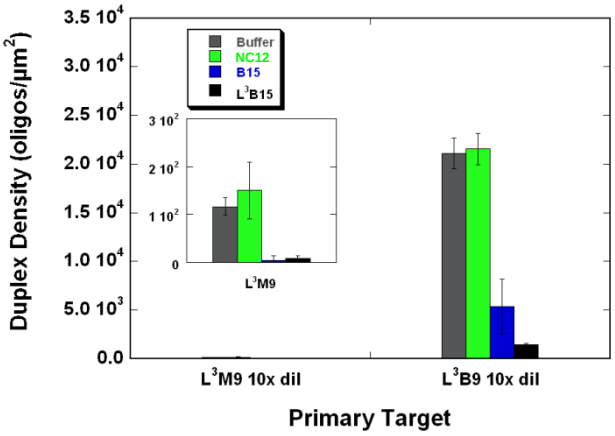

Figure 2.2.3. Surface density of LNA-LNA duplexes remaining after incubation with various secondary DNA (**NC12** or **B15**) or LNA (**L^{3}B15**) target strands at 37 °C. Notably, the coupling agent, EDAC, was diluted 10× to 7.1 mM to mimic the probe coupling conditions used for assembly and disassembly experiments. Reprinted from Eze and Milam.[21]

2.2.4 Analysis of Nuclease Resistance

Figure 2.2.4 shows the duplex stability under various temperature conditions in the absence and presence of DNase I for three primary targets (**B9**, **L^{3}B9**, or **L^{3}M9**) hybridized to immobilized **L^{3}A20** probes. DNase I is an endonuclease that hydrolyzes double-stranded DNA.[2,4] Room temperature and 37 °C controls (without DNase I) are included to determine the extent to which thermal dissociation contributes to any observed decrease in duplex density.

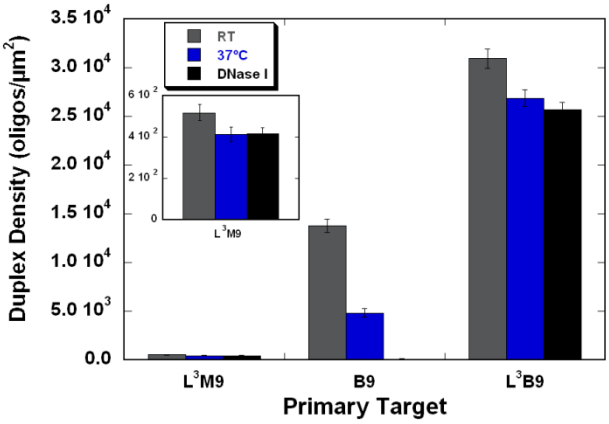

Figure 2.2.4. Primary duplex density remaining between **L^{3}A20** probes and various DNA (**B9**) and LNA (**L^{3}M9** or **L^{3}B9**) targets, following incubation for 24 h at room temperature, 37 °C, and 37 °C with DNase I (1 U/mL). Reprinted from Eze and Milam.[21]

The 13.1% and 20.1% decreases in duplex densities for **L^{3}A20**:**L^{3}B9** and **L^{3}A20**:**L^{3}M9**, respectively, after incubation at elevated temperature indicate that most of these primary duplexes remain hybridized at 37 °C. Only 35.1% of primary duplexes, however, remain hybridized for **L^{3}A20**:**B9** at 37 ºC. Following incubation with DNase I (digest) at 37 °C, the duplex density for **L^{3}A20**:**B9** decreases by 98.5% relative to the 37 °C control. The duplex densities for both LNA targets, **L^{3}B9** and **L^{3}M9**, on the other hand, remain relatively unchanged following incubation with DNase I with only a 4.4% and 0.2% decrease in duplex density, respectively. Thus, both **L^{3}A20**:**L^{3}B9** and

L^{3}A20:**L^{3}M9** exhibit nuclease resistance after 24 h, whereas **L^{3}A20**:**B9** is nearly completely degraded indicating that LNA–DNA duplexes are more susceptible to both nuclease hydrolysis and thermal dissociation than LNA–LNA duplexes. The more promising, nuclease-resistant LNA-LNA sequences (**L^{3}A20**:**L^{3}B9** and **L^{3}A20**:**L^{3}M9**) were next explored in assembly and disassembly studies.

2.2.5 Colloidal Assembly via Primary Hybridization

Figure 2.2.5 shows confocal micrographs of colloidal satellite assembly studies involving mixtures of nonfluorescent microspheres functionalized with **L^{3}A20** probe strands and fluorescent 200 nm particles functionalized with (a) **L^{3}A20**, (b) **L^{3}M9**, or (c) **L^{3}B9** target strands in both fluorescence only mode to better visualize the assemblies (top) and in DIC mode with fluorescence overlay to verify colocalization of fluorescent nanoparticles with Analogous 3D compilations are provided in Supporting Information (Figure S1). Unlike the shorter, soluble targets in the flow cytometry studies, 20 base-long primary target strands are now immobilized on a second population of smaller particles, and assembly formation is monitored via confocal microscopy.

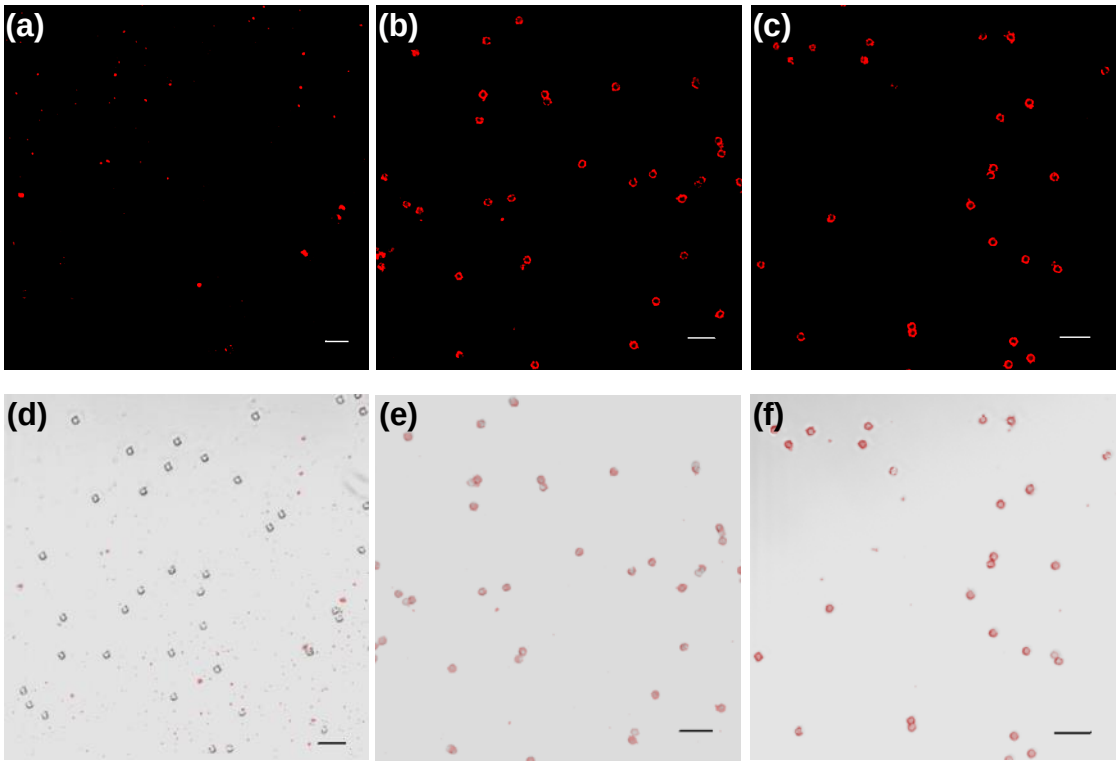

Figure 2.2.5. Confocal micrographs of colloidal satellite assemblies formed between nonfluorescent microspheres functionalized with **L^{3}A20** probe strands and fluorescent 200 nm particles functionalized with (a,d) **L^{3}A20**, (b,e) **L^{3}M9**, or (c,f) **L^{3}B9** target strands. Each micrograph consists of (a-c) a single focal plane taken in fluorescence-only mode or (d-f) a 1D rendering of a 3D z-stack compilation taken in DIC mode with fluorescence overlay. Scale bar is 5 μm. Reprinted from Eze and Milam.[21]

To first assess the possible role of nonspecific interactions in driving particle adhesion events, a negative control in which both particle populations are functionalized with **L^{3}A20** was explored. The fluorescence micrograph from this negative control in Figure 2.2.5(a) shows that essentially no assembly occurs between small fluorescent nanoparticles and the larger microspheres. The micrograph directly below in Figure 2.2.5(d) further indicates that little, if any, homogeneous aggregation occurs between either nonfluorescent microspheres or fluorescent nanoparticles. The lack of assembly or aggregation for this case demonstrates that nonspecific, attractive interactions between LNA-functionalized colloidal particles are not significant. For the complementary particle cases shown in Figure 2.2.5(b)–(c), however, extensive satellite assembly for-

mation is evident for both perfectly-matched (**L^{3}B9**) and mismatched (**L^{3}M9**) cases. While nanoparticle coverage is more difficult to assess in these micrographs involving a single confocal slice through the assemblies, the renderings of three-dimensional compilations of the confocal slices suggest that nanoparticle coverage may be more extensive for the perfectly matched LNA bridges as shown in Figure 2.2.5(e)–(f). This difference in the extent of nanoparticle coverage on colloidal satellites is consistent with the flow cytometry data trends in Figure 2.2.1 in which the primary hybridization activity at room temperature for the **L^{3}B9** target exceeds that of the **L^{3}M9** target. Despite the exceedingly low duplex density for **L^{3}A20**:**L^{3}M9**, however, robust assemblies that can withstand wash steps (to remove excess, nonadherent nanoparticles) are observed here as well as in our prior work.[25] In all complementary cases, the suspensions contained well-dispersed satellite assemblies with few, if any, dimers or trimers.

2.2.6 Disassembly via Competitive Displacement Events

Figure 2.2.6 and Figure 2.2.7 show confocal micrographs of **L^{3}B9**- and **L^{3}M9**-linked assemblies, respectively, formed at room temperature and then incubated with a noncomplementary secondary target (**NC12**) or with a complementary secondary target (**B15** or **L^{3}B15**) at 37 °C. Analogous 3D compilations are provided in each figure.

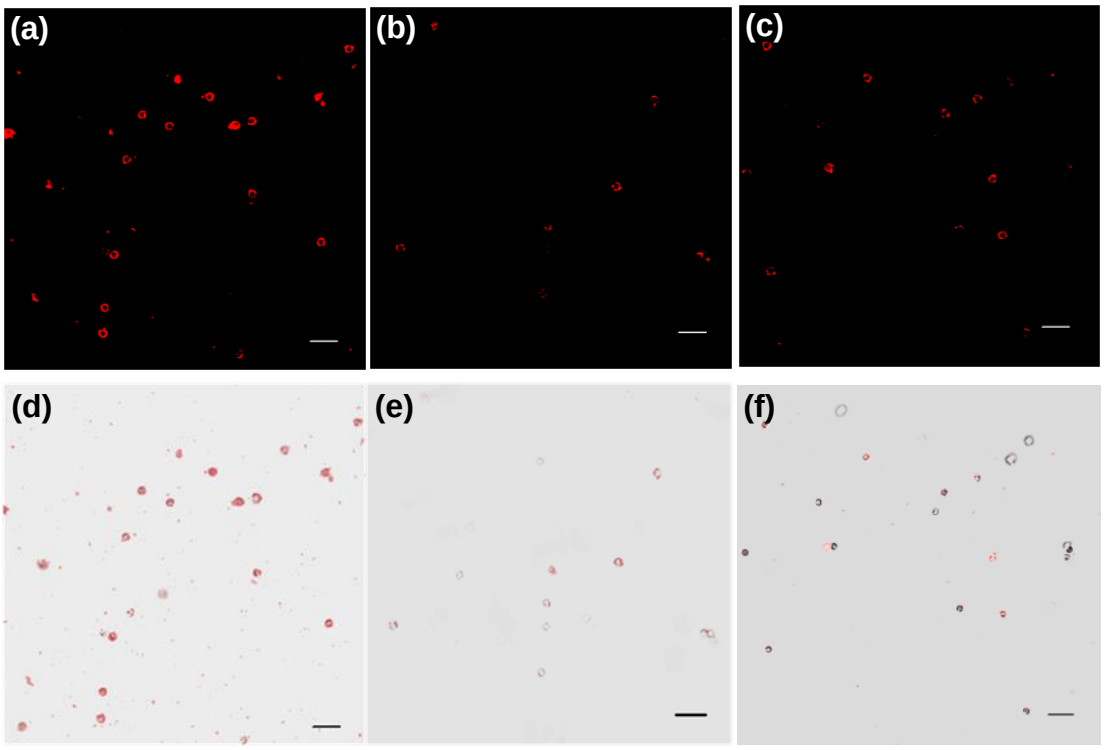

Figure 2.2.6. Suspensions of LNA-linked (**L^{3}A20:L^{3}B9**) colloidal satellite assemblies following a 24 h incubation at 37 °C with (a,d) **NC12**, (b,e) **B15**, or (c,f) **L^{3}B15** secondary targets. Each micrograph consists of (a-c) a single focal plane taken in fluorescence-only mode or (d-f) a 1D rendering of a 3D z-stack compilation taken in DIC mode with fluorescence overlay. Scale bars are 5 μm. Reprinted from Eze and Milam.[21]

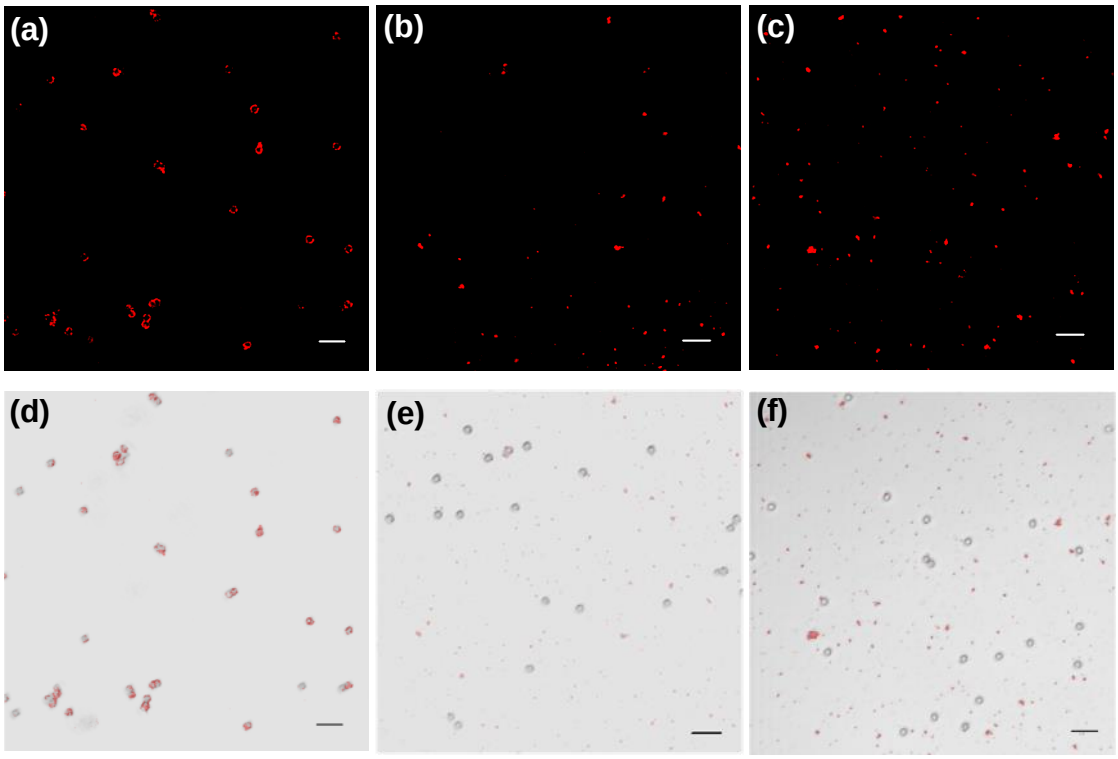

Figure 2.2.7. Suspensions of LNA-linked (**L^{3}A20:L^{3}M9**) colloidal satellites following a 24 h incubation at 37 °C with (a) **NC12**, (b) **B15**, or (c) **L^{3}B15** secondary targets. Each micrograph consists of (a-c) a single focal plane taken in fluorescence-only mode or (d-f) a 1D rendering of a 3D z-stack compilation taken in DIC mode with fluorescence overlay. Scale bars are 5 µm. Reprinted from Eze and Milam.[21]

Similar to flow cytometry studies to evaluate competitive displacement activity, the buffer control (not shown) evaluates the thermostability of the assemblies at 37 °C. Although significant thermal dissociation (~35% and 22% for **L^{3}B9** and **L^{3}M9**, respectively for diluted probe coupling conditions) at 37 °C was noted in flow cytometry studies discussed earlier, the lack of disassembly in the presence of **NC12** secondary target indicates that thermal dissociation alone does not induce nanoparticle release, as shown in Figure 2.2.6(a) and Figure 2.2.7(a). The **L^{3}B9**-linked assemblies remain fairly intact following incubation with either **L^{3}B15** or **B15** secondary targets as shown in Figure 2.2.6(b)–(c). Thus, despite the extensive competitive displacement activity shown in Figure 2.2.3 (e.g., ~5×10^3 duplexes per µm^2 remaining following incubation with **B15**

secondary targets) a sufficient number of duplex bridges must reside between satellite and template particles following incubation with secondary targets. Extensive disassembly, however, occurs after incubation of **L^{3}M9**-linked assemblies with the complementary DNA or LNA secondary targets, likely leaving unattached nanoparticles and relatively bare, nonfluorescent probe-functionalized microspheres as evident in Figure 2.2.7(e)–(f). This extensive disassembly behavior for the mismatched duplex case follows the nearly complete competitive displacement activity shown in Figure 2.2.3 from flow cytometry studies with soluble primary targets. Collectively, these results indicate that LNA-mediated colloidal assembly is achieved, but extensive disassembly via competitive displacement events is favored only by employing the weakest LNA partner strands as duplex bridges.

2.3 Conclusions

LNA is employed in the current study as a bio-inspired materials assembly tool. By optimizing the sequence length, duplex concentration and LNA content in the probe and target strands, the affinity between hybridization partners was successfully tuned allowing for colloidal disassembly. The sequence length-dependent displacement of mismatched primary targets exhibiting similar initial primary duplex densities indicates that the surface density of primary duplexes alone may not be a sufficient comparative indicator of duplex affinity. Using flow cytometry and confocal microscopy as analytical tools, these studies establish strategies for nuclease-resistant, LNA-mediated assembly and disassembly of colloidal particles for physiologically relevant applications.

We find that incorporation of LNA residues (~33%) into either one or both primary hybridization partner strands typically results in a higher duplex density than for isosequential DNA strands. Mismatched primary hybridization partners with sequence length of 11-15 bases have similar initial primary duplex densities. The extent of displacement of mismatched strands by 15 base-long, perfectly matched competitive target

strands, however, does depend on the base length of the original mismatched partner strand. Confocal microscopy confirms that substantial colloidal assembly occurs for both perfectly-matched and mismatched LNA sequences that are 9 bases in length. Extensive disassembly, however, was only observed for the mismatched case through the introduction of 15 base-long competitive DNA or LNA target strands. The results demonstrate that LNA can be used to programmatically assemble and disassemble colloidal particles.

2.4 References

1. Koshkin, A. A.; Nielsen, P.; Meldgaard, M.; Rajwanshi, V. K.; Singh, S. K.; Wengel, J. LNA (locked nucleic acid): An RNA mimic forming exceedingly stable LNA:LNA duplexes. *J. Am. Chem. Soc.* **1998,** *120* (50), 13252-13253.

2. Kaur, H.; Babu, B. R.; Maiti, S. Perspectives on chemistry and therapeutic applications of locked nucleic acid (LNA). *Chem. Rev.* **2007,** *107* (11), 4672-4697.

3. Jepsen, J. S.; Pfundheller, H. M.; Lykkesfeldt, A. E. Downregulation of p21((WAF1/CIP1)) and estrogen receptor alpha in MCF-7 cells by antisense oligonucleotides containing locked nucleic acid (LNA). *Oligonucleotides* **2004,** *14* (2), 147-156.

4. Grunweller, A.; Wyszko, E.; Bieber, B.; Jahnel, R.; Erdmann, V. A.; Kurreck, J. Comparison of different antisense strategies in mammalian cells using locked nucleic acids, 2 '-o-methyl RNA, phosphorothioates and small interfering RNA. *Nucleic Acids Res.* **2003,** *31* (12), 3185-3193.

5. Singh, S. K.; Nielsen, P.; Koshkin, A. A.; Wengel, J. LNA (locked nucleic acids): Synthesis and high-affinity nucleic acid recognition. *Chem. Commun.* **1998,** (4), 455-456.

6. Singh, S. K.; Wengel, J. Universality of LNA-mediated high-affinity nucleic acid recognition. *Chem. Commun.* **1998,** (12), 1247-1248.

7. Wengel, J.; Petersen, M.; Nielsen, K. E.; Jensen, G. A.; Håkansson, A. E.; Kumar, R.; Sørensen, M. D.; Rajwanshi, V. K.; Bryld, T.; Jacobsen, J. P. LNA (locked nucleic acid) and the diastereoisomeric α-l-LNA: Conformational tuning and high-affinity recognition of DNA/RNA targets. *Nucleosides, Nucleotides Nucleic Acids* **2001,** *20* (4-7), 389-396.

8. Wengel, J.; Petersen, M.; Nielsen, K. E.; Jensen, G. A.; Hakansson, A. E.; Kumar, R.; Sorensen, M. D.; Rajwanshi, V. K.; Bryld, T.; Jacobsen, J. P. LNA (locked nucleic

acid) and the diastereoisomeric alpha-l-LNA: Conformational tuning and high-affinity recognition of DNA/RNA targets. *Nucleos. Nucleot. Nucl.* **2001,** *20* (4-7), 389-396.

9. Singh, S. K.; Nielsen, P.; Koshkin, A. A.; Wengel, J. LNA (locked nucleic acids): Synthesis and high-affinity nucleic acid recognition. *Chem. Commun.* **1998,** (4), 455-456.

10. Nielsen, K. E.; Rasmussen, J.; Kumar, R.; Wengel, J.; Jacobsen, J. P.; Petersen, M. NMR studies of fully modified locked nucleic acid (LNA) hybrids: Solution structure of an LNA : RNA hybrid and characterization of an LNA : DNA hybrid. *Bioconjugate Chem.* **2004,** *15* (3), 449-457.

11. Bruylants, G.; Boccongelli, M.; Snoussi, K.; Bartik, K. Comparison of the thermodynamics and base-pair dynamics of a full LNA:DNA duplex and of the isosequential DNA:DNA duplex. *Biochemistry* **2009,** *48* (35), 8473-8482.

12. Tolstrup, N.; Nielsen, P. S.; Kolberg, J. G.; Frankel, A. M.; Vissing, H.; Kauppinen, S. Oligodesign: Optimal design of LNA (locked nucleic acid) oligonucleotide capture probes for gene expression profiling. *Nucleic Acids Res.* **2003,** *31* (13), 3758-3762.

13. You, Y.; Moreira, B. G.; Behlke, M. A.; Owczarzy, R. Design of LNA probes that improve mismatch discrimination. *Nucleic Acids Res.* **2006,** *34* (8), e60.

14. Owczarzy, R.; You, Y.; Groth, C. L.; Tataurov, A. V. Stability and mismatch discrimination of locked nucleic acid-DNA duplexes. *Biochemistry* **2011,** *50* (43), 9352-9367.

15. Frieden, M.; Christensen, S. M.; Mikkelsen, N. D.; Rosenbohm, C.; Thrue, C. A.; Westergaard, M.; Hansen, H. F.; Orum, H.; Koch, T. Expanding the design horizon of antisense oligonucleotides with alpha-l-LNA. *Nucleic Acids Res.* **2003,** *31* (21), 6365-6372.

16. Natsume, T.; Ishikawa, Y.; Dedachi, K.; Tsukamoto, T.; Kurita, N. Effect of base mismatch on the electronic properties of DNA-DNA and LNA-DNA double strands: Density-functional theoretical calculations. *Chem. Phys. Lett.* **2007,** *446* (1-3), 151-158.

17. Nielsen, K. E.; Singh, S. K.; Wengel, J.; Jacobsen, J. P. Solution structure of an LNA hybridized to DNA: NMR study of the

d(CT(L)GCT(L)T(L)CT(L)GC):d(GCAGAAGCAG) duplex containing four locked nucleotides. *Bioconjugate Chem.* **2000,** *11* (2), 228-238.

18. SantaLucia, J.; Hicks, D. The thermodynamics of DNA structural motifs. *Annu. Rev. Biophys. Biomol. Struct.* **2004,** *33*, 415-440.

19. Tison, C. K.; Milam, V. T. Reversing DNA-mediated adhesion at a fixed temperature. *Langmuir* **2007,** *23* (19), 9728-9736.

20. Zuker, M. a. M., Nicholas R. The dinamelt web server. http://mfold.rna.albany.edu/?q=DINAMelt/Two-state-melting (accessed 10/8/2013).

21. Eze, N. A.; Milam, V. T. Exploring locked nucleic acids as a bio-inspired materials assembly and disassembly tool. *Soft Matter* **2013,** *9* (8), 2403-2411.

22. Parpart, S. T.; Tison, C. K.; Milam, V. T. Effects of mismatches on DNA as an isothermal assembly and disassembly tool. *Soft Matter* **2010,** *6* (16), 3832-3840.

23. SantaLucia, J.; Allawi, H. T.; Seneviratne, A. Improved nearest-neighbor parameters for predicting DNA duplex stability. *Biochemistry* **1996,** *35* (11), 3555-3562.

24. McTigue, P. M.; Peterson, R. J.; Kahn, J. D. Sequence-dependent thermodynamic parameters; for locked nucleic acid (LNA)-DNA duplex formation. *Biochemistry* **2004,** *43* (18), 5388-5405.

25. Baker, B. A.; Milam, V. T. DNA density-dependent assembly behavior of colloidal micelles. *Langmuir* **2010,** *26* (12), 9818-9826.

CHAPTER 3

QUANTIFYING *IN SITU* KINETICS OF PRIMARY HYBRIDIZATION BETWEEN IMMOBILIZED PROBES AND SOLUBLE TARGETS

Introduction

While the hybridization activity of natural oligonucleotide solutions has been studied for decades, less is known about the hybridization activity of these newer synthetic oligonucleotides. Existing reports on LNA hybridization have largely focused on thermodynamic studies of oligonucleotide solutions in which no strands are conjugated to a material surface,[1-5] or on biotechnological applications of LNA hybridization[6-9] such as microarrays or gene targeting, in which LNA strands may or may not be immobilized to a surface. It has been demonstrated that solution-based studies (e.g., salt concentration) of DNA or LNA do not necessarily allow for accurate predictions of hybridization kinetics for immobilized strands.[10-13]

Expanding on previous work[14] that studied *in situ* DNA hybridization kinetics on microspheres and to obtain a more detailed understanding of early LNA hybridization events, in the absence of wash steps, flow cytometry is used to monitor *in situ* hybridization between single-stranded DNA or LNA probes immobilized on microspheres and a family of single-stranded soluble DNA and LNA targets. The hybridization activity of single-stranded DNA and locked nucleic acid (LNA) sequences on microspheres was quantified *in situ* using flow cytometry as a high throughput analytical technique. In contrast to conventional sample preparation techniques for flow cytometry that involve several wash steps, the oligonucleotide-functionalized microsphere suspensions are directly sampled during primary hybridization events. The kinetics studies presented in

this dissertation are an important first step for this expanding LNA-functionalized microsphere system into a multi-functional biomaterials system with biomedical applications.

3.1 Materials and Methods

3.1.1 Oligonucleotide Selection and Particle Preparation

All DNA sequences (IDT Technologies, Coralville, IA) and LNA sequences (Exiqon, Woburn, MA) were purchased from the manufacturer and purified by HPLC prior to arrival. The sequences in Table 3.1.1 are based on previous work.[15] Briefly, upon arrival, the lyophilized sequences are suspended at a 100 μM concentration in Tris-EDTA (TE) buffer either at pH 8.0, for sequences that are fluorescently labeled with 6-carboxyfluorescein (FAM), or at pH 7.4 for sequences that are aminated. All sequences are aliquoted and then stored at -20 °C until use.

The nomenclature of the sequences is as follows: complementary strands used for primary hybridization are labeled either **A** or **B** according to their function as either a probe or target, respectively. This letter is followed by either the total number of bases in the immobilized probe strands and soluble, labeled targets. For the targets, this number is also equivalent to the number of bases intended to participate in hybridization events, whereas several nonhybridizing bases (up to 11 bases, depending on target base length) are included in the 20 base-long immobilized probe. Incorporation of LNA at every third base is designated by the term $\mathbf{L^3}$ which precedes the **A**/**B** label. For example, the 20 base-long LNA probe is labeled $\mathbf{L^3A20}$, whereas a 9 base-long, perfectly matched DNA target is labeled **B9**. Mismatched targets include the letter **M** in their nomenclature instead of the letter **B**. All primary targets are fluorescently tagged with FAM at their 5′ end. Multiple copies of the probe sequence (**A20** or $\mathbf{L^3A20}$) are immobilized on carboxylated polystyrene microspheres (Bangs Laboratories, Fishers, IN) for *in situ* primary hybridization experiments using 1-ethyl-3[3-dimethylaminopropyl]-carbodiimide hydro-

chloride (EDAC) at a 7.1 mM concentration as a coupling agent, as described in earlier work.[16,14].

Table 3.1.1 List of the function and nomenclature of various DNA and LNA sequences. Values of Gibbs free energy of hybridization at 37 °C, ΔG_{hyb}, are provided for duplexes comprised of DNA probes and DNA targets. Sequence names that contain an "L^3" prefix have been designed with an LNA base substituted at every third residue, which are marked by a superscript "L" to the right of the base. An underlined base indicates the location of a single, center mismatch. The ΔG_{hyb} values for **A20** probe and DNA target duplexes were determined using the IDT OligoAnalyzer Hetero-Dimer function (https://www.idtdna.com/analyzer/Applications/OligoAnalyzer/; accessed 08/08/2012).[17] Notably, analogous analytic tools for determining ΔG_{hyb} values for hybridization between strands possessing LNA residues were not available.

Function	**Sequence**		**ΔG_{hyb} (kcal/mol)**
immobilized DNA probe	**A20** =	3'–TAGTCGGCGTTAGGTTTTTT–5'	
immobilized LNA probe	**L^3A20** =	3'–TA^{L}GTC^{L}GGC^{L}GTT^{L}AGG^{L}TTTTTT	
soluble DNA 1° targets	**B9** =	5'–ATCAGCCGC–3'	-19.6
	B15 =	5'–ATCAGCCGCAATCCA–3'	-31.5
soluble LNA 1° targets	**L^3B9 =**	5'–AT^{L}CAG^{L}CCG^{L}C–3'	
	L^3M9=	5'–AT^{L}CA<u>C</u>^{L}CCG^{L}C–3'	
	L^3B15 =	5'–AT^{L}CAG^{L}CCG^{L}CAA^{L}TCC^{L}A–3'	
noncomplementary target	**NC14** =	5'–TAGTCGGCGTTAGG–3'	-3.6

3.1.2 *In Situ* Primary Hybridization Measurements on Microspheres

In situ primary hybridization experiments were performed similarly as described in a previous DNA study.[14] Briefly, a 2.5 µL volume of **A20**- or **L^3A20**-functionalized microspheres (at 1% w/v loading in PBS/Tween) is added to a 1 mL volume of a 1 µM primary target solution (**B9**, **B15**, **L^3M9**, **L^3B9**, or **L^3B15**) in PBS/Tween, quickly vortexed, and then introduced to the flow cytometer. PBS/Tween is a 0.2% v/v solution of Tween-20 in phosphate buffered saline. After a reliable signal is obtained (~30 s after

vortexing), two separate measurements (each containing 10,000 events) are taken within the first minute followed by measurements every minute for the next 29 minutes. Each timed measurement is completed in less than 10 s. Following the 30 min experimental time frame, for the *in situ* studies, the remaining suspension volume (*i.e.*, not run through the flow cytometer) is prepared for post-wash analysis by first pelleting the suspensions and quickly removing the supernatant. The suspensions are washed three times in 100 µL PBS/Tween and then resuspended in 100 µL of the same buffer. The "washed" microsphere suspensions are then evaluated via flow cytometry to quantify any loss of associated fluorescently-labeled primary target. For the experiments performed at the 24 h time point, the samples are prepared as follows: a 4 µL volume of either **A20**- or **L^{3}A20**-functionalized microspheres (at 1% w/v loading) is resuspended into 200 µL PBS/Tween and then mixed by vortexing with 200 µL of a 10 µM primary target solution in TE buffer pH 8.0 (with a final primary target concentration of 5 µM). After incubating for 24 h on a rotamixer, 200 µL of the suspension is used for pre-wash analysis and the remaining 200 µL is washed three times in 100 µL of PBS/Tween for post-wash analysis using flow cytometry.

3.1.3 Flow Cytometry

A Becton Dickinson LSRII flow cytometer (Becton Dickinson, San Jose, CA) was used to quantify FAM-labeled duplexes on populations of microspheres for all 30 min *in situ*, 30 min post-wash, and 24 h pre-wash and post-wash analysis. For both the 30 min *in situ* post-wash and the 24 h pre- and post-wash experiments, the final resuspension volumes are diluted to 1 mL in PBS/Tween or in PBS/Tween with additional NaCl for the high salt hybridization studies. Data acquisition to obtain the average fluorescence associated with the microsphere population of interest was carried out using FACSDiva software (Becton Dickinson). The molecules of equivalent soluble fluorochrome (MESF) units obtained from Quantum FITC-5 standards (Bangs Laboratories) are used along with

Quickcal template software (Bangs Laboratories) to convert the mean fluorescence value measured for each sample into the average number of fluorescently labeled targets associated with each microsphere to then calculate the average surface density of associated target, σ, for the 1.1 μm microspheres. In addition to the MESF standards, probe-functionalized microspheres were (a) run alone (to assess the autofluorescence baseline), (b) incubated with noncomplementary **NC14** targets (to determine the extent of nonspecific target binding to the polystyrene microsphere surface or to the probe strands), or (c) incubated with complementary targets (to record the accumulation of hybridized targets on microspheres over time).

3.1.4 Analysis of Time-Dependent Primary Hybridization Activity on Microspheres

In addition to reporting the surface density of associated target, σ, over time, the rate constant for primary hybridization between immobilized, single-stranded probes and soluble, single-stranded targets, k_1, was determined through two-parameter curve fits of σ as a function of time, t, as shown in Equation 3.1 below.

$$\sigma = \sigma_\infty(1 - \exp(-k_1 t)) \tag{3.1}$$

where σ_∞ corresponds to the σ value at the 30 min time point.

3.2 Results & Discussion

3.2.1 Flow Cytometry Histograms Generated during *in situ* Measurements

The *in situ* primary hybridization activity between either immobilized DNA or immobilized LNA probes and various soluble targets was investigated using flow cytometry immediately after introducing suspensions of **A20**- and **L^{3}A20**-functionalized microspheres to DNA (**NC14, B9,** or **B15**) and LNA (**L^{3}M9, L^{3}B9,** or **L^{3}B15**) targets. Wash steps prior to flow cytometry measurements are commonly used to remove unhybridized target or target weakly bound to probe-functionalized microspheres through nonspecific

attractive interactions.[16, 18-25] In the absence of wash steps, however, these *in situ* measurements allow for direct quantification of hybridization events as they occur between the probe-functionalized microspheres and fluorescently labeled targets while also avoiding potential wash-induced target dissociation, especially of weak hybridization partners. A noticeable shift to higher fluorescence intensity values is observed at the two earliest time points (30 s and 40 s) in the representative flow cytometry histograms shown in Figure 3.2.1 for **L^{3}A20**-functionalized microspheres incubated with either (a) **B9** or (b) **L^{3}B15** targets. Rightward shifts in fluorescence intensity continue at longer times, but the shifts are far less dramatic, thus indicating that target association is rapid and quickly reaches a plateau. Converting these relative fluorescence intensity values into surface densities of associated target, σ, then allows one to compare the hybridization kinetics for several probe-target combinations.

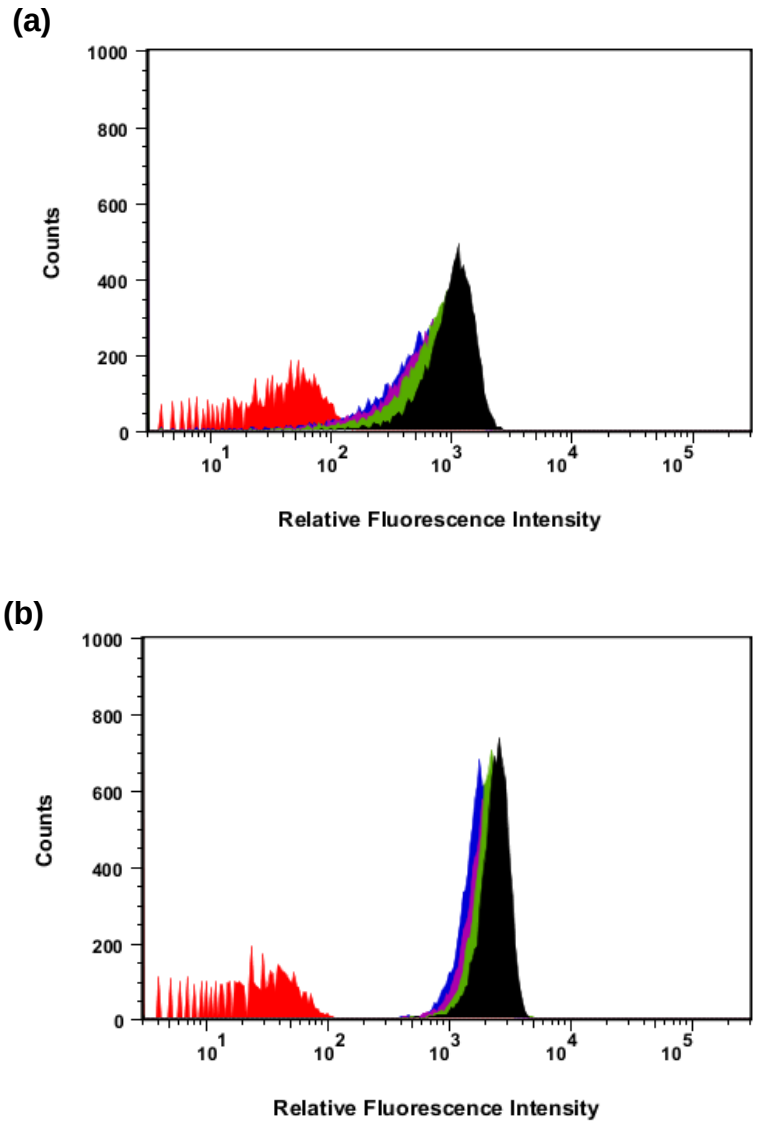

Figure 3.2.1 Flow cytometry histograms of particle counts as a function of the relative fluorescence intensity associated with a population of $\mathbf{L^3A20}$-functionalized microspheres incubated with a solution of (a) **B9** DNA targets or (b) $\mathbf{L^3B15}$ LNA targets for the following amounts of time: 0 s (red), ~30 s (blue), ~40 s (purple), ~1 min (green), or ~2 min (black).

3.2.2 Assessing *in situ* Primary Hybridization Kinetics

As shown in Figure 3.2.2, for DNA-functionalized microspheres, time-dependent association of all complementary or nearly complementary targets increases rapidly and reaches a plateau value within the first 2 min of target incubation. This trend indicates

that an apparent equilibrium is reached within the experimental timeframe explored here, regardless of the base length or LNA content of the targets employed. Importantly, the lack of noncomplementary target (**NC14**) association with **A20**-functionalized microspheres indicates that nonspecific association of primary targets either to the immobilized DNA probes or to the microsphere surface is low (100 oligos/μm^2, or 2.5% of the weakest hybridization pair **A20:L^{3}M9**). In contrast, the 15 base-long LNA target, **L^{3}B15**, exhibits the highest target density on the **A20**-functionalized microspheres indicating that this LNA target has the highest relative affinity for immobilized DNA probes. Given the nearly negligible association of noncomplementary DNA to these microspheres (even in the absence of conventional wash steps), these target density values appear to directly correspond to the density of primary duplexes formed on the surface of the microspheres.

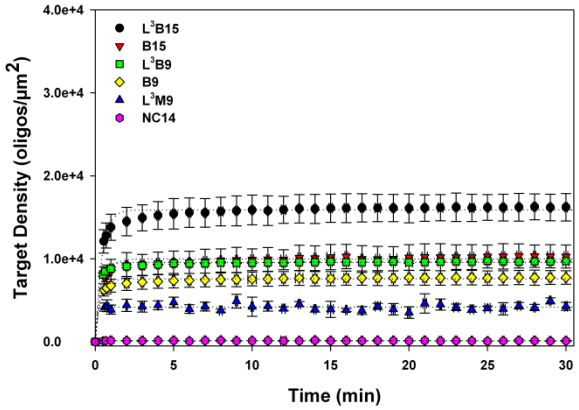

Figure 3.2.2. *In situ* measurements of hybridization activity between **A20**-functionalized microspheres and soluble, fluorescently labeled DNA targets [**NC14** (pink diamonds); **B9** (yellow diamonds); or **B15** (red inverted triangles)] or LNA targets [**L^{3}M9** (blue triangles); **L^{3}B9** (green squares); or **L^{3}B15** (black circles)]. Dotted lines represent curve fits to Equation 3.1. Error bars indicating standard deviation for duplex density and time values for the average of three suspension samples are shown.

Comparisons within subgroups of related, perfectly matched LNA or DNA primary targets reveal that longer sequences consistently result in higher primary duplex densities.

For example, **A20:L^{3}B15** exhibits a higher duplex density than **A20:L^{3}B9** (16,200 vs. 9700 oligos/μm^2), while **A20:B15** has a higher duplex density than **A20:B9** (10,200 vs. 7700 oligos/μm^2). Comparisons between subgroups of LNA and DNA targets, however, do not have clear target length or content behavior. For example, **A20:B15** and **A20:L^{3}B9** have similar duplex densities despite an additional six DNA bases in the **B15** target. Though the overall target length is shorter in **L^{3}B9**, incorporation of LNA residues at every third base appears to increase the hybridization affinity of this LNA target for its DNA probe, resulting in comparable duplex densities to **B15**. The greater difference in duplex density values between longer duplexes of **A20:L^{3}B15** and **A20:B15** than between shorter duplexes of **A20:L^{3}B9** and **A20:B9**, however, indicates that sequence length and/or LNA content effects on the resulting hybridization activity are apparently additive.

To examine the effects of a base mismatch on the kinetics and extent of hybridization activity, an intentional mismatch is introduced to the center of the LNA target. Not surprisingly, of all of the DNA and LNA targets examined, the mismatched **A20:L^{3}M9** pair has the lowest duplex density (4300 oligos/μm^2) which is approximately two-fold lower than that of the perfectly matched **A20:L^{3}B9** pair (9700 oligos/μm^2). The reduced duplex density is likely due to the combined effect of incorporating a center mismatch on an LNA residue. Notably, the DNA analog of **L^{3}M9** was not explored in the current study due to its exceedingly low hybridization activity in prior work.[15]

The extent of hybridization for various primary targets with LNA-functionalized microspheres in Figure 3.2.3 follows many of the same trends as with the DNA-functionalized microspheres shown in Figure 3.2.2. Once again, the **L^{3}B15** target ultimately exhibits the highest target density (22,800 oligos/μm^2), **L^{3}M9** has the lowest target density (6600 oligos/μm^2), and the noncomplementary target (**NC14**) exhibits nearly negligible binding activity. Thus, nonspecific target binding to LNA-functionalized microspheres appears negligible, and *in situ* duplex densities can be

directly measured. Ultimately, as with the DNA probe cases discussed earlier, the 15 base-long targets, **L^{3}B15** and **B15,** result in higher duplex densities (22,800 and 20,200 oligos/μm^2, respectively) than the 9 base-long targets, **L^{3}B9** and **B9** (21,200 and 13,600 oligos/μm^2, respectively). Similar to the DNA probe cases, incorporation of LNA residues affords the shorter LNA **L^{3}B9** target a comparable duplex density to the longer DNA **B15** target (21,200 vs. 20,200 oligos/μm^2), indicating that two sequence design tools, increased target base length or the incorporation of LNA residues into a shorter target sequence, can lead to similar duplex densities for both DNA and LNA probes. As with the DNA probe cases, incorporation of LNA residues at every third base in the target significantly increases the resulting duplex density of **L^{3}A20:L^{3}B9** compared to **L^{3}A20:B9**. However, unlike the DNA probe cases, there is a greater difference in duplex density values between **L^{3}A20:L^{3}B9** and **L^{3}A20:B9** than between **L^{3}A20:L^{3}B15** and **L^{3}A20:B15**, which indicates limited additive LNA content effects on hybridization activity if both probe and target possess LNA moieties. Such diminishing effects of incorporating additional LNA substitutions on the duplex melting temperature, a commonly reported indicator of LNA hybridization affinity, have been observed previously in oligonucleotide solutions.[26-28]

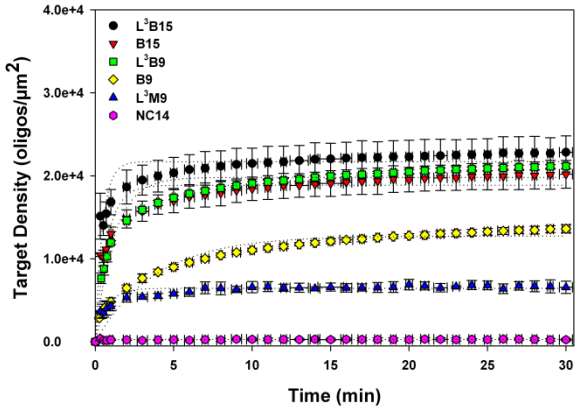

Figure 3.2.3. *In situ* measurements of hybridization activity between **L^{3}A20**-functionalized microspheres and soluble, fluorescently labeled DNA targets [**NC14** (pink diamonds); **B9** (yellow diamonds); or **B15** (red inverted triangles)] or LNA targets [**L^{3}M9** (blue triangles); **L^{3}B9** (green squares); or **L^{3}B15** (black circles)]. Dotted lines represent curve fits to Equation 3.1. Error bars indicating standard deviation for duplex density and time values the average of three suspension samples are shown.

In all cases, however, the target density for LNA probes is always higher than that obtained with DNA probes for the same target sequences. Moreover, the extent of hybridization is similar for **B9**, **L^{3}B9**, and **B15** for the DNA probe cases, whereas for the LNA probe cases, **L^{3}B9**, **B15**, and **L^{3}B15** exhibit similar target density values. Finally, unlike the DNA probe case in which a plateau in target densities is reached within the first 2 min (see Figure 3.2.2), only the **L^{3}M9** and **L^{3}B15** target cases appear to have clearly reached a plateau in duplex density values for **L^{3}A20**-functionalized microspheres within the 30 min experimental time frame shown in Figure 3.2.3. This slower duplex formation with the LNA probe is underscored by the significantly slower times to reach half the maximum target densities which range from ~26–162 s, compared to ~12–19 s for the DNA probe cases. This slower accumulation of bound targets indicates that more time is needed to reach an apparent equilibrium, likely due to the significantly greater extent of primary hybridization for LNA probe cases.

3.2.3 Post-washing Effects on Primary Duplex Density

Next, the effects of wash steps on the primary hybridization activity following *in situ* measurements are assessed. Although the post-wash primary duplexes follow a similar sequence trend to the pre-wash duplexes in terms of the relative target densities for various targets, there is a significant reduction in primary duplex density following washing steps for all probe:target pairs as indicated in Figure 3.2.4. First, it is important to point out that the nearly complete loss of noncomplementary target associated with the oligonucleotide-functionalized microspheres after washing for the noncomplementary **A20:NC14** control indicates that the signal observed during the *in situ* measurements was likely due to negligibly weak, nonspecific attractive interactions between the noncomplementary target and immobilized probe and/or microsphere surface. The amount of primary target lost due to wash steps becomes smaller as the primary target base length increases or with the incorporation of LNA residues.

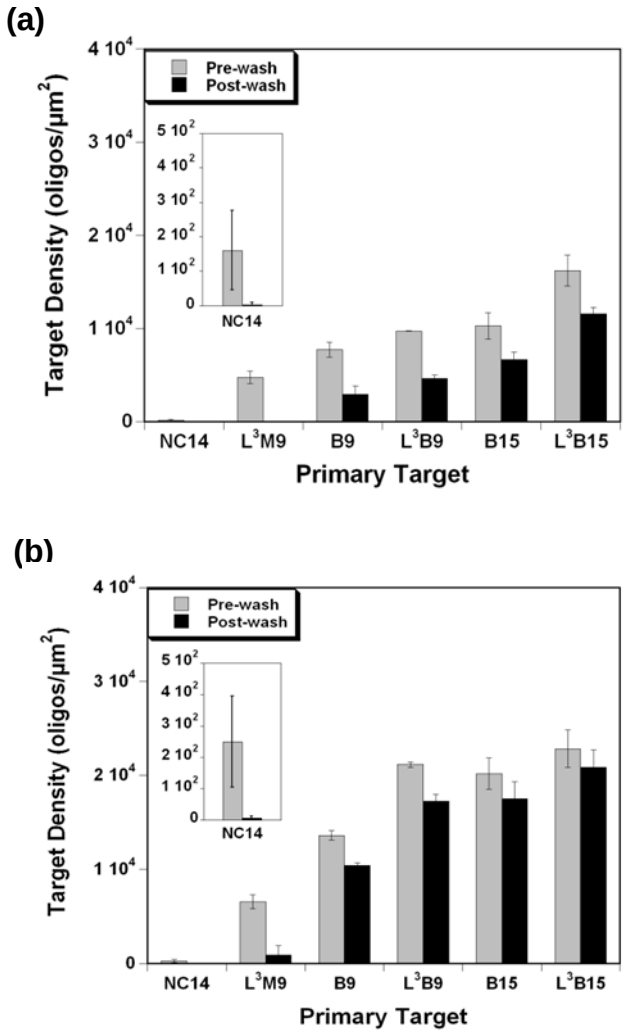

Figure 3.2.4. Surface density of primary duplexes at the 30 min time point following *in situ* primary hybridization measurements (pre-wash) and immediately following wash steps (post-wash). Primary duplexes formed between fluorescently labeled DNA (**NC14, B9,** or **B15**) or LNA (**L^{3}M9, L^{3}B9,** or **L^{3}B15**) targets and either (a) immobilized **A20** probes or (b) immobilized **L^{3}A20** probes.

Table 3.2.1 lists the percent decrease in target density after three wash steps are performed for the probe:target pairs in Figure 3.2.4. Nearly all of the noncomplementary target and much of the mismatched target is lost for both the DNA and LNA probe-functionalized microspheres. There is some washing-induced loss of target (9-23%) for all other LNA probe-target pairs. Since nonspecific binding appears negligible and even

the strongest probe:target pair (**L^{3}A20**: **L^{3}B15**) appears susceptible to target loss, washing steps must induce target dissociation.

Table 3.2.1. Percent decrease in target density that occurs upon washing. Following a 30 min incubation to allow for primary duplexes to form between DNA (**NC14**, **B9**, or **B15**) or LNA (**L^{3}M9**, **L^{3}B9**, or **L^{3}B15**) targets and immobilized (a) **A20** probes or (b) **L^{3}A20** probes. Table calculations based on Figure 3.2.4.

Primary Target	**Percent Decrease (%)**	
	A20	**L^{3}A20**
NC14	97.7	97.4
L^{3}M9	99.7	86.2
B9	61.9	23.4
L^{3}B9	52.3	18.4
B15	35.1	13.2
L^{3}B15	28.5	8.7

In agreement with previous DNA-based studies,[14, 20] washing even after a 24 h incubation in normal (150 mM NaCl) or high (up to 1000 mM NaCl) ionic strength solution still results in a reduction in primary duplex density as shown in Figure 3.2.5 and Figure 3.2.6, respectively. Incubations in target-free solution also had a similar effect. To then assess the effect of salt concentration on the extent of primary hybridization activity, soluble primary targets (1 µM) were incubated for 24 h with either **A20-** or **L^{3}A20-**functionalized microspheres in PBS/Tween buffer containing 150 mM, 500 mM, or 1000 mM NaCl, and were then analyzed by flow cytometry prior to any wash steps (pre-wash) and following a series of three washes in PBS/Tween buffer, in which the original salt concentration is maintained. As shown in Figure 3.2.6, increasing the salt concentration from 150 mM to 1000 mM NaCl increases the duplex density observed for both **A20:B9** and **L^{3}A20:B9**. There is still, however, significant loss of primary duplexes occurs following washes, even for the highest ionic strength conditions. For **L^{3}A20:B9**, for

example, there is a 23% reduction in the duplex density in 150 mM NaCl upon washing, compared to a 26% reduction in 1000 mM NaCl.

In the presence of excess soluble targets (i.e., in the bulk solution surrounding oligonucleotide-functionalized microspheres), the apparent equilibrium reached in Figure 3.2.2 and Figure 3.2.3 is likely to be dynamic with dissociation and reassociation of targets occurring within the target-rich duplex brush layer on the microspheres. Following washes, however, any loss of target from this "target-rich zone" to the now target-poor bulk solution makes target reassociation less likely particularly for weaker hybridization partners as shown in prior studies.[14, 29] Another possible explanation for wash-induced target dissociation could stem from targets that are only weakly bound due to partial hybridization to two neighboring probes.[29-30]

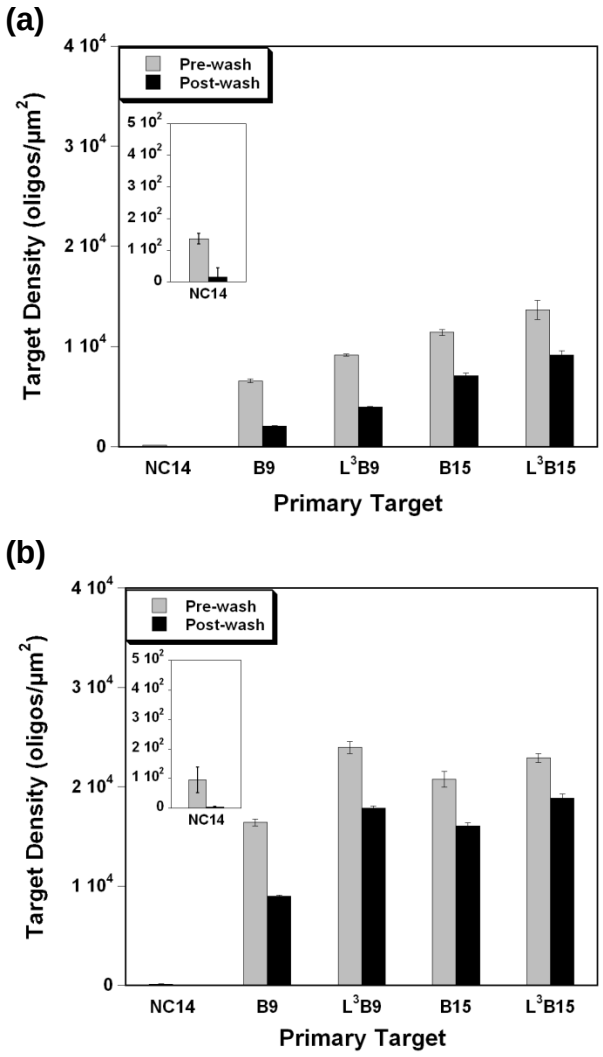

Figure 3.2.5. Surface density of primary duplexes at the 24 h time point following primary hybridization measurements (pre-wash, gray) at the higher 5 μM primary target concentration and following immediate wash steps (post-wash, black). Primary duplexes formed between fluorescently labeled DNA (**NC14**, **B9**, or **B15**) or LNA (**L^{3}B9** or **L^{3}B15**) targets and immobilized (a) **A20** probes or (b) **L^{3}A20** probes.

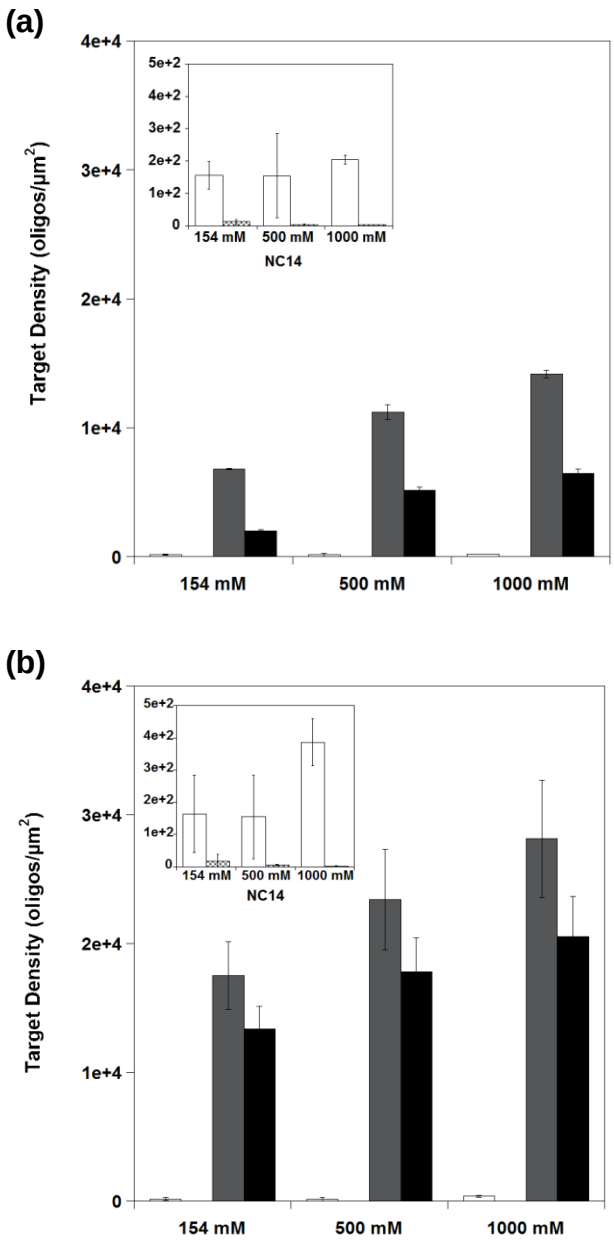

Figure 3.2.6. Primary duplex density of fluorescently labeled **NC14** (inset) and **B9** primary targets hybridized to (a) **A20** probes or (b) **L^3A20** probes immobilized onto nonfluorescent microspheres for 24 h in 150 mM, 500 mM, and 1000 mM NaCl conditions, prior to any wash steps (pre-wash, dark gray) and following wash steps (post-wash, black). Fluorescently labeled noncomplementary **NC14** (inset) is included under the same salt conditions, pre-wash (white) and post-wash (cross-hatch).

To consider this alternate explanation, the highest target density obtained (22,800 oligos/μm^2, for **L^3A20**:**L^3B15** after 30 min time point) is used as an estimate of the immobilized probe density. The reciprocal of this probe density value ($4.4 \cdot 10^{-5}$ μm^2/oligo), which can be used to estimate the average spacing between immobilized probes. Assuming a circular cross-sectional area for each immobilized probe projected onto the microsphere surface, the probe-to-probe spacing is approximately 8 nm. Based on an average interphosphate spacing for single-stranded DNA of 0.59 nm, the shortest 9 base target is ~5 nm long in its extended conformation, while the maximum length (including a 6 carbon spacer) for an extended 20 base-long probe is ~12 nm. Given the flexibility of single-stranded DNA, which does not favor extended conformations, the prospect of target sharing between two probe strands is not likely.

Although moderate washing-induced target dissociation from immobilized probes has been observed previously as a result of wash steps,[20, 29] wash steps are included during preparation of double-stranded probes for *in situ* displacement studies in order to remove excess primary targets from the surrounding solution and assess only the effects stemming from having only secondary targets initially in the surrounding solution. The effect of wash steps makes the *in situ* hybridization results, obtained prior to wash steps, of even greater interest for understanding of the hybridization of immobilized LNA sequences. Most significantly, the mismatched **A20:L^3M9** pair does not withstand the wash steps well, with 99.7% of the prewashing primary duplex density lost, as shown in Table 3.2.1, indicating the exceedingly low post-wash probe:target hybridization.

Similar to the DNA probe cases, for the LNA probe, there is a sequence length dependent increase in primary duplex density both for LNA primary targets and especially for DNA primary targets. As with the DNA probe cases, there is a significant reduction in primary duplex density following wash steps for all probe-target pairs though nonspecific target binding is nearly negligible. Most significantly, the mismatched **L^3A20:L^3M9** pair does not withstand the wash steps well, with 86% of the prewashing primary duplex density lost (6,600 vs. 900 oligos/μm^2). Interestingly, increasing both the incubation time (to 24

h) and the target concentration (to 5 μM) does not result in higher pre- or post-wash densities for any of the targets (see Table 3.2.1 and

Table 3.2.2). Although washing may drive dissociation of soluble **L^{3}M9** targets, the LNA duplex bridges that form between immobilized LNA probes and immobilized **L^{3}M9** targets are collectively strong enough to mediate colloidal assembly.[15] Similar to the DNA probe case, the loss of complementary targets or nearly complementary targets is attributed to the steep concentration gradient between target-rich microspheres and the target-poor surrounding solution following wash steps.

Table 3.2.2. Percent decrease in target density that occurs upon washing following a 24 h incubation to allow for primary duplexes to form between DNA (**NC14**, **B9**, or **B15**) or LNA (**L^{3}B9** or **L^{3}B15**) targets and immobilized (a) **A20** probes or (b) **L^{3}A20** probes. Table calculations are based on data shown in Figure 3.2.6.

Primary Target	**Percent Decrease (%)**	
	A20	**L^{3}A20**
NC14	88.4	96.6
B9	69.0	45.1
L^{3}B9	56.9	25.4
B15	38.0	22.6
L^{3}B15	33.0	17.7

3.2.4 *In situ* Kinetics of Primary Hybridization

In addition to measuring the extent of primary hybridization, the kinetics of primary hybridization was investigated using curve fits of the data to Equation 3.1, which are represented by dotted lines in Figure 3.2.2 and Figure 3.2.3. The rate constants for hybridization of various primary targets to DNA and LNA probes are reported in Table 3.2.3. Notably, the perfectly matched **L^{3}A20:B9** duplex is an order of magnitude slower than any other probe:target pairs. For the remaining DNA and LNA probe cases, the values for the primary hybridization rate constant, k_1, have the same order of magnitude for all other primary target sequences. For a given target, however, hybridization to DNA

probes was slightly faster than for LNA probes. Moreover, for the DNA probe cases, the 9 base-long primary targets have slightly larger k_1 values than the 15 base-long sequences, and the values seem to be largely independent of LNA content. The LNA probe cases, however, exhibit the opposite trend for perfectly matched duplexes, with the 15 base-long targets having slightly larger k_1 values than the 9 base-long sequences. These overall differences in k_1 values (except for **L^{3}A20:B9**) were very modest. The values for k_1 do not appear to correlate with the extent of primary duplex formation. For example, the rate constant for the mismatched **L^{3}A20:L^{3}M9** pair is quite similar to that for the perfectly matched **L^{3}A20:B15** pair, despite a large difference in the extent of hybridization ($\Delta\sigma$ = 13,600 oligos/μm^2).

Table 3.2.3 Observed rate constants for primary duplex formation, k_1, as determined from *in situ* experiments with both DNA **A20**- and LNA **L^{3}A20**-functionalized microspheres and various primary targets listed below.

	k_1 (s^{-1})	
Primary Target	DNA Probe	LNA Probe
L^{3}B15	3.98×10^{-2}	2.70×10^{-2}
B15	3.73×10^{-2}	1.75×10^{-2}
L^{3}B9	5.84×10^{-2}	1.23×10^{-2}
B9	4.66×10^{-2}	4.29×10^{-3}
L^{3}M9	---	1.73×10^{-2}

The values for the primary hybridization rate constant, k_1, for both the DNA and LNA probes are in agreement with previously reported k_1 values for *in situ* primary duplex formation between DNA-functionalized microspheres and DNA primary targets.[14] Due to the small number of studies on surface-based LNA hybridization kinetics,[12-13] solution-based studies of the kinetics of LNA hybridization can provide some insight, though the few studies available do not entirely agree with one another. In general,

hybridization kinetics in oligonucleotide solutions has been shown to be faster than on surfaces.[11, 31-33] Assuming a two-state model for dissociation in which two strands are either hybridized or completely dissociated,[32, 34-35] and since the primary target concentration [T_1] is in excess and effectively constant, then the observed rate constant of primary duplex formation, k_1, can be related to the second-order association rate constant, k_a, by the equation $k_1 = k_a[T_1] + k_r$. This equation can be approximated as $k_1 \sim k_a[T_1]$ if the dissociation rate constant, k_r, of the primary duplexes is assumed to be small. This assumption seems reasonable since the dissociation rate constants for LNA-modified duplexes are reportedly even lower than those for DNA sequences.[12, 36] LNA modifications, however, do not appear to increase the association rate constants over that of analogous DNA. Interestingly, despite the reportedly lower k_r values for LNA,[12, 36] overall there was no change in k_1 values for incorporation of LNA residues into the probe or target strands, indicating that substituting one-third of the sequence with LNA residues did not greatly affect the hybridization kinetics, similar to previous reports on LNA solutions.[34, 36] It is interesting to note that there were increases in duplex formation for LNA-based targets over analogous DNA targets in Figure 3.2.2 and Figure 3.2.3. With the exception of the **L^{3}A20:B9** case, the values of k_a for target hybridization to the LNA and DNA probes are ~2-3 × 10^4 $M^{-1}s^{-1}$ and ~4-6 × 10^4 $M^{-1}s^{-1}$, respectively. These values are in good agreement with values reported for hybridization between soluble DNA targets to DNA probes immobilized on planar substrates[31, 37] and on microspheres[10, 14, 38].

For the **L^{3}A20:B9** case, the observed rate constant of primary duplex formation was an order of magnitude lower than for all other cases, including the mismatched LNA target. The basis for this reduced rate constant does not appear to correlate with trends in the plateau duplex density values shown in Figure 3.2.2 since the **B9** target is not the weakest target. Suppression of hybridization kinetics has been reported for surface-immobilized DNA relative to soluble species due to steric and electrostatic hindrance, conformational restriction of the immobilized probe, and high probe density.[11, 33, 39] These

parameters are, however, nearly the same for all samples, and neither the **L^{3}A20** probe nor the **B9** target have any stable intrastrand secondary structures (e.g., self-loops) at room temperature (LNA: Exiqon Oligo Optimizer Tool;[40] DNA: Zuker mfold server[41]) which have previously been shown to suppress the kinetics of hybridization.[33] Although there were differences in the extent of hybridization, none of the other 9 base-long targets studied (**L^{3}B9** or mismatched **L^{3}M9**) resulted in such a decrease in the kinetics observed. Additionally, hybridization of **B9** to **A20** exhibited a faster hybridization rate, although the resulting duplex density was lower than when hybridized to **L^{3}A20**. Thus, perhaps the combination of **B9** target sequence length which is too short to complete a helical turn and the lack of LNA nucleotides to further stabilize the duplex ultimately drives even slower duplex formation of **B9** with the LNA probe.

We then assessed the effect of ionic strength on the kinetics of hybridization between the slowest hybridization partners, **L^{3}A20:B9**. Figure 3.2.7 shows that primary duplex formation occurs more quickly at the high salt concentration (1000 mM NaCl) and that a plateau in target density is apparently reached within 7 min, whereas at the low salt concentration (150 mM NaCl), an apparent plateau in target density is not reached within the experimental timeframe, consistent with results in Figure 3.2.2. The extent of hybridization is higher at 1000 mM NaCl than at 150 mM NaCl (16,300 vs. 13,600 oligos/μm^2), an expected result based on the 24 h post-wash target densities shown in Figure 3.2.6. The rate constant for primary hybridization, k_1, is more than five-fold greater in the buffer containing 1000 mM NaCl than in the buffer containing 150 mM NaCl (2.40×10^{-2} s^{-1} vs. 4.29×10^{-3} s^{-1}). This increase in the rate constant of primary hybridization makes the originally slowest **L^{3}A20:B9** pair the second fastest LNA probe:target pair, behind the **L^{3}A20:L^{3}B15** pair. Increasing the ionic strength has also reportedly increased the kinetic parameters of LNA-DNA hybridization on a planar substrate.[12]

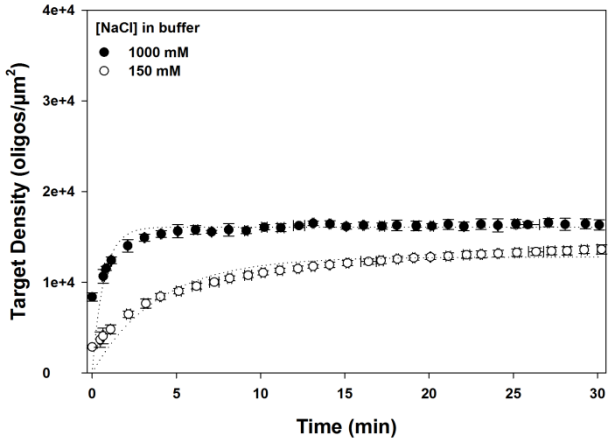

Figure 3.2.7. *In situ* measurements of hybridization activity between **L^{3}A20**-functionalized microspheres and soluble, fluorescently labeled **B9** DNA targets in 150 mM (open circles) and 1000 mM (closed circles) NaCl conditions. Dotted lines represent curve fits to Equation 3.1. Error bars indicating standard deviation for duplex density and time values for the average of three suspension samples are shown.

3.3 Conclusions

Using flow cytometry, we have monitored the early hybridization events between immobilized oligonucleotide probes and fluorescently labeled oligonucleotide targets, without the use of wash steps. Based on experiments investigating pre-wash and post-wash effects on the resulting target density, target length and LNA content have a noticeable effect on the extent of hybridization. Despite the dissociation of duplexes upon washing or incubation in target-free buffer, the overall trends in the extent of hybridization between various probe:target pairs were comparable to those in the *in situ* hybridization studies without washing. Additionally, it was found that a low duplex density does not correlate with slower hybridization kinetics, as with the **L^{3}A20:L^{3}M9** pair. In fact, similar rate constants were observed for nearly all probe:target pairs with a wide range in duplex density values ($\Delta\sigma$ = 18,500 duplexes/μm^2). The one exception occurs with the **L^{3}A20:B9** pair, which exhibits moderate, but slower hybridization

activity. However, the kinetics of hybridization were substantially enhanced for this slowest hybridization pair by increasing the ionic strength of the buffer.

3.4 References

1. Petersen, M.; Nielsen, C. B.; Nielsen, K. E.; Jensen, G. A.; Bondensgaard, K.; Singh, S. K.; Rajwanshi, V. K.; Koshkin, A. A.; Dahl, B. M.; Wengel, J.; Jacobsen, J. P. The conformations of locked nucleic acids (LNA). *J. Mol. Recognit.* **2000,** *13* (1), 44-53.

2. Nielsen, K. E.; Singh, S. K.; Wengel, J.; Jacobsen, J. P. Solution structure of an LNA hybridized to DNA: NMR study of the d(CT(L)GCT(L)T(L)CT(L)GC):d(GCAGAAGCAG) duplex containing four locked nucleotides. *Bioconjugate Chem.* **2000,** *11* (2), 228-238.

3. Kaur, H.; Arora, A.; Wengel, J.; Maiti, S. Thermodynamic, counterion, and hydration effects for the incorporation of locked nucleic acid nucleotides into DNA duplexes. *Biochemistry* **2006,** *45* (23), 7347-7355.

4. Hughesman, C. B.; Turner, R. F. B.; Haynes, C. A. Role of the heat capacity change in understanding and modeling melting thermodynamics of complementary duplexes containing standard and nucleobase-modified LNA. *Biochemistry* **2011,** *50* (23), 5354-5368.

5. Owczarzy, R.; You, Y.; Groth, C. L.; Tataurov, A. V. Stability and mismatch discrimination of locked nucleic acid-DNA duplexes. *Biochemistry* **2011,** *50* (43), 9352-9367.

6. Kaur, H.; Babu, B. R.; Maiti, S. Perspectives on chemistry and therapeutic applications of locked nucleic acid (LNA). *Chem. Rev.* **2007,** *107* (11), 4672-4697.

7. Lundin, K. E.; Højland, T.; Hansen, B. R.; Persson, R.; Bramsen, J. B.; Kjems, J.; Koch, T.; Wengel, J.; Smith, C. I. E. Biological activity and biotechnological aspects of locked nucleic acids. In *Advances in genetics,* Theodore Friedmann, J. C. D.; Stephen, F. G., Eds. Academic Press: 2013; Vol. Volume 82, pp 47-107.

8. Karlsen, K. K.; Wengel, J. Locked nucleic acid and aptamers. *Nucleic Acid Therapeutics* **2012,** *22* (6), 366-370.

9. Veedu, R. N.; Wengel, J. Locked nucleic acids: Promising nucleic acid analogs for therapeutic applications. *Chem. Biodiversity* **2010,** *7* (3), 536-542.

10. Sekar, M. M. A.; Bloch, W.; St John, P. M. Comparative study of sequence-dependent hybridization kinetics in solution and on microspheres. *Nucleic Acids Res.* **2005,** *33* (1), 366-375.

11. Henry, M. R.; Wilkins Stevens, P.; Sun, J.; Kelso, D. M. Real-time measurements of DNA hybridization on microparticles with fluorescence resonance energy transfer. *Anal. Biochem.* **1999,** *276* (2), 204-214.

12. Arora, A.; Kaur, H.; Wengel, J.; Maiti, S. Effect of locked nucleic acid (LNA) modification on hybridization kinetics of DNA duplex. *Nucleic Acids Symposium Series* **2008,** *52* (1), 417-418.

13. Mohrle, B. P.; Kumpf, M.; Gauglitz, G. Determination of affinity constants of locked nucleic acid (LNA) and DNA duplex formation using label free sensor technology. *Analyst* **2005,** *130* (12), 1634-1638.

14. Hardin, J. O.; Milam, V. T. Measuring in situ primary and competitive DNA hybridization activity on microspheres. *Biomacromolecules* **2013,** *14* (4), 986-992.

15. Eze, N. A.; Milam, V. T. Exploring locked nucleic acids as a bio-inspired materials assembly and disassembly tool. *Soft Matter* **2013,** *9* (8), 2403-2411.

16. Tison, C. K.; Milam, V. T. Reversing DNA-mediated adhesion at a fixed temperature. *Langmuir* **2007,** *23* (19), 9728-9736.

17. IDT oligoanalyzer. http://www.idtdna.com/analyzer/Applications/OligoAnalyzer/ (accessed 08/08/2012).

18. Zhang, Y.; Milam, V. T.; Graves, D. J.; Hammer, D. A. Differential adhesion of microspheres mediated by DNA hybridization i: Experiment. *Biophys. J.* **2006,** *90* (11), 4128-4136.

19. Milam, V. T.; Hiddessen, A. L.; Crocker, J. C.; Graves, D. J.; Hammer, D. A. DNA-driven assembly of bidisperse, micron-sized colloids. *Langmuir* **2003,** *19* (24), 10317-10323.

20. Baker, B. A.; Milam, V. T. Hybridization kinetics between immobilized double-stranded DNA probes and targets containing embedded recognition segments. *Nucleic Acids Res.* **2011,** *39* (15).

21. Biancaniello, P. L.; Crocker, J. C.; Hammer, D. A.; Milam, V. T. DNA-mediated phase behavior of microsphere suspensions. *Langmuir* **2007,** *23* (5), 2688-2693.

22. Kim, A. J.; Biancaniello, P. L.; Crocker, J. C. Engineering DNA-mediated colloidal crystallization. *Langmuir* **2006,** *22* (5), 1991-2001.

23. Walsh, M. K.; Wang, X.; Weimer, B. C. Optimizing the immobilization of single-stranded DNA onto glass beads. *J. Biochem. Biophys. Methods* **2001,** *47* (3), 221-231.

24. Steinberg, G.; Stromsborg, K.; Thomas, L.; Barker, D.; Zhao, C. Strategies for covalent attachment of DNA to beads. *Biopolymers* **2004,** *73* (5), 597-605.

25. Seferos, D. S.; Giljohann, D. A.; Rosi, N. L.; Mirkin, C. A. Locked nucleic acid-nanoparticle conjugates. *ChemBioChem* **2007,** *8* (11), 1230-1232.

26. You, Y.; Moreira, B. G.; Behlke, M. A.; Owczarzy, R. Design of LNA probes that improve mismatch discrimination. *Nucleic Acids Res.* **2006,** *34* (8), 11.

27. Singh, S. K.; Nielsen, P.; Koshkin, A. A.; Wengel, J. LNA (locked nucleic acids): Synthesis and high-affinity nucleic acid recognition. *Chem. Commun.* **1998,** (4), 455-456.

28. Koshkin, A. A.; Nielsen, P.; Meldgaard, M.; Rajwanshi, V. K.; Singh, S. K.; Wengel, J. LNA (locked nucleic acid): An RNA mimic forming exceedingly stable LNA:LNA duplexes. *J. Am. Chem. Soc.* **1998,** *120* (50), 13252-13253.

29. Zhang, Y.; Hammer, D. A.; Graves, D. J. Competitive hybridization kinetics reveals unexpected behavior patterns. *Biophys. J.* **2005,** *89* (5), 2950-2959.

30. Livshits, M. A.; Mirzabekov, A. D. Theoretical analysis of the kinetics of DNA hybridization with gel-immobilized oligonucleotides. *Biophys. J.* **1996,** *71* (5), 2795-2801.

31. Tawa, K.; Yao, D.; Knoll, W. Matching base-pair number dependence of the kinetics of DNA–DNA hybridization studied by surface plasmon fluorescence spectroscopy. *Biosens. Bioelectron.* **2005,** *21* (2), 322-329.

32. Porschke, D.; Uhlenbec.Oc; Martin, F. H. Thermodynamics and kinetics of helix-coil transition of oligomers containing gc base pairs. *Biopolymers* **1973,** *12* (6), 1313-1335.

33. Gao, Y.; Wolf, L. K.; Georgiadis, R. M. Secondary structure effects on DNA hybridization kinetics: A solution versus surface comparison. *Nucleic Acids Res.* **2006,** *34* (11), 3370-3377.

34. Christensen, U.; Jacobsen, N.; Rajwanshi, V. K.; Wengel, J.; Koch, T. Stopped-flow kinetics of locked nucleic acid (LNA)-oligonucleotide duplex formation: Studies of LNA-DNA and DNA-DNA interactions. *Biochem. J.* **2001,** *354* (3), 481-484.

35. Stevens, P. W.; Henry, M. R.; Kelso, D. M. DNA hybridization on microparticles: Determining capture-probe density and equilibrium dissociation constants. *Nucleic Acids Res.* **1999,** *27* (7), 1719-1727.

36. Christensen, U. Thermodynamic and kinetic characterization of duplex formation between 2′-o, 4′-c-methylene-modified oligoribonucleotides, DNA and RNA. *Biosci. Rep.* **2007,** *27* (6), 327-333.

37. Liebermann, T.; Knoll, W.; Sluka, P.; Herrmann, R. Complement hybridization from solution to surface-attached probe-oligonucleotides observed by surface-plasmon-field-enhanced fluorescence spectroscopy. *Colloids Surf., A* **2000,** *169* (1–3), 337-350.

38. Rogers, W. B.; Sinno, T.; Crocker, J. C. Kinetics and non-exponential binding of DNA-coated colloids. *Soft Matter* **2013,** *9* (28), 6412-6417.

39. Peterson, A. W.; Heaton, R. J.; Georgiadis, R. M. The effect of surface probe density on DNA hybridization. *Nucleic Acids Res.* **2001,** *29* (24), 5163-5168.

40. Tolstrup, N.; Nielsen, P. S.; Kolberg, J. G.; Frankel, A. M.; Vissing, H.; Kauppinen, S. Oligodesign: Optimal design of LNA (locked nucleic acid) oligonucleotide capture probes for gene expression profiling. *Nucleic Acids Res.* **2003,** *31* (13), 3758-3762.

41. Zuker, M. Mfold web server for nucleic acid folding and hybridization prediction. *Nucleic Acids Res.* **2003,** *31* (13), 3406-3415.

CHAPTER 4

ASSESSING *IN SITU* KINETICS OF COMPETITIVE DISPLACEMENT OF PRIMARY TARGETS BY SECONDARY TARGETS FROM IMMOBILIZED PROBES

Introduction

Although DNA is a more popular tool for surface-based hybridization, synthetic oligonucleotides, such as locked nucleic acids (LNA), provide nuclease resistance and stronger hybridization interactions. Prior work has demonstrated the potential for displacement of double-stranded (ds) LNA mixmers (i.e., sequences containing a mix of LNA and DNA nucleotides) by cellular mRNA targets by quantifying the transfection efficiency and inducible gene expression of dsLNA probes.[1] *In situ* measurements of LNA-based displacement events involving material surfaces, however, are lacking in the literature. This dissertation extends prior work[2] on *in situ* measurements of hybridization kinetics of DNA sequences as well as the colloidal disassembly studies between immobilized sequences, by subsequently investigating the *in situ* competitive displacement kinetics of select pairs of sequences. In the current study, we measure *in situ* strand displacement of LNA primary targets from duplexes with either LNA or DNA probes immobilized onto microspheres in the presence of an LNA or DNA competitive target. To the best of our knowledge, the work in this chapter is the first report of competitive displacement rate constants for LNA-based sequences and mixed LNA/DNA systems (for simplicity, these mixmers will be referred to as LNA or LNA-based strands throughout).

4.1 Materials and Experimental Methods

4.1.1 Materials

Table 4.1.1 lists all sequences used for the *in situ* measurements. The sequence design approach was based on previous work for the regular probes[3] and the flip probe.[4] DNA sequences were obtained from Integrated DNA Technologies (IDT, Coralville, IA), and LNA sequences were purchased from Exiqon (Woburn, MA). All sequences were purified using HPLC by the respective manufacturer. Immobilized probes were designed with five thymine bases and a six carbon moiety as a spacer between the hybridizing bases and an amino moiety either at the 5′ end (regular probes) or at the 3′ end (flip probe) for subsequent covalent attachment to 1.1 µm diameter carboxylated polystyrene beads (Bangs Laboratories, Fishers, IN) using the crosslinking agent 1-ethyl-3-(3-dimethylaminopropyl)carbodiimide (EDAC) at a 7.1 mM concentration, similarly as described before.[5] All primary targets are labeled with 6-carboxyfluorescein (FAM) on the 5′ end. FAM is a more hydrolytically stable isomer of fluorescein, as well as a spectral mimic. FAM-labeled primary targets are resuspended to a 100 µM concentration in Tris-EDTA buffer at pH 8.0 upon receiving and stored at -20°C. Aminated probes and unlabeled secondary targets are resuspended to a 100 µM concentration in Tris-EDTA buffer at pH 7.4 and are stored at -20°C. lists all sequences used for the *in situ* measurements.

Table 4.1.1 List of the function and nomenclature of various DNA and LNA sequences. Sequences that contain LNA residues are indicated by the "L^3" prefix in the sequence nomenclature; the "3" superscript denotes the frequency of LNA substitution, at every third base. The location of LNA bases is marked by an "L" superscript to the right of a base. Fluorescently labeled sequences contain an "F" suffix, whereas unlabeled sequences contain a "U" suffix. An underlined base signifies a mismatch. The flip probe has an external toehold orientation for competitive hybridization compared to the internal toehold orientation of the other probe sequences.

Function	Nomenclature
immobilized DNA probe	**A20** = 3′-TAGTCGGCGTTAGGTTTTTT-5′
immobilized LNA probes	**L^3A20** = 3′-TA^{L}GTC^{L}GGC^{L}GTT^{L}AGG^{L}TTTTTT-5′
	L^3A20-flip = 3′-TTTTTTA^{L}GTC^{L}GGC^{L}GTT^{L}AGG^{L}T-5′
soluble LNA 1° targets	**L^3B9F** =5′-AT^{L}CAG^{L}CCG^{L}C-3′
	L^3M9F = 5′-AT^{L}CA<u>C</u>^{L}CCG^{L}C-3′
soluble DNA 2° target	**B15U** = 5′-ATCAGCCGCAATCCA-3′
soluble LNA 2° target	**L^3B15U** = 5′- AT^{L}CAG^{L}CCG^{L}CAA^{L}TCC^{L}A-3′

4.1.2 Sequence Nomenclature

The sequence nomenclature is as follows: probe sequences, intended for immobilization onto polystyrene microspheres, contain an **A**, whereas target sequences, which are soluble, contain a **B**. Mismatched target sequences, however, contain instead an **M**, to indicate the presence of a single, center mismatch. This letter is followed by the total number of bases, for probes, and for targets, the number of bases intended for hybridization. LNA sequences are indicated by an **L^3** prefix, which signifies the substitution of an LNA residue at every third base. Fluorescently labeled primary targets have an **F** suffix, whereas unlabeled secondary targets carry a **U** suffix. The sequence composition of primary duplexes is notated as follows: probe:primary target (e.g., **L^3A20:L^3B9F**). The sequence composition of primary duplexes in the presence of secondary targets is notated as follows: probe:primary target/secondary target (e.g., **L^3A20:L^3B9F/L^3B15U**).

4.1.3 Flip Probe

The regular probes were designed such that when the nine base-long targets are hybridized, there is a six base-long toehold region between the 3′ end of the target and the spacer segment of the probe, which is attached to the microsphere surface and includes

the amine functional group, a six carbon spacer moiety, and five nonhybridizing thymine bases. This toehold region can serve as the nucleation site for the competitive target to form a duplex with the probe strand. For the flip probe, the spacer segment was transferred from the 5′ to the 3′ end of the probe, and the toehold region for the flip probe was effectively flipped from an internal location near the microsphere surface to an external one at the free end of the strand. Because the orientation of the bases in the hybridization region remains unchanged, the same primary and secondary targets that are used for the other probe studies can be used with the flip probe, allowing for direct comparison of the effect of toehold location on the kinetics of hybridization.

4.1.4 Flow Cytometry

Flow cytometry was performed on a Becton Dickinson (BD) LSRII flow cytometer and data were collected using BD FACSDiva software (BD, San Jose, CA). A histogram of counts vs. relative fluorescence intensity was obtained for each sample, which allowed for determination of the molecules of equivalent soluble fluorochrome (MESF) associated with each probe-functionalized particle, when used with Quantum FITC-5 MESF standards (Bangs Laboratories). Samples were prepared by first incubating probe-functionalized microspheres with various FAM-labeled primary targets (5 μM) for 24 h (0.01% w/v) at room temperature in a total volume of 200 μL phosphate buffered saline containing 0.2% v/v Tween-20 (PBS/Tween), for a final microsphere loading of 0.01% w/v. Following incubation, the samples were resuspended in 100 μL PBS/Tween after washing three times in 100μL PBS/Tween, with centrifugation at 9900×*g* for 3.5 min to pellet the microspheres and vortexing to resuspend the pellet.

At the beginning of each *in situ* competitive displacement run, a 2.5 μL volume of fluorescently labeled primary duplex-functionalized microspheres was pipetted into a 1 mL volume of 1 μM unlabeled DNA or LNA competitive target and immediately vortexed. After a brief equilibration time (~15 s), the sample is introduced to the flow

cytometer and the first three readings are taken between ~30 s to <1 min, and then the remaining 29 readings are taken every minute.

4.1.5 Kinetics of Competitive Hybridization

Analysis of *in situ* flow cytometry experiments yields information about the primary target density (oligos/μm^2), σ, remaining in the presence of various competitive targets. To calculate the fraction of primary duplexes, f_{pd}, shown in Equation 4.1 normalization by the initial primary target density, σ_0, is required. However, direct measurement of the true σ_0 is not possible in the positive control samples because displacement events occur quickly. Indeed linear regression analyses of the positive control samples (in the presence of competitive targets) led to a severe underestimation of the initial duplex density (based on duplex densities obtained in target-free buffer). Similar to our prior work on DNA strands,[2] to find values for σ_0, a linear regression was performed through the first three data points, using the average of three runs for each primary target, of the samples containing the noncomplementary **NC12U** as the competitive target (**probe:1° target/NC12U**). For example, the linear regression performed on **A20:L^{3}B9F/NC12U** was applied to both **A20:L^{3}B9F/B15U** and **A20:L^{3}B9F/L^{3}B15U**, but not to **L^{3}A20:L^{3}B9F/B15U** and **L^{3}A20:L^{3}B9F/L^{3}B15U** (regression based on **L^{3}A20:L^{3}B9F/NC12U** was applied to these).

$$f_{pd} = \sigma/\sigma_0 \tag{4.1}$$

where f_{pd} is the fraction of primary duplexes, σ is the primary target density remaining in oligos/μm^2, and σ_0 is the initial primary target density in oligos/μm^2.

The fraction of primary targets released from primary duplexes in the presence of competitive target, f_r, is shown in Equation 4.2. This fraction of primary targets released is then used to calculate the fraction of primary target displaced by competitive targets, f_d,

after normalizing for primary target dissociation caused by nonspecific interactions of the noncomplementary secondary target, $f_{r,NC}$, in Equation 4.3. Because f_r consists of potential contributions from both the dissociative pathways, whereas $f_{r,NC}$ consists only of contributions from the dissociative pathway, it is possible to obtain solely the contribution of the displacement pathway from f_r by subtracting out the dissociative effects associated with $f_{r,NC}$. The average value and error bars from three runs are shown for each combination of probe:1° target/2° target. The observed displacement rate constant, k_d, was obtained by performing a fit to data of the fraction displaced as a function of time using Equation 4.4. As discussed elsewhere,[2, 6-7] $k_d = k_2[T_2]$, where k_2 is the rate constant for the formation of an intermediate complex involving the probe, primary target, and competitive target, and where $[T_2]$ is the concentration of the competitive target. The fitting parameters (f_∞ and k_d) obtained for the displacement plots were determined using SigmaPlot software (Systat Software Inc., San Jose, CA). Parameters for which $p > 0.05$ are not reported.

$$f_r = 1 - f_{pd} \tag{4.2}$$

where f_{pd} is the fraction of primary duplexes and f_r is the fraction of primary targets released from the probe.

$$f_d = (f_r - f_{r,NC})/(1 - f_{r,NC}) \tag{4.3}$$

where f_d is the fraction of primary targets displaced by a competitive secondary target, f_r is the fraction of primary targets released from the probe in the presence of competitive secondary target, and $f_{r,NC}$ is the fraction of primary targets released from the probe in the presence of noncomplementary secondary target.

$$f_d = f_\infty(1 - \exp(-k_d t)) \tag{4.4}$$

where f_d is the fraction of primary targets displaced by a competitive secondary target, f_∞ is a time-dependent fitting parameter, and k_d is the rate constant for competitive displacement.

4.1.6 Analysis of Observed Displacement Rate Constant

The kinetics of soluble DNA strand displacement was first modeled by Reynaldo *et al.*[7] whereby an unlabeled competitive DNA target, T_2, replaced an identical, labeled DNA target originally that was hybridized to an unlabeled DNA probe strand in the primary duplex PT_1^*, to form an unlabeled duplex, PT_2., as indicated in Figure 4.1.1. According to Reynaldo, replacement of T_1^* in the original hybridization duplex by T_2 to form the new PT_2 duplex could proceed via either dissociation or sequential displacement. In the dissociative pathway, PT_1^* completely dissociates, which then allows for rapid hybridization of P and T_2. In the sequential displacement pathway, however, PT_1^* becomes partly denatured (likely due to random base pair fluctuations) and forms an intermediate complex, $PT_1^*T_2$, with T_2, followed by rapid branched migration to displace T_1^*. The dissociative pathway dominates near the T_m of the primary duplex, whereas the sequential displacement pathway dominates near room temperature and when the competitive target is used in excess, which are the conditions relevant for this study.

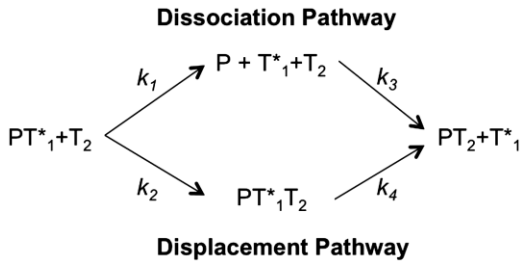

Figure 4.1.1. The two replacement pathways proposed for exchanging a labeled primary target in the PT_1^* duplex with an unlabeled secondary target to form the unlabeled PT_2 duplex. The rate constants for these pathways are indicated as follows: k_1 is the dissociation rate constant, k_2 is the intermediate complex formation rate constant, k_3 is the association rate constant between P and T_2, and k_4 is the rate constant for the formation of PT_2 from the $PT_1^*T_2$ intermediate complex. Reproduced from Baker and Milam[6] by permission of Oxford University Press.

Reynaldo *et al*. make an important assumption that the reverse process, rehybridization of the displaced T_1^* strand, does not occur due to the excess concentration of T_2 used. This assumption is not unreasonable for this system in which an excess of competitive target is used because our sequence design characteristics (increased sequence length and additional LNA bases) are intended to give the competitive targets a higher affinity than the primary targets for the probes. Reynaldo combined the contributions of both pathways into an expression that yields an observed displacement rate constant. In our work, however, the competitive targets are designed to have an increased affinity for the probe, in addition to having an excess concentration. This sequence design makes it less likely for the dissociative pathway to be significant. Moreover, the data in our displacement analysis has been normalized for the fraction of T_1^* lost due both to thermal dissociation and to nonspecific oligonucleotide interactions. Using these modifications of Reynaldo's work to account for this normalization,[2, 6] we use Equation 4.4 to fit our displacement data and to report observed displacement rate constants for primary target loss in the displacement pathway.

4.2 Results and Discussion

4.2.1 *In situ* Target Release and Competitive Displacement Profiles

The effects of LNA content for both the probe strand and the competitive target, of mismatch substitution in the primary target, and of toehold orientation are investigated in this study. A decrease in the relative fluorescence intensity of the sample can be observed, as shown in Figure 4.2.1 by the leftward progression of the fluorescence peaks toward lower mean fluorescence values over time, which indicates increased loss of fluorescently labeled primary target in the presence of competitive target. Using Quickcal template software (Bangs Laboratories), the MESF values obtained were converted into target densities.

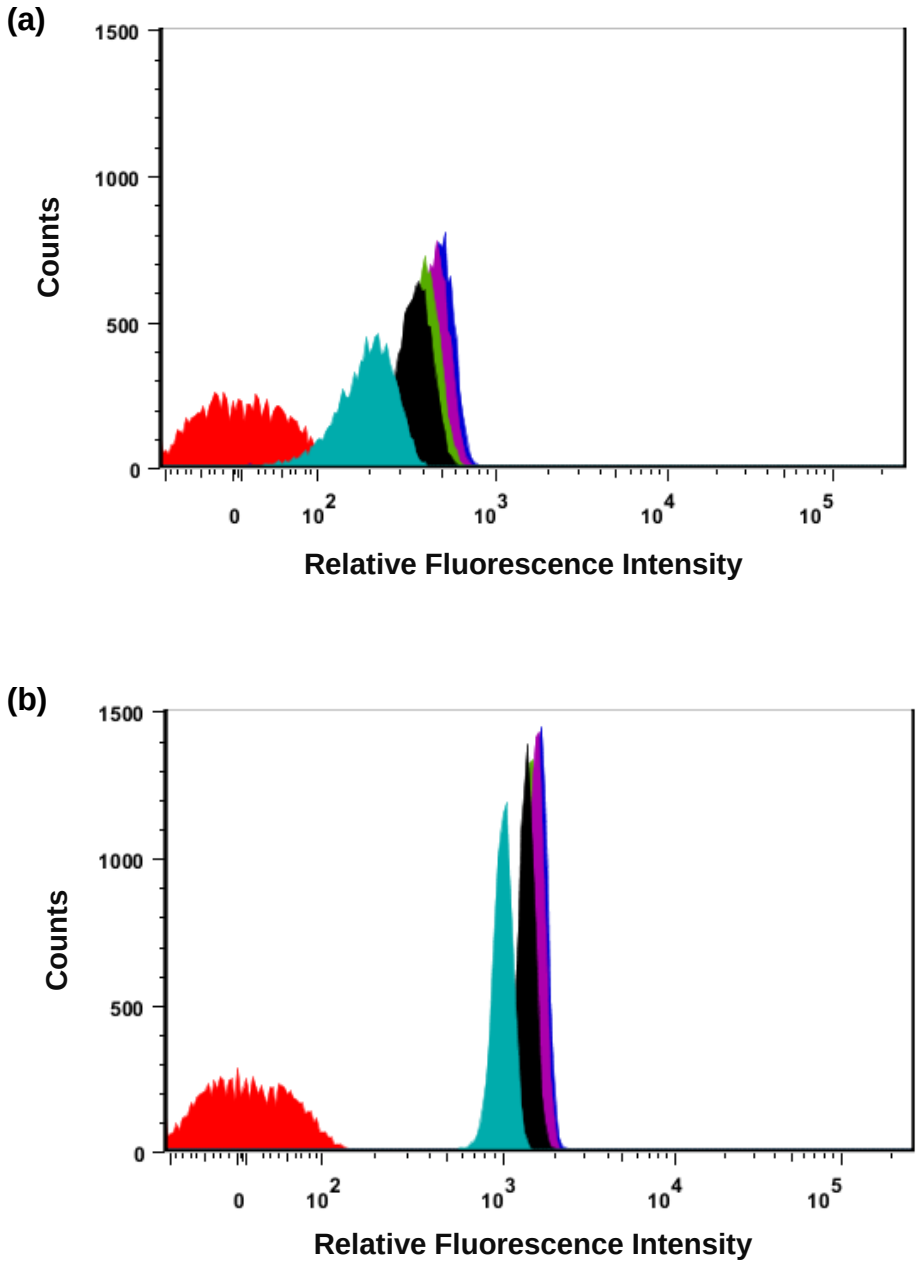

Figure 4.2.1. Flow cytometry histograms of counts vs. relative fluorescence intensity for the *in situ* competitive displacement of **L^{3}B9F** from (a) **A20**-functionalized microspheres when incubated in a solution of **L^{3}B15U** LNA secondary targets for the following amounts of time: 0 s (red), ~30 s (blue), ~40 s min (purple), ~1 min (green), ~2 min (black), and ~30 min (teal).

The primary duplex densities of **A20:L^{3}B9F** and **L^{3}A20:L^{3}B9F** remaining in the presence of various secondary targets over time were measured *in situ* and are plotted in Figure 4.2.2 below. The stark difference in the primary duplex densities at early time points for the DNA and LNA probes indicates the greater affinity of the primary target for the LNA probe. The duplex densities at early time points are in agreement with data reported in Chapter 3 for post-wash primary duplex densities. These plots show the effect of complementary secondary targets in reducing the primary duplex density compared to the nearly unnoticeable effect of the noncomplementary secondary target.

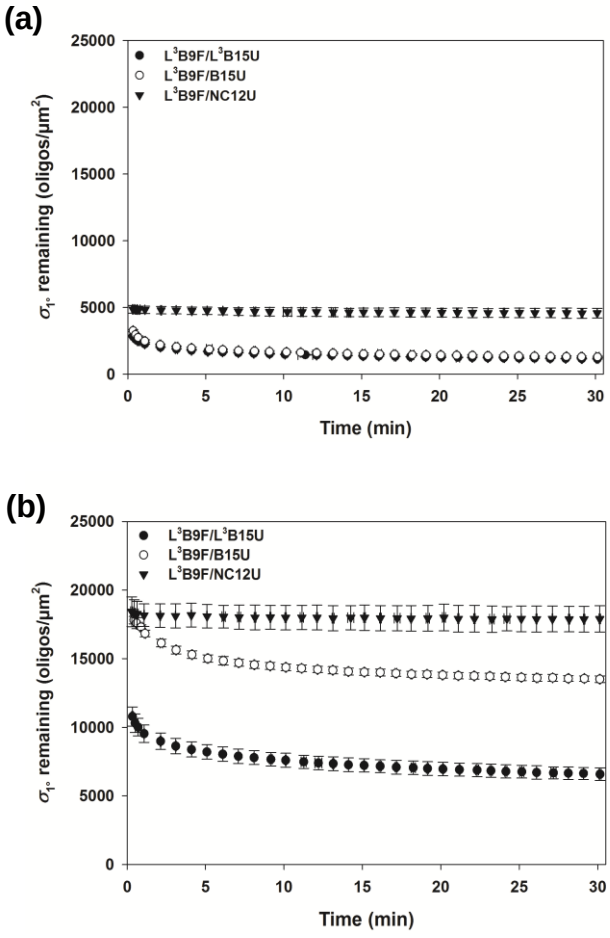

Figure 4.2.2. *In situ* measurements of the primary duplex density of perfectly matched **L^{3}B9F** remaining hybridized to (a) **A20** DNA probes or (b) **L^{3}A20** LNA probes in the presence of **L^{3}B15U** (closed circles), **B15U** (open circles), and **NC12U** (closed triangles).

Figure 4.2.3 shows the release profiles of a perfectly matched LNA primary target, **L^{3}B9F**, from a duplex with either a DNA or an LNA probe in the presence of various secondary targets. For the DNA probe case, there is an extensive and nearly equivalent fraction released of **L^{3}B9F** LNA primary target in the presence of either the **B15U** DNA or the **L^{3}B15U** LNA secondary targets (f_r(30 min) ~ 0.73 and 0.77, respectively), with only a small fraction of primary target release occurring in the presence of a noncomplementary target (f_r(30 min) ~0.06). Together, these release profiles indicate that most of the primary target release is due to competitive displacement by longer secondary targets rather than duplex dissociation events. For the LNA probe case, however, extensive release of **L^{3}B9F** occurs only in the presence of the LNA secondary target (f_r(30 min) ~ 0.64), while more modest primary target release occurs in the presence of the DNA secondary target (f_r(30 min) ~ 0.27). As with the DNA probe case, there is only a small fraction of primary target release (f_r(30 min) ~ 0.03) in the presence of noncomplementary secondary target indicating that most of the primary target release is due to displacement interactions with complementary, but longer secondary targets.

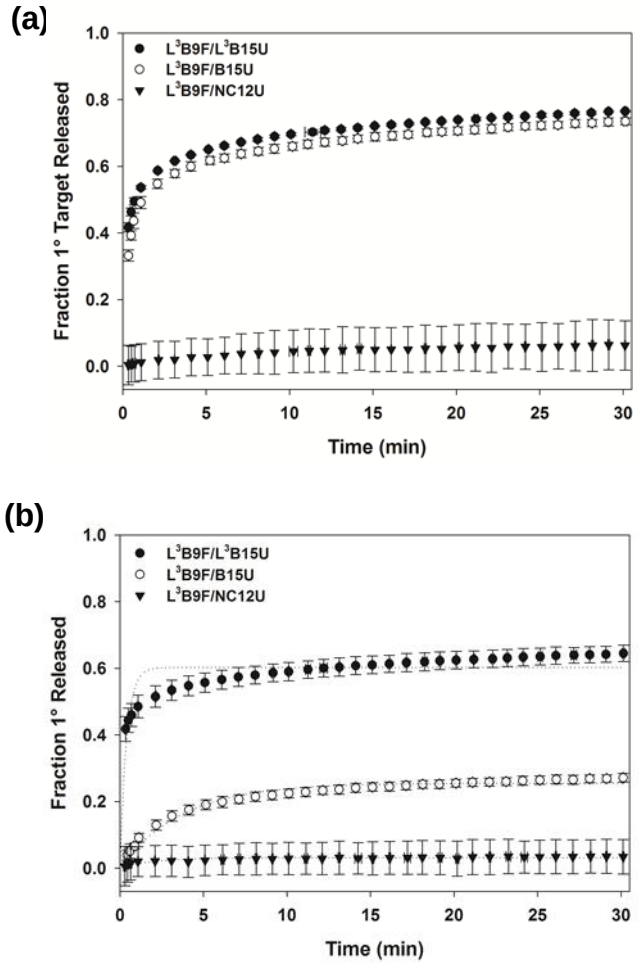

Figure 4.2.3. *In situ* measurements of the fraction of fluorescently labeled **L^{3}B9F** LNA primary target released from (a) **A20** DNA- or (b) **L^{3}A20** LNA-functionalized microspheres in the presence of unlabeled **L^{3}B15U** LNA (closed circles), **B15U** DNA (open circles), or noncomplementary **NC12U** DNA (closed triangles) competitive targets.

As detailed in the Materials and Methods section, release profiles shown in Figure 4.2.3 were converted to displacement profiles shown in Figure 4.2.4 to pinpoint the role of partner exchange events from duplex dissociation events. Figure 4.2.4 shows the displacement profiles of perfectly matched, 9 base-long primary LNA targets from either DNA or LNA probes by 15 base-long competitive DNA or LNA targets. For the DNA probe, there is little difference in the displacement activity of **L^{3}B9F** by either the **B15U** DNA or **L^{3}B15U** LNA secondary targets. For the LNA probe, however, the **L^{3}B15U**

LNA competitive target displaces more than 2.5× the amount of primary target as the **B15U** DNA competitive target. In fact, the fraction of primary target displaced is similar for three DNA and LNA probe cases (f_d(30 min) ~ 0.63–0.75), but is substantially lower for the case involving the LNA probe and DNA secondary target (f_d(30 min) ~ 0.25). It appears that substitution of LNA nucleotides into the probe lowers the displacement capabilities of the secondary DNA target, despite its longer sequence length and six base-long toehold segment on the probe strand. Studies in Chapter 3 measuring *in situ* primary hybridization activities for these sequences, however, indicate nearly identical duplex densities of **A20:B15F** and **A20:L^{3}B9F** occur suggesting that any affinity differences between these two targets and the DNA probe may be modest. Despite their similarities in primary duplex densities from these separate studies, the displacement profiles in Figure 4.2.4(a) indicate that the longer **B15U** DNA secondary target must have a sufficiently greater affinity for the DNA probe to drive displacement of the shorter **L^{3}B9F** LNA primary target. Intriguingly, these same prior studies indicated lower duplex densities occur for **L^{3}A20:B15F** (20,200 oligos/μm^2) compared to **L^{3}A20: L^{3}B9F** (21,200 oligos/μm^2). Despite these differences in primary hybridization activity, modest displacement of **L^{3}B9F** is still achieved by the **B15U** DNA secondary target in Figure 4.2.4(b) indicating that the toehold segment must play a substantial role in enabling any displacement activity in our current involving pure DNA and LNA-DNA mixmers. Furthermore, it is important to note that displacement activity in Figure 4.2.4, while substantial, is not nearly complete for any these probe-target combinations and may help explain why this displacement strategy does not promote complete disassembly of colloidal particles linked together with these perfectly-matched LNA-based duplex bridges.

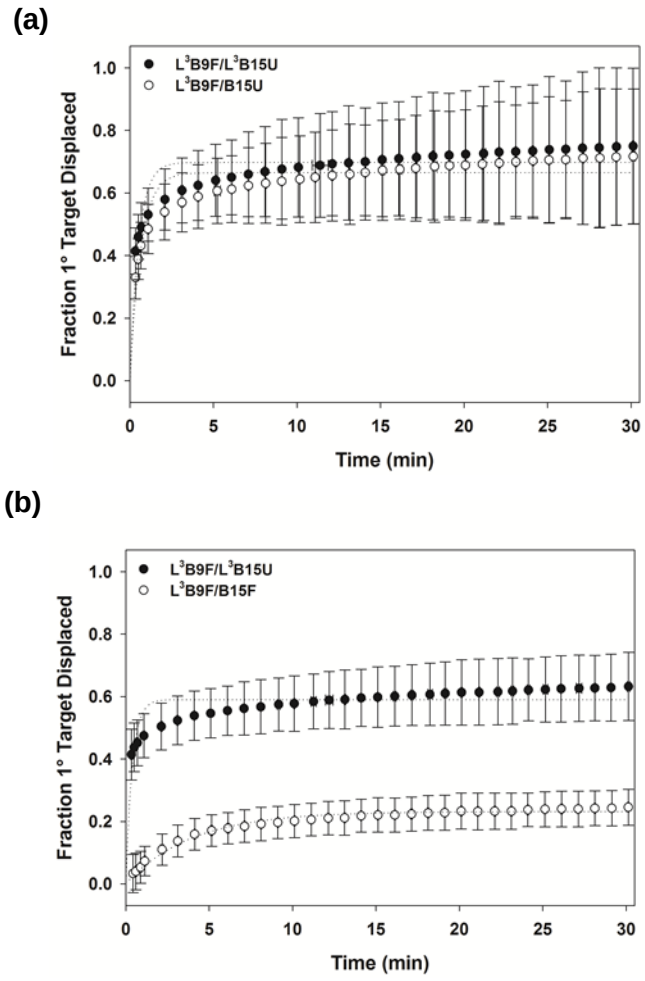

Figure 4.2.4. Measurements of the *in situ* competitive displacement of **L^{3}B9F** from (a) **A20**- or (b) **L^{3}A20**-functionalized microspheres by **L^{3}B15U** (closed circles) or **B15U** (open circles). Dotted lines represent curve fits to Equation 4.4.

Figure 4.2.5 shows the *in situ* measurements of the fraction of mismatched **L^{3}M9F** primary target released from the LNA probe in the presence of various secondary targets. Substantial but incomplete release of this mismatched target occurs in the presence of the **B15U** DNA secondary (f_r(30 min) ~ 0.67). Notably, however, the release profiles in the presence of **B15U** and the noncomplementary **NC12U** secondary target nearly overlap during the first 15 min indicating that most of these early release events can be attributed to dissociation of **L^{3}A20:L^{3}M9F** duplexes. Although not directly obtainable from online

calculators, an estimation for the T_m of the **L[3]A20:L[3]M9F** duplex of 38 °C is discussed in Appendix B and may help explain the release profiles observed in Figure 4.2.5.

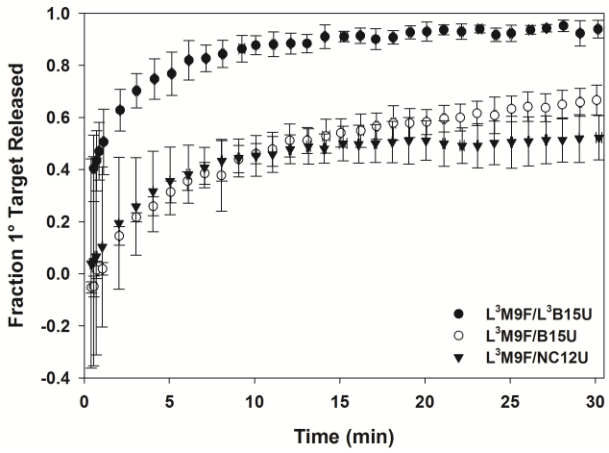

Figure 4.2.5. *In situ* measurements of the fraction of **L[3]M9F** mismatched LNA primary target released from **L[3]A20**-functionalized microspheres in the presence of unlabeled **L[3]B15U** (closed circles), **B15U** (open circles), or noncomplementary **NC12U** (closed triangles) competitive targets.

To demonstrate the ease with which the mismatched **L[3]M9F** primary target is un-hybridized from the probe in the presence of various targets, the duplex density of **L[3]M9F** remaining hybridized to **L[3]A20** is plotted in Figure 4.2.6. In the presence of the **L[3]B15U** LNA competitive target, there is nearly complete loss of **L[3]M9F** target within the 30 min experimental time frame. In the presence of the **B15U** DNA competitive target, however, there is a greater amount of primary target remaining hybridized to the probe as expected. Upon inspection of the noncomplementary **NC12U** secondary target, which has a similar amount of primary target remaining hybridized to the probe as for the **B15U** case, it appears that much of the primary target loss is due to thermal dissociation events, corroborating the weak hybridization interaction between **L[3]M9F** and the **L[3]A20** LNA probe.

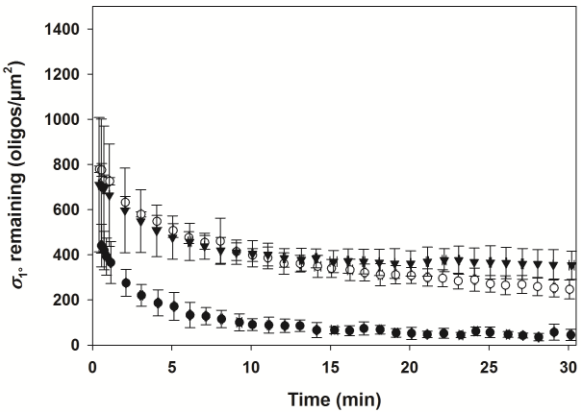

Figure 4.2.6. *In situ* measurements of the primary duplex density of mismatched **L^{3}M9F** remaining hybridized to **L^{3}A20** LNA probes in the presence of **L^{3}B15U** (closed circles), **B15U** (open circles), or **NC12U** (closed triangles).

In collectively comparing all the release profiles of the mismatched LNA target, it is apparent that additional, in fact, nearly complete primary target release is achieved in the presence of the **L^{3}B15U** LNA secondary target (f_r(30 min) ~ 0.94) at all time points tested. Thus, while substantial dissociation of the mismatched primary duplex does occur, this additional release must be due to successful displacement activity. In agreement with the fraction released profiles, the *in situ* profiles of the fraction of mismatched **L^{3}M9F** primary targets displaced from **L^{3}A20**-functionalized microspheres, shown in Figure 4.2.7, indicate that the primary target is quite weak. Not surprisingly, given the extensive overlap in fraction released profiles with the noncomplementary control, the fraction displaced profile of the **L^{3}M9F** primary target in the presence of the **B15U** DNA competitive target did not allow for a fit to Equation 4.4, and is thus not shown in Figure 4.2.7. For the LNA competitive target case, however, there is an exponential rise to a maximum fraction displaced of 0.87, which is lower than the fraction displaced for the displacement of the perfectly matched target in Figure 4.2.4.

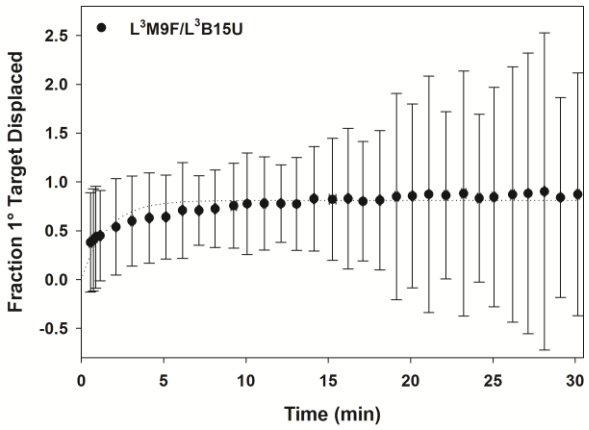

Figure 4.2.7. Measurements of the *in situ* competitive displacement of **L^{3}M9F** from **L^{3}A20**-functionalized microspheres by **L^{3}B15U**. Dotted lines represent curve fits to Equation 4.4.

4.2.2 *In situ* Measurements of the Flip Probe System

As expected for the flip probe case in Figure 4.2.8, the **L^{3}B15U** LNA competitive target leads to a higher fraction primary target displaced than the **B15U** DNA competitive target (0.51 vs. 0.31). This difference, however, is not as dramatic as that for the regular LNA probe case in Figure 4.2.4. Interestingly, the initial immobilized primary duplex densities for the LNA flip probe are not as high as those densities obtained for the regular LNA probe. In fact, the opposite result was expected because the toehold of the original duplex is oriented near the particle surface, whereas that of the flip system is oriented toward the oligonucleotide solution, ostensibly facilitating the arrival and attachment of the competitive target, which no longer has to penetrate the oligonucleotide brush layer as deeply to hybridize to the toehold region of the probe strand. It is possible, however, that covalent attachment of the probe at the 3′ end is less efficient. A previous study reported increased duplex densities for the 3′ attached probe. It has been shown that for immobilized aptamers, the effect of orientation of immobilization is aptamer-specific.[8] Prompted by concerns that the flip system in which the FAM fluorophore is in proximity with the

microsphere surface would lead to quenching of the FAM signal,[9] **L^{3}B9F** sequences were designed with a 3′ FAM fluorophore both with and without a 3-6 C spacer out of concern for quenching by the penultimate 3′ guanine residue (data not shown). Surprisingly, the primary duplex densities obtained with these modifications that move the FAM fluorophore further away from the microsphere surface resulted in even lower duplex densities than with the original 5′ labeled **L^{3}B9F** target, as shown in Table 4.2.1. Thus, the 5′ labeled **L^{3}B9F** target was used as the primary target in the flip probe study. It appears that flipping the toehold region to a more exposed location led to both lower initial σ values, but also lower f_d values.

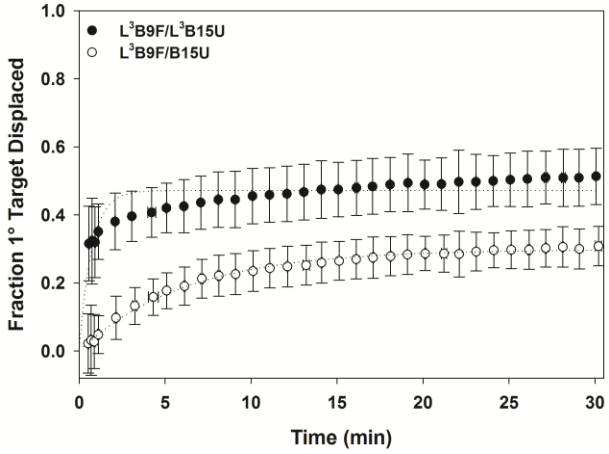

Figure 4.2.8. Measurements of the *in situ* competitive displacement of **L^{3}B9F** from **L^{3}A20(flip)**-functionalized microspheres by **L^{3}B15U** (closed circles) and **B15U** (open circles). Dotted lines represent curve fits to Equation 4.4.

Table 4.2.1. List of the post-wash primary duplex densities obtained with **L^{3}A20-** or **L^{3}A20(flip)**-functionalized microspheres incubated with **L^{3}B9F** primary targets containing a regular 5′ FAM fluorophore or a 3′ FAM fluorophore, with or without a 3-carbon spacer (indicated by 3C).

	Duplex Density (oligos/μm^2)	
Primary Target	**L^{3}A20 probe**	**L^{3}A20(flip) probe**
L^{3}B9-5′FAM	23114	8073
L^{3}B9-3′FAM	10055	6093
L^{3}B9-3C-3′FAM	6870	4680

4.2.3 *In situ* Competitive Displacement Kinetics

The observed displacement rate constant, k_d, was obtained from fits of the fraction displaced curves to Equation 4.4 for all probes and targets used. The kinetics of competitive displacement for the LNA competitive target are essentially independent of whether an LNA or DNA probe is used, whether the primary target is perfectly matched or mismatched, or whether the toehold region is relatively buried or exposed. The DNA competitive target, however, is somewhat more sensitive to its environment, with the fastest kinetics when a DNA probe is used, and a penalty of approximately one order of magnitude decrease in the displacement rate constant, when an LNA probe is used. Furthermore, for the mismatched primary target case, k_d could not be determined. Notably, the displacement kinetics of the DNA and LNA competitive targets are quite similar when displacing a shorter perfectly matched LNA primary target from a DNA probe. These differences between the LNA and DNA competitive targets are interesting, because although the LNA competitive target has been shown to have a higher affinity for the probe than the DNA competitive target, its primary hybridization kinetics for the same probe are quite similar to those of the DNA competitive target, as reported in Chapter 3.

The observed *in situ* displacement rate constants that are listed in Table 4.2.2 fall within the range of previously reported *in situ*[2] and post-wash[10] displacement rate constants for similar DNA sequences hybridized to DNA-functionalized colloidal particles. These values in Table 4.2.2 are larger by 2-3 orders of magnitude than those reported for dissimilar DNA sequences hybridized to DNA-functionalized colloidal particles,[6, 11] although these differences could arise from differences in particle size and functional group density, as well as differences in the immobilized probe length or length of the toehold region. Notably, as far as the authors are aware, there have been no reports of the dissociation rate constants of LNA sequences due to competitive displacement (rather than thermal dissociation experiments) either in solution or on substrates.

Table 4.2.2. Observed displacement rate constants, k_d, for primary LNA and DNA targets incubated with secondary LNA and DNA targets.

Probe	1° Target	k_d (s^{-1})	
		LNA 2° Target	**DNA 2° Target**
L^3A20	**L^3B9F**	4.31×10^{-2}	4.21×10^{-3}
	L^3M9F	1.06×10^{-2}	---
A20	**L^3B9F**	3.21×10^{-2}	2.54×10^{-2}
L^3A20-flip	**L^3B9F**	2.29×10^{-2}	2.70×10^{-3}

4.3 Conclusions

We have presented the first *in situ* study of the kinetics of LNA-based competitive hybridization. The current study investigates the dual challenge of retaining high primary duplex density and stability in the presence of noncomplementary targets and of inducing highly responsive displacement in the presence of competitive targets. Overall, we find that the time scales for competitive displacement are similar for DNA and LNA. Addi-

tionally, the displacement rate constants using an LNA competitive target do not vary by more than 3× when the nature of the probe (DNA or LNA), primary target (perfectly matched or mismatched), or toehold region (buried or exposed) are changed. There is, however, some variability in the displacement rate constants using a DNA competitive target; an immobilized LNA probe slows the displacement rate constant by an order of magnitude. Moreover, it appears that the location of the toehold region does not greatly affect the kinetics of competitive displacement. Importantly, we show that for a DNA probe, the DNA and LNA competitive targets are essentially interchangeable in terms of the kinetics of competitive displacement (both fraction primary target displaced and displacement rate constants). The ready displacement of a shorter LNA primary target from a DNA probe by a longer DNA competitive target suggests that LNA sequences can be incorporated into double-stranded probe systems, allowing for detection of natural oligonucleotide or possibly aptamer targets. This study demonstrates the potential of a mixed LNA-DNA double-stranded probe for *in situ* nucleic acid detection assays.

4.4 References

1. Riahi, R.; Dean, Z.; Wu, T.-H.; Teitell, M. A.; Chiou, P.-Y.; Zhang, D. D.; Wong, P. K. Detection of mRNA in living cells by double-stranded locked nucleic acid probes. *Analyst* **2013,** *138* (17), 4777-4785.

2. Hardin, J. O.; Milam, V. T. Measuring in situ primary and competitive DNA hybridization activity on microspheres. *Biomacromolecules* **2013,** *14* (4), 986-992.

3. Eze, N. A.; Milam, V. T. Exploring locked nucleic acids as a bio-inspired materials assembly and disassembly tool. *Soft Matter* **2013,** *9* (8), 2403-2411.

4. Baker, B. A. Employing double-stranded DNA probes on colloidal substrates for competitive hybridization events. Georgia Institute of Technology, Atlanta, GA, 2010.

5. Tison, C. K.; Milam, V. T. Reversing DNA-mediated adhesion at a fixed temperature. *Langmuir* **2007,** *23* (19), 9728-9736.

6. Baker, B. A.; Milam, V. T. Hybridization kinetics between immobilized double-stranded DNA probes and targets containing embedded recognition segments. *Nucleic Acids Res.* **2011,** *39* (15).

7. Reynaldo, L. P.; Vologodskii, A. V.; Neri, B. P.; Lyamichev, V. I. The kinetics of oligonucleotide replacements. *J. Mol. Biol.* **2000,** *297* (2), 511-520.

8. Cho, E. J.; Collett, J. R.; Szafranska, A. E.; Ellington, A. D. Optimization of aptamer microarray technology for multiple protein targets. *Anal. Chim. Acta* **2006,** *564* (1), 82-90.

9. Tirri, M.; Wahlroos, R.; Meltola, N.; Toivonen, J.; Hänninen, P. Effect of polystyrene microsphere surface to fluorescence lifetime under two-photon excitation. *J. Fluoresc.* **2006,** *16* (6), 809-816.

10. Tison, C. K.; Milam, V. T. Programming the kinetics and extent of colloidal disassembly using a DNA trigger. *Soft Matter* **2010,** *6* (18), 4446-4453.

11. Baker, B. A.; Mahmoudabadi, G.; Milam, V. T. Using double-stranded DNA probes to promote specificity in target capture. *Colloids Surf., B* **2013,** *102*, 884-890.

CHAPTER 5

SUMMARY AND FUTURE WORK

5.1 Summary

This dissertation details the use of competitive displacement events to induce the isothermal disassembly of LNA-linked colloidal microspheres at 37 °C, as well as the kinetics of hybridization and displacement events at room temperature. Here, the concept of competitive displacement is applied to the programmable disassembly of LNA-linked colloidal satellites each comprised of a central microsphere surrounded by a layer of nanoparticles. The use of a nucleic acid analogue, such as LNA, is critical for any physiological applications of this process because the advantageous backbone chemistry that confers nuclease resistance and increased specificity on LNA make it an attractive component compared to DNA which is readily cleaved *in vivo* by nucleases outside of the cell nucleus environment. By optimizing the affinity, duplex concentration, and LNA content in the probe and target strands, the extent of colloidal disassembly can be tuned. Although most of the primary targets investigated would likely be able to drive colloidal satellite assembly, their utility in a reversible scheme would likely have been limited, as the extent of displacement and disassembly are found to be determined more by the overall primary target affinity, which is not necessarily directly correlated to target:probe duplex density values. After the fundamentals of isothermal, LNA-mediated assembly and redispersion are understood, experiments elucidating the hybridization kinetics of immobilized probes are then performed. This project is an important step in developing a multifunctional colloid-based biomaterial system with potential for future use in biomedical systems.

5.2 Directions for Future Work

Current work in the Milam lab has turned toward DNA aptamers. There is potential for extending the work in this dissertation to these projects. Aptamers are oligonucleotide sequences that, in addition to their affinity for their complementary strands, have high affinity for non-nucleotide targets, such as gold, proteins, or chemical compounds. Current lab research is investigating the following: 1) identification of DNA aptamers for gold nanospheres and nanorods that can then precipitate gold nanoparticles from a gold salt solution and 2) competitive displacement of a nonnucleotide target through the introduction of an oligonucleotide target (or vice versa) to an immobilized aptamer. Selection of a gold aptamer involves amplification of the candidate aptamers remaining via several polymerase chain reaction (PCR) steps. Currently, LNA modification of known DNA-based aptamer sequences occurs after the selection process occurs because the natural polymerases that are used in PCR do not recognize LNA nucleotides.[1-3] There is ongoing research,[4-5] however, to modify natural polymerases so that they can incorporate LNA bases into a DNA (or RNA sequence) during PCR, thus allowing for amplification of LNA-based aptamer target candidates during the selection process. Some studies,[6-8] however, indicate that LNA modification of aptamers is not quite as straightforward as for hybridization to oligonucleotide targets, as a decrease in affinity between aptamer and target has been observed in some cases. An aptamer displacement kinetics study could determine if a double-stranded probe system with LNA modification of either the aptamer or its complementary oligonucleotide hybridization partner would inhibit or slow down displacement of the complementary oligonucleotide strand by the nonnucleotide target. Having a bead-based system would potentially allow for *in situ* quantification of displacement events as well as aptamer-target binding kinetics using flow cytometry. Similar to the first ongoing studies to identify DNA aptamer sequences for gold, the effect of LNA modification of an aptamer on the specificity and strength of the aptamer-target interaction could be investigated.

The applications of this dissertation go beyond the current work in progress in the Milam lab, and would also be useful for cell-based studies. The development of a functional drug delivery vehicle would entail (1) reducing the size of the satellite assembly to below 200 nm; (2) replacing polystyrene, which is used here as a model material, with another more biocompatible material; (3) accommodating for surface chemistry effects on probe conjugation and density; (4) determining the appropriate probe density to eliminate nonspecific particle aggregation issues (a lower coupling agent concentration was required going from a 5 μm particle in previous work[9] to a 1 μm template particle used in this work). Cellular uptake of oligonucleotide-functionalized gold nanoparticles readily occurs without transfection agents, and subsequent specific gene knockdown in the presence of these nanoparticles has previously been demonstrated.[10] In this future system, genomically relevant sequences must be used to achieve the desired effect. One possibility is to use LNA-modified, immobilized aptamers to scavenge for toxins or to bind undesirable aptamer targets. If an LNA-modified aptamer is designed with a sufficiently high affinity that binding a toxin is essentially irreversible, the toxin can be prevented from associating with its intended cellular target, or can be displaced from the target, allowing for clearance by the reticuloendothelial system. Of course, with such a high affinity, the specificity of the aptamer-toxin interaction must be demonstrated so as to avoid unintentional binding of, for example, nutrient-based ligands to aptamers rather than receptors.

Yet, although several challenges remain to understanding LNA-based binding events, this nuclease-resistant biomacromolecule presents exciting opportunities in designing and implementing designer materials systems.

5.3 References

1. Darfeuille, F.; Hansen, J. B.; Orum, H.; Primo, C. D.; Toulmé, J. J. LNA/DNA chimeric oligomers mimic RNA aptamers targeted to the tar RNA element of hiv-1. *Nucleic Acids Res.* **2004,** *32* (10), 3101-3107.

2. Schmidt, K. S.; Borkowski, S.; Kurreck, J.; Stephens, A. W.; Bald, R.; Hecht, M.; Friebe, M.; Dinkelborg, L.; Erdmann, V. A. Application of locked nucleic acids to improve aptamer *in vivo* stability and targeting function. *Nucleic Acids Res.* **2004,** *32* (19), 5757-5765.

3. Karlsen, K. K.; Wengel, J. Locked nucleic acid and aptamers. *Nucleic Acid Therapeutics* **2012,** *22* (6), 366-370.

4. Pinheiro, V. B.; Taylor, A. I.; Cozens, C.; Abramov, M.; Renders, M.; Zhang, S.; Chaput, J. C.; Wengel, J.; Peak-Chew, S.-Y.; McLaughlin, S. H.; Herdewijn, P.; Holliger, P. Synthetic genetic polymers capable of heredity and evolution. *Science* **2012,** *336* (6079), 341-344.

5. Veedu, R. N.; Vester, B.; Wengel, J. Efficient enzymatic synthesis of LNA-modified DNA duplexes using kod DNA polymerase. *Org. Biomol. Chem.* **2009,** *7* (7), 1404-1409.

6. Bonifacio, L.; Church, F.; Jarstfer, M. Effect of locked-nucleic acid on a biologically active G-quadruplex. A structure-activity relationship of the thrombin aptamer. *Int. J. Mol. Sci.* **2008,** *9* (3), 422-433.

7. Shangguan, D.; Tang, Z.; Mallikaratchy, P.; Xiao, Z.; Tan, W. Optimization and modifications of aptamers selected from live cancer cell lines. *ChemBioChem* **2007,** *8* (6), 603-606.

8. Hernandez, F. J.; Kalra, N.; Wengel, J.; Vester, B. Aptamers as a model for functional evaluation of LNA and 2′-amino LNA. *Bioorganic & Medicinal Chemistry Letters* **2009,** *19* (23), 6585-6587.

9. Tison, C. K.; Milam, V. T. Programming the kinetics and extent of colloidal disassembly using a DNA trigger. *Soft Matter* **2010,** *6* (18), 4446-4453.

10. Seferos, D. S.; Giljohann, D. A.; Rosi, N. L.; Mirkin, C. A. Locked nucleic acid-nanoparticle conjugates. *ChemBioChem* **2007,** *8* (11), 1230-1232.

APPENDIX A

HYBRIDIZATION AFFINITY BETWEEN LNA BASES

Table A.1 List of oligonucleotide sequence function and nomenclature. Values of Gibbs Free Energy of Hybridization, ΔG_{hyb}, are provided for select DNA probe-target duplexes.

Function	Nomenclature		ΔG_{hyb} (kcal/mol)
immobilized DNA probe	**A20** =	3'–TAGTCGGCGTTAGGTTTTTT–5'	
immobilized LNA probe	**L^{3}A20** =	3'–TA^{L}GTC^{L}GGC^{L}GTT^{L}AGG^{L}TTTTTT–5'	
soluble DNA 1° target	**B9** =	5'–ATCAGCCGC–3'	-19.6 kcal/mol
soluble LNA 1° target	**L^{3}B9** =	5'–AT^{L}CAG^{L}CCG^{L}C–3'	
soluble DNA 1° target	**M9** =	5'–ATCA<u>C</u>CCGC –3'	
soluble LNA 1° targets	**L^{3}M9** =	5'–AT^{L}CA<u>C</u>^{L}CCG^{L}C–3'	
	L^{3}M11 =	5'–AT^{L}CAG^L<u>G</u>CG^{L}CAA^L–3'	
	L^{3}M13 =	5'–AT^{L}CAG^{L}C<u>G</u>G^{L}CAA^{L}TC–3'	
	L^{3}M15 =	5'–AT^{L}CAG^{L}CC<u>C</u>^{L}CAA^{L}TCC^{L}A–3'	
immobilized LNA 1° targets	**L^{3}B9** =	5'–TTTTTTTTTTTTAT^{L}CAG^{L}CCG^{L}C–3'	
	L^{3}M9 =	5'–TTTTTTTTTTTTAT^{L}CA<u>C</u>^{L}CCG^{L}C–3'	
soluble DNA 2° target	**B15** =	5'–ATCAGCCGCAATCCA–3'	-31.5 kcal/mol
soluble LNA 2° target	**L^{3}B15** =	5'–AT^{L}CAG^{L}CCG^{L}CAA^{L}TCC^{L}A–3'	
soluble target	**NC14** =	5'–GGATTGCGGCTGAT–3'	-3.6 kcal/mol

[a] Superscript "3" in sequence nomenclature indicates LNA base at every third residue. Superscript "L" after base indicates LNA base. Underlined base indicates a mismatch. ΔG_{hyb} values for **A20** probe and DNA targets were determined using IDT OligoAnalyzer, Hetero-Dimer function (https://www.idtdna.com/analyzer/Applications/OligoAnalyzer/; date accessed: 08/08/2012). Notably, analogous analytic tools for determining ΔG_{hyb} values for strands possessing mismatches or LNA residues were unavailable.

The thermodynamics of base pair hybridization for DNA-DNA interactions is well understood, with a functional model that allows for accurate assessment of the thermodynamic contributions of each base pair by also considering the sequence context.[1] The strength of each **A:T** or **C:G** pair is highly dependent on the adjacent base on either side, i.e., the sequence context, as well as the temperature and salt concentration. The sequence context is accounted for in a nearest-neighbor model that considers the thermodynamic contributions of nearest-neighbor bases and assumes that the interactions of nucleotides further away can be ignored.[1] LNA bases are even more sensitive than DNA bases to the effect of sequence context on base pairing stability. The thermodynamics of base pair hybridization for LNA-DNA interactions has been studied to a lesser extent than DNA. A nearest-neighbor model for LNA-DNA hybridization has been created under the following conditions: (1) LNA bases are restricted to one strand and (2) each LNA base hybridizes to a DNA base (whether complementary as with **A^L:T** or noncomplementary as with **A^L:A**) on the partner strand.[2-3] No comparable models exist, however, for LNA-

LNA base pair interactions. In this work, hybridization of LNA mixmer sequences, such as **L^{3}A20:L^{3}B9F**, was designed so that the LNA bases in one strand would pair with complementary LNA bases in the partner strand. Additionally, all of the base pairing interactions between two LNA strands involve only LNA-LNA and DNA-DNA base pairing, in order to maximize the effect of LNA addition on the resulting duplex. These LNA-LNA interactions likely stabilized the mismatched 9 base-long **L^{3}M9F** sequence enough to allow for reversible colloidal assembly (Chapter 2) and kinetic rate analysis (Chapters 3 and 4). The model for LNA hybridization cannot be applied to duplexes of this nature. However, hybridization of an LNA strand with a DNA strand, such as **L^{3}A20:B9F** or **A20:L^{3}B9F**, results in LNA-DNA and DNA-DNA base pairing, and these sequences can be analyzed using the currently available models.

The nearest neighbor model parameters are reported using hybridization conditions of 37 °C and 1 M NaCl. Typically for DNA, a temperature correction is performed by assuming the heat capacity, C_p, is constant over the temperature range of interest. However, it has been shown that such an assumption for both DNA-DNA and LNA-DNA duplexes is not necessarily valid.[4] Accordingly, the parameters in Table A.2 are reported for hybridization conditions at 37 °C.

A salt correction for the experiments that were performed in this work at 150 mM NaCl is obtained in Equation A.1 from SantaLucia[5]:

$$\Delta G^\circ_{37}[Na^+] = \Delta G^\circ_{37}[1\text{ M NaCl}] - 0.114 \times N/2 \times \ln[Na^+] \quad \text{(A.1)}$$

where ΔG°_{37} is the Gibbs free energy for Watson Crick base pairing at 37 °C, N is the total number of phosphates in the duplex, and $[Na^+]$ is the concentration of all monovalent cations in solution. Because the online calculators currently use DNA-based salt corrections for LNA-containing duplexes, Equation A.1 is used to calculate the LNA thermodynamic parameters at 150 mM, which are listed in Table A.2 below.

In general, at each salt concentration, the change in the Gibbs free energy of hybridization for each nearest neighbor pairing is more negative in the LNA-DNA case than in the DNA-DNA case. As expected, the ΔG°_{37} values for duplexes formed at 1 M NaCl are greater than those at 154 mM. Some LNA substitutions, however, have little effect, such as TG/AC to TG^{L}/AC and AT/TA to $A^{L}T$/TA. Interestingly, the stabilizing effect of certain LNA substitutions can be mimicked by certain DNA pairs. For example, AT^{L}/TA is less stabilizing than CT/GA, a pure DNA duplex. The DNA doublets GC/CG and CG/GC are more stabilizing than all but three of the LNA-DNA doublets. Although studies in the past have been concerned with designing the most stable LNA strand with the highest melting temperature, such an aim would contradict the aims of this dissertation, which include the design of an LNA primary target that is strong enough to induce colloidal satellite assembly, yet weak enough to be completely removed by competitive displacement events during disassembly.

Table A.2 Nearest-neighbor ΔG°_{37} parameters for DNA-DNA and LNA-LNA base pairs from the sequences used, at 154 mM and 1 M [NaCl] and 37 °C. The values at 1 M are reported from the literature;[2, 5] the values at 150 mM are corrected from reported values.[5] The sequences are listed in antiparallel orientation, as for hybridization (TG/AC signifies that 5′-TG-3′ hybridizes to 3′-AC-5′). A terminal AT penalty is added for each end of a duplex that terminates in an AT pair.

DNA-DNA	ΔG°_{37} (kcal/mol) 154 mM	1 M	LNA-DNA	ΔG°_{37} (kcal/mol) 154 mM	1 M
TG/AC	-1.02	-1.45	TG^{L}/AC	-1.13	-1.56
GG/CC	-1.41	-1.84	$G^{L}G$/CC	-2.11	-2.54
GA/CT	-0.87	-1.30	GA^{L}/CT	-1.31	-1.74
AT/TA	-0.45	-0.88	AT^{L}/TA	-0.76	-1.19
TT/AA	-0.57	-1.00	$T^{L}T$/AA	-0.70	-1.13
GC/CG	-1.81	-2.24	GC^{L}/CG	-2.35	-2.78
CG/GC	-1.74	-2.17	$C^{L}G$/GC	-2.07	-2.50
CT/GA	-0.85	-1.28	$C^{L}T$/GA	-1.52	-1.95
			$A^{L}T$/TA	-0.46	-0.89
Penalties:					
Initiation		+1.96			
Terminal AT		+0.05			
Self-complementarity		+0.43			

A.1 References

1. SantaLucia, J.; Allawi, H. T.; Seneviratne, A. Improved nearest-neighbor parameters for predicting DNA duplex stability. *Biochemistry* **1996,** *35* (11), 3555-3562.

2. Owczarzy, R.; You, Y.; Groth, C. L.; Tataurov, A. V. Stability and mismatch discrimination of locked nucleic acid-DNA duplexes. *Biochemistry* **2011,** *50* (43), 9352-9367.

3. You, Y.; Moreira, B. G.; Behlke, M. A.; Owczarzy, R. Design of LNA probes that improve mismatch discrimination. *Nucleic Acids Res.* **2006,** *34* (8), 11.

4. Bruylants, G.; Boccongelli, M.; Snoussi, K.; Bartik, K. Comparison of the thermodynamics and base-pair dynamics of a full LNA:DNA duplex and of the isosequential DNA:DNA duplex. *Biochemistry* **2009,** *48* (35), 8473-8482.

5. SantaLucia, J.; Hicks, D. The thermodynamics of DNA structural motifs. *Annu. Rev. Biophys. Biomol. Struct.* **2004,** *33*, 415-440.

Appendix B

Estimating the Melting Temperature for the Mismatched Primary Target

The extensive thermal dissociation that occurs is not surprising, given the low calculated melting temperature values of **A20:M9F** of 19.4 °C and **A20:L^{3}M9F** of 15.9 °C (calculated at IDT Biophysics website).[1] Because existing calculators only allow for determination of thermodynamic properties for the hybridization of an LNA-containing sequence to an all-DNA sequence (i.e., only one strand can contain LNA bases), the T_m of **L^{3}A20:L^{3}M9F** could not be determined. However, the IDT Biophysics website, which allows corrections for mismatches and one base-long dangling ends for sequences of different lengths, was used to obtain T_m values for the analogous **A20:M9F** and **A20:L^{3}M9F** duplexes. Only one report could be found in the literature regarding the change in melting temperature of an LNA-LNA base pairing interaction relative to a DNA-DNA reference. Based on data provided on the thermodynamic effects of **A^L**:**T^L** base pairs,[2] a rough assumption can be made that each base pairing LNA-LNA interaction contributes +11 °C relative to the DNA analogues. A single mismatched DNA-LNA (C:C^L) base pair appears to decrease the melting temperature of **A20:M9F** by ΔT_m= -7.7 °C. It is likely that the LNA-LNA mismatch in **L^{3}A20:L^{3}M9F** is even more destabilizing, but the thermodynamic data is currently lacking. Given these approximations of the LNA stabilization and mismatch destabilization, a reasonable T_m for **L^{3}A20:L^{3}M9F** is approximately 34 °C. Taking into account the additional destabilization of an LNA-LNA mismatch, the actual T_m for the duplex could be near room temperature, meaning that the dissociative pathway would become a key replacement route for this target. Interestingly, in our previous work, when both probe and primary target were immobilized, the **L^{3}A20:L^{3}M9** duplexes were stable when incubated for 24 h in the presence of noncomplementary target and even after multiple wash steps.[3]

B.1 References

1. Laurence, T. A.; Kong, X.; Jäger, M.; Weiss, S. Probing structural heterogeneities and fluctuations of nucleic acids and denatured proteins. *Proc. Natl. Acad. Sci. U. S. A.* **2005,** *102* (48), 17348-17353.

2. Koshkin, A. A.; Nielsen, P.; Meldgaard, M.; Rajwanshi, V. K.; Singh, S. K.; Wengel, J. LNA (locked nucleic acid): An RNA mimic forming exceedingly stable LNA:LNA duplexes. *J. Am. Chem. Soc.* **1998,** *120* (50), 13252-13253.

3. Eze, N. A.; Milam, V. T. Exploring locked nucleic acids as a bio-inspired materials assembly and disassembly tool. *Soft Matter* **2013,** *9* (8), 2403-2411.

VITA

Ngozi Eze was born in Wisconsin but grew up in Worcester, Massachusetts. She attended Bancroft School for most of her formative years before graduating from MIT in 2005 with a Bachelor of Science in Chemistry. She then worked in a microbiology lab affiliated with Massachusetts General Hospital pinpointing the effect of certain pathogenic *Shigella* proteins on host cell signaling cascades during cell invasion. Wanting to combine her interests in chemistry and biology, Ngozi decided to pursue a doctorate in Materials Science and Engineering at the Georgia Institute of Technology in 2008 with Dr. Valeria Milam.